2D ICE TRAJECTORY IN THE FLOW FIELD OF JOUKOWSKI AIRFOIL

by

Mahdi KAMOUSI ALAMDARI

THESIS PRESENTED TO ÉCOLE DE TECHNOLOGIE SUPÉRIEURE
IN PARTIAL FULFILLMENT FOR A MASTER'S DEGREE
WITH THESIS IN MECHANICAL ENGINEERING
M.A.Sc.

MONTREAL, MARCH 27, 2018

ÉCOLE DE TECHNOLOGIE SUPÉRIEURE
UNIVERSITÉ DU QUÉBEC

BOARD OF EXAMINERS

THIS THESIS HAS BEEN EVALUATED

BY THE FOLLOWING BOARD OF EXAMINERS

Mr. François Morency, Thesis Supervisor
Department of Mechanical Engineering, École de technologie supérieure

Mr. Stéphane Hallé, President of the Board of Examiners
Department of Mechanical Engineering, École de technologie supérieure

Mr. François Garnier, Member of the jury
Department of Mechanical Engineering, École de technologie supérieure

THIS THESIS WAS PRENSENTED AND DEFENDED

IN THE PRESENCE OF A BOARD OF EXAMINERS AND PUBLIC

ON MARCH 22, 2018

AT ÉCOLE DE TECHNOLOGIE SUPÉRIEURE

ACKNOWLEDGEMENT

I would like to thank my thesis advisor Prof. François Morency at École de technologie supérieure. The door to Prof. Morency office was always open whenever I ran into a trouble spot or had a question about my research or writing. He consistently allowed this paper to be my own work, but steered me in the right direction whenever he thought I needed it.

I must express my very profound gratitude to my parents and to my family for providing me with unfailing support and continuous encouragement throughout my years of study and through the process of researching and writing this thesis. This accomplishment would not have been possible without them. Thank you.

Mahdi Kamousi Alamdari

TRAJECTOIRE 2D DE LA GLACE DANS UN ÉCOULEMENT AUTOUR D'UN PROFIL DE JOUKOWSKI

Mahdi KAMOUSI ALAMDARI

RÉSUMÉ

Le givrage en vol et le dégivrage sont des problèmes important dans l'industrie de l'aviation et ont été étudié ces dernières décennies expérimentalement et numériquement. Au cours des dernières années, l'approche numérique a été privilégiée pour simuler la création de la glace et la trajectoire des pièces de glace en raison de son coût et de son efficacité temporelle. Cette étude vise à étudier l'influence des différents paramètres de la pièce de glace et du profil aérodynamique sur la probabilité d'ingestion de glace par un moteur monté à l'arrière d'un avion. Pour y parvenir, le profil d'écoulement de Joukowski et la trajectoire 2D d'une pièce de glace carrée dans ce champ d'écoulement seront étudiés.

Le champ de vitesse autour d'un profil de Joukowski est simulé et sera utilisé pour calculer les forces aérodynamiques sur la pièce de glace carrée. Les trajectoires des particules de glace en forme de plaques carrées dans des champs d'écoulement uniformes sont comparées à la littérature pour valider l'approche numérique. Comme le dégivrage est associé à des incertitudes sur les conditions initiales, la méthode de Monte-Carlo est utilisée pour faire une étude statistique sur le phénomène étudié. La probabilité de collision de glace autour du profil aérodynamique est calculée pour étudier l'influence des paramètres aérodynamiques tels que l'épaisseur, la courbure et l'angle d'attaque ainsi que l'influence de la forme et de la masse de la glace sur la trajectoire de la glace. Le dégivrage est étudié séparément pour l'intrados et l'extrados du bord d'attaque.

Les conditions initiales du dégivrage sont un facteur important dans les trajectoires de glace. Les résultats montrent que la probabilité d'ingestion de glace varie en fonction des paramètres de l'aile et de la pièce de glace. Les profils plus épais et plus incurvés imposent moins de risque d'ingestion de glace. L'angle d'attaque du profil aérodynamique a une influence différente sur la probabilité d'ingestion en fonction de l'emplacement du dégivrage. Les particules de glace rectangulaires et sphériques sont plus susceptibles de frapper le moteur que les morceaux de glace carrés. En outre, il est démontré que l'effet Magnus a une influence importante sur les trajectoires de la glace qui ne peut être ignorée dans les simulations.

Mots clés : CFD, trajectoire de la glace, profil de Joukowski, ingestion de glace, givrage en vol, dégivrage

2D ICE TRAJECTORY IN THE FLOW FIELD OF THE JOUKOWSKI AIRFOIL

Mahdi KAMOUSI ALAMDARI

ABSTRACT

Inflight icing and ice shedding as an important problem in the aviation industry have been studying in recent decades both experimentally and numerically. In recent years, the numerical approach has been privileged to simulate ice accretion and ice piece trajectory due to its cost and time efficiency. This study aims to investigate the influence of the different characters of the ice piece and airfoil on the probability of ice ingestion by an aft-mounted engine. In this order, the flow field of the Joukowski airfoil and 2D trajectory of a square plate ice piece in this flow field will be simulated.

Velocity field of Joukowski airfoil is simulated and used to compute aerodynamic forces on the square plate ice piece. Trajectories for square plate ice particles in uniform flow fields are compared with the literature to validate the developed code. As the ice shedding is associated with uncertainties regarding its initial conditions, Monte-Carlo method is used to have a statistical study on this phenomenon. Ice pass probability map around the airfoil is generated to investigate the influence of airfoils' parameters such as thickness, camber and angle of attack as well as the influence of ice's shape and mass on the trajectory of the ice piece. Ice shedding is investigated separately for upside and downside of the leading edge.

Initial condition of ice shedding is found to be an important factor in ice trajectories. Results show that ice ingestion probability by engine changes for different set of parameters of airfoil and ice piece. Thicker and more curved airfoils impose less ice ingestion risk. Airfoil's angle of attack has different influence on the probability map depending on the location of the ice shedding. Rectangular and sphere ice particles are more likely than square ice pieces to pass through the engine. Also it is shown that Magnus effect has an important influence on the ice trajectories which cannot be ignored in ice trajectory simulations.

Key words: CFD, Ice trajectory, Joukowski airfoil, Ice ingestion, Inflight icing, Ice shedding

TABLE OF CONTENTS

Page

LIST OF TABLES

Page

LIST OF FIGURES

Page

LIST OF SYMBOLS

Mathematical symbols:

C_L	Lift Coefficient
C_D	Drag Coefficient
C_M	Moment coefficient
U_∞	Flow velocity
U_{flow}	Vertical component of the flow velocity
W_{flow}	Horizontal component of the flow velocity
u_{ice}	Horizontal velocity component of the ice particle
w_{ice}	Horizontal velocity component of the ice particle
α	Angle of the relative velocity with horizontal axis
γ	Angle of attack of the ice particle
C_{ice}	Normal force coefficient
D	Drag force on the ice particle
L	Lift force on the ice particle
M	Moment on the ice particle
g	Gravity acceleration
I	Moment of inertia on the ice particle
m_{ice}	Mass of the ice particle
N	Normal force on the ice particle
S	Reference area of the ice particle
t	time
β	Angle of the circles offset
ρ	Density
ω	Angular velocity
l	Length of the ice particle
L	Width of the ice particle

e	Thickness of the ice particle
c	Distance of the pressure center with the center of ice
C_{Dr}	Drag coefficient caused by Magnus effect
C_{Lr}	Lift Coefficient caused by Magnus effect
C_{Mr}	Moment coefficient caused by Magnus effect
Z	The Plane of the Joukowski airfoil
ζ	The plane of the circular cylinder

Units:

m	Meter, unit of length
$ft.$	Feet, unit of length
m/s	Meter per second, unit of velocity
kg/m^3	Kilogram per cubic meter, unit of density
sec	Second, unit of time
°	Degree, unit of angle
$°C$	Degree Celsius , unit of temperature

Abbreviations:

2D	Two-Dimensional
3D	Three-Dimensional
AOA	Angle of Attack
CFD	Computational Fluid Dynamic
LWC	Liquid Water Content
NACA	National advisory Committee for Aeronautics
DOF	Degree of Freedom
TWC	Total Water Content
FAR	Federal Aviation Regulations

INTRODUCTION

Ice accretion on aircraft is one of the hazardous phenomena that can cause catastrophic accidents. This issue has been under investigation for several decades and especially in recent years to solve the problems related to icing and ice shading in the aviation industry. Although many empirical and computational methods have been implemented, but icing problem still remains as an important threat to aircraft safety and efficiency. Icing during the flight brings about degradation of the aircraft's performance and shading of the accreted ice can damage the downstream components of an aircraft such as engines.

In recent years, Computational Fluid Dynamic (CFD) has been considered as a privileged approach to study icing and ice shedding phenomenon. Due to the efficiency of this method regarding time and cost, CFD models have been widely used to predict the ice accretion on the component of the aircraft such as leading edges, control surfaces and engine nacelles. Also this numerical approach is used to study the trajectory of the ice particles shed from the geometry of the aircraft (Shimoi, 2010) (Suares, 2005).

Ice trajectory simulations have been carried out to trace the path of the shed ices and compute the ice pass probability and their strike with the component of the aircraft. Studies concern both two-dimensional and three-dimensional movement of the ice mass. While in the majority of the 2D simulation, the ice piece has three Degrees of Freedom (DOF) of movement, in 3D simulations DOF vary from three to six. The flow fields used in the simulations can be uniform or non-uniform. The uniform flow field can be a representative of the wind tunnel flow and the non-uniform flow fields can be the flow field of airfoil, wing or an aircraft as a whole.

The shape of the ice fragment plays an important role in ice trajectory results. Aerodynamic force and moment coefficients, which are mostly calculated through empirical methods, differ for each shape of the ice piece. Although the shape of shed ice pieces is random, simulations are conducted for some ice shapes such as square plates, rectangular plats, spheres, semi sphere and disk shape ice shapes (Shimoi, 2010).

The ice piece moves in a flow field due to the imposed forces and moments. Both aerodynamic and gravitational forces govern the acceleration of the ice mass. While the forces translate the ice piece in the flow filed, moments are in charge of the angular movement of the particle. In some research all the forces and moments are taken into account and some others have limited their studies by neglecting some of the aerodynamic forces such as Magnus effect, generated by the angular velocity of the ice piece.

This research project will consider the trajectory of a square plate ice in a two-dimensional flow field. DOF for the ice piece will be three for two linear movements in the directions of the horizontal and vertical axis of the plane and an angular movement around the axis perpendicular to the plane of the 2D flow field. Lift and drag forces as well as the moment on the ice piece will be calculated using both the static aerodynamic coefficients and the aerodynamic coefficients generated by the angular velocity of the ice particle (Magnus effect).

The flow fields used in this research project are uniform and non-uniform flow fields. The trajectories run in the uniform flow field will serve for validation of the simulation code and non-uniform flow field will be used to draw the results of the research. Joukowski airfoil is the geometry which the flow field around it will be simulated.

Ice trajectory will be simulated in a 2D flow field using differential equation of the movement. The velocity and the position of the ice piece will be computed by integrating these differential equations in each time step of the trajectory. Aerodynamic and gravitational forces will be used to obtain the linear acceleration of the ice body and moment of inertia will be used to compute angular acceleration of the ice fragment.

The random nature of the ice shedding makes the statistical study inevitable for this phenomenon (Suares, 2005), (Shimoi, 2010). The initial condition of the ice shedding is associated with uncertainties regarding ice piece's shape, location, orientation and linear and initial angular velocities. A code developed for Monte-Carlo method will be integrated with the code of ice trajectory. This code generates a large number of initial conditions and plot the footprint of the ice pieces around the airfoil. Using this integrated code, the probability of the ice trajectory through the defined areas in the study plane will be possible.

This research will be presented in three chapters. First chapter will deal with the background of the icing problem and ice trajectory simulation. First comes an introduction for in-flight icing problems. The meteorological conditions in which the probability of in-flight icing is higher and the process of ice accretion on the components of the aircraft, in particular inside the engine, will be presented. The possible approaches to analyze icing problems and currently used de-icing systems in the aviation will be mentioned briefly. These sections will be followed by a literature review related to the ice trajectory simulation methods.

Chapter two is dedicated to the methodology of the research project. it will offer the mathematical model, equations and coefficients used in the simulation code. In addition, the condition of the flow fields and properties of ice particles simulated in the research will be mentioned. In another section, the simulation tools used in the project will be described by illustrating the flow chart of the Matlab codes developed during the research.

Chapter three contains the results of the research project. The results will be validated, verified and discussed for Joukowski airfoil, single trajectories and Monte-Carlo method. The figures generated by the simulation code will show the probability maps around the airfoil in different situations. This chapter will discuss the impact of the airfoil's angle of attack, airfoil thickness and its camber on the trajectory of the ice piece. Also, the possibility of the ice ingestion by downstream engines will be verified when the ice piece has different shapes such as square, rectangular and sphere shape and different masses.

CHAPTER 1

LITERATURE REVIEW

1.1 In-flight icing and the engine of aircraft

According to Bin and Yanpei (Bin and Yanpei, 2011), the source of the ice accreted on the propulsion system can be different, but usually, engine icing is caused by freezing of cloud droplets, or super cooled water droplets. Super cooled water droplets maintain their liquid state even at temperatures well below the freezing degree. When these droplets impinge on the aircraft's engine during the flight, they can bring about anomalies such as non-recoverable or repeating surge, stall rollback or flameout, and may also cause the gas path ice blockage in core engine (Bin and Yanpei, 2011).

The presence of high altitude ice crystals which exist in the deep convective clouds of strong tropical and sub-tropical storms is known to be the other causation of this problem. These ice crystals do not have good reflectivity for radar echoes, so it is difficult to prevent passage of aircraft through these clouds (Califf and Knezevici, 2014). According to Haggerty, McDonough et al. (Haggerty, McDonough et al., 2012), several aeronautic accidents which are attributed to engine icing, have occurred in flight conditions where super cooled liquid droplets were not present. In these cases, ice crystal particles in surrounding clouds are considered to have the main role in degradation of engine power. Since the mid-1990's, more than 100 documented engine power loss events are attributed to this phenomenon known as ice particle icing. The majority of accidents related to ice particle icing phenomenon, have occurred in the vicinity of tropical thunderstorms, particularly over the western tropical Pacific Ocean. It is hypothesized that ice particles accrete on warm surfaces inside the engine. These Ice masses deform the aerodynamic shape of the blades and may block the airflow passage inside the engine. Also, accreted ices can shed into the engine which is hazardous for downstream components. All these factors reduce performance of the engine dramatically (Haggerty, McDonough et al., 2012).

Veres, Jorgenson et al. (Veres, Jorgenson et al., 2012) estimate that ingested ice crystals into the engine will confront with higher temperatures in core part of the engine. This condition will melt a portion of the ice crystals. It will make a mixture of ice and water which consequently enhances the stickiness power of ice particles on the metal surfaces of the compressor components. Thus, the engine experiences airflow blockage on its stationary parts such as stator vanes (Veres, Jorgenson et al., 2012).

According to Veres, Jorgenson et al. (Veres, Jorgenson et al. 2012), local wet-bulb temperature and minimum local melt ratio are two key parameters that play main roles to provide favorable condition for ice accretion. It is known that this favorable condition takes place when the local wet-bulb temperature is near and blow freezing and the local melt ratio is 10%. These criteria can be used to determine the possibility of icing due to ice crystals. The degree of ice blockage can be estimated by using an empirical model of ice growth rate and the impingement duration of ice crystals (Veres, Jorgenson et al. 2012).

Liquid water content (LWC), total water content (TWC), flight Mach number, particle impingement angle and particle size are the factors that determine the sticking efficiency of ice crystals particles (Currie, Fuleki et al., 2014). A former research (Currie, Fuleki et al., 2014) suggests that the sticking efficiency remains finite at all particle impingement angles when TWC is more than 10 g/m^3 and the flight Mach number is low (0.25). At higher Mach numbers, smaller ice crystal particles stick more efficiently to engine components.

Over the past decades, aircraft flight accidents related to icing has been reported all over the world. According to Cao, Wu et al. (Cao, Wu et al., 2015), in America, statistic data of flight accidents during 1973 to 1977 showed that 2.56% of the total flight accidents are due to the icing problem. During 1976 and 1988, flight accidents attributed to ice accretion reached up to 542. American Safety Advisor statistic data concerning iced- aircraft flight accidents from 1990 to 2000 indicates that 12% of all the flight accidents in adverse weather conditions occurred in icing condition and in-flight icing was the reason for 92% of the iced-induced accidents (Cao, Wu et al., 2015).

Since 1990, many of jet engine power loss incidents have been attributed to the icing problem, which have been occurred at altitude higher than 22,000 ft., the level which is recognized as the extreme upper limit for the existence of super cooled liquid water (Mason, Strapp et al., 2006). Mason, Strapp et al estimate that at this level the hydrometeors are expected to exist in the form of ice particles which can be individual ice crystals or in larger size spanning from microns to centimeters. Previous to these events, it was believed that ice particles are harmless for the airframe and the engine due to the fact that frozen particles don't stick to these components and bounce off from the surface. Recent engine power loss events since 1990, initiated deeper investigation of ice particles influence on jet engines. More than 240 icing related events have been documented worldwide since the 90s, which 62 of them are believed to be due to ice particle icing (Mason, Strapp et al., 2006).

According to Mason, Strapp et al. (Mason, Strapp et al., 2006), documented icing incidents and accidents show that most of the ice crystal icing occurs during aircraft flights through convective clouds. Convective clouds have updraft cores that cause the movement of low-level air to higher altitudes in which the temperature drops and water vapor condense continuously. This phenomenon can increase the liquid water content (LWC) and/or ice water content (IWC) in a limited region. It is assumed that condensing vapor goes directly to the ice phase above the freezing level. The maximum level of IWC is about 9 g/m^3 at 30,000 ft. and as the altitude increases above this level, IWC decreases. Previous observations show that Atlantic hurricane convection clouds are almost completely glaciated at -5°C which means rapid conversion of LWC to ice above the freezing level and no significant super cold LWC exist at temperature below -12°C (Mason, Strapp et al., 2006).

The accreted ice on the aircraft's surfaces can be in two general forms. These forms are called glaze ice and rime ice. As Borigo (Borigo, 2014) describes, glaze ice is a clean and hard ice that usually does not have an aerodynamic shape. When droplets do not freeze instantaneously and run downstream the result will be a glaze ice accretion. Because of its non-aerodynamic shape, it is more vulnerable to shedding. The creation of rime ice is very fast and as soon as droplets impinge with the surface, freezing occurs and ice traps some air which makes it milky and white. Rime ice has greater adhesion properties and lower density (Bin and Yanpei, 2011).

Rime ice usually grows in low temperature (-40°C to -10°C) at lower speeds and at low LWC conditions but glaze ice typically accretes at temperatures closer to freezing (-18°C to 0°C) at higher speeds and LWC (Borigo, 2014).

An engine of aircraft should pass icing test to get its certification. An engine should be able to work steadily without any problem under a specific icing condition (Bin and Yanpei, 2011). These requirements are mentioned in FAR Section 33.68. This Section requires that each engine which is equipped with ice protection system should be able to sustain its power during flight phases without ice accretion on components and run steadily under icing condition at least for 30 minutes at ground idle setting and then demonstrate its takeoff thrust by being able to accelerate without any problem. This performance requirement is defined in appendix C of FAR part 25. Engine does not use its auto-recovery system during icing test, since it is a back-up device for aircraft during the icing problem (Bin and Yanpei, 2011).

Icing can be analyzed both experimentally and numerically. The experimental approach to analyze icing can be done during a real flight or in the wind tunnel. Both of these approaches are suitable to analyze a system, but they cannot be used in the design platform (Pellissier, 2010). Testing an aircraft during a real flight would be very expensive and it can be used just after production of the aircraft. This method is time consuming and finding an icing condition in flight to examine the performance of the engine is very difficult. Inflight-testing is dangerous and difficult to run and all the icing conditions outlined in aviation safety regulation such as the FAA's FAR (Federal Airworthiness Regulations) Part 25 Appendix C or the EASA's CS (Certification Specifications) Part 25 Appendix C cannot be reproduced (Pellissier, 2010).

Using wind-tunnel can be a solution for problems associated with in flight testing but it has its own limitations. Icing test facilities utilize freezing super cooled droplets or ice shavers to simulate icing condition. There are differences between an artificial ice crystal produced in icing wind tunnel and a natural ice crystal which can be found at high altitude. Since the shape of the crystal is a key element to study the trajectory of ice particles, such inadequate simulation of ice crystals misleads the analyses of the icing dynamics (Nilamdeen, 2010). The number of icing wind tunnels is very limited and manufacturers own most of the wind tunnels, so there are few facilities in research domain that are accessible for researchers. The price of using

these wind tunnels is expensive and even ignoring the cost will not help much due to the fact that most of the good facilities that can produce icing condition are booked in advance for a long time.

Beside the experimental methods, computational models are used to compute ice accretion, evaluate the performance degradation caused by icing, study and design anti-icing systems and evaluate their efficiency. According to Rios (Rios Pabon, 2012), the complicity of analyzing the ice crystal trajectory and the problems of experimental approach favor the use of computational methods. By using these methods ice shape and its trajectory can be simulated more efficiently. The time and money needed to run these analyzes are significantly less than experimental methods.

1.2 Ice trajectory simulation

A literature review was conducted to establish the state of the art in the fields related to ice shedding and ice piece trajectory simulation. This literature review concerned the ice trajectory simulation methods and the probabilistic methods for numerical studies on this phenomenon. Following is the results of a literature review which introduces works done in the ice trajectory simulation.The ice trajectory simulation as a numerical tool to investigate the inflight icing and ice shedding has been considered and developed in recent decades and there are not many available papers and data in the literature. Most of the works done to simulate the trajectories are in the field of wind engineering and to simulate the trajectories of the debris in the storms (Tachikawa, 1983), (Kordi, 2009), (Holmes, 2006). However, some researchers have applied this knowledge in the field of ice shedding problem and ice piece trajectories (Shimoi, 2010), (Suares, 2005).

This research has been done with different considerations. Two general categories in the ice piece trajectory simulations are the trajectories which are simulated in 2D flow fields and the trajectories which are carried out in 3D flow fields. Moreover, the degree of freedom of the movement of the ice piece is confined in the research and can vary from 2 DOF to 6 DOF.

The flow fields in which ice trajectories are studied are divided to uniform and non-uniform flow fields. The trajectories in the uniform flow field are mostly used to validate the data of the simulations with the experimental data and results of the wind tunnel experiments. The non-uniform flow fields used in the simulations are the flow field of the aircraft's geometry as a whole or the flow field of components of the aircraft such a wing.

Tachikawa (Tachikawa, 1983) is a pioneer researcher in the field of the trajectory simulation. He has carried out several 2D experiments in the wind tunnel to determine the aerodynamic force coefficients on the different shape of the plates. He has measured the lift and drag forces and moments on the plate in a low-speed wind tunnel. Magnus effect is taken into account to simulate the trajectories and the results are compared with the experimental trajectories with different initial conditions for different plates. In his research he has shown that the initial orientation of the plate plays an important rule to determine the path of the plate.

Holmes et al. (Holmes, 2006) has conducted plate type debris trajectory simulation in 2D uniform flow field experimentally and numerically. He has investigated the trajectory of three different square flat plate debris with different dimensions and density in the uniform horizontal flow fields with different velocities. The differential equations of movement are used to calculate the trajectory of the debris. He has used aerodynamic force coefficients which are a function of the angle of attack, to calculate the lift, drag and moment forces on the plate. The Magnus effect in the simulation of Holmes is only considered for lift force and he has compared the trajectories with and without Magnus effect. Holmes has compared their trajectories with experimental data of Texas Tech University. In the article of Holmes there are some examples of trajectories for different plate pieces with different initial conditions for the angle of attack of the ice piece and its initial velocity to compare the influence of the initial conditions on the trajectories of the plate debris.

Kordi and Kopp (Kordi, 2009) have simulated the trajectory of the square flat plate in 2D uniform flow field. They have used differential equations of motion to trace the movement of the ice particle. The aerodynamic coefficients generated by the angular velocity of the ice piece are added to the static coefficients to take into account the Magnus effect, in this order, the

equations of Iverson (Iverson, 1979) are used based on the ice piece's tip speed and the speed of the tip of the auto rotational point.

Suares (Suares, 2005) has performed a broad research on the trajectory simulation of ice pieces in uniform and non-uniform flow field. He has simulated the ice trajectory in 2D and 3D for uniform flow and flow fields of the airfoil and wing. The ice piece samples used in the trajectories are square plates, rectangular plates and semicircular shells and the research includes 3,4 and 6 degrees of freedom for the movement of the ice piece samples. Suares has developed codes in FORTRAN and MSC.Easy5 for ice trajectory simulation and by using Monte-Carlo method the strike possibility of the ice piece with downstream engines in different conditions has been studied.

Chandrasekharan and Histion (Chandrasekharan, 2003) have simulated the trajectory of the ice pieces shed from the surface of the aircraft to analyze the probability of the ice ingestion by downstream engines when the minor modifications are made in the dimension of the fuselage. The VSAERO code has been utilized to compute the flow field and velocity field around the geometry of the Learjet 40 and Learjet 45 business jets. In the simulation, the lift and side forces on the ice particle have been dismissed and the movement of the ice fragment and its acceleration in the flow field is calculated only using the drag forces and gravitational forces. The project includes the simulations of disk and plate shape ice pieces. The disk ice particle has a diameter of four inches and a thickness of one inch and start its shedding from the radome of the aircraft. Two plate form ice pieces with dimensions of $3" \times 1" \times 1"$ and $1.5" \times 1.5" \times 0.3"$ are used to simulate the ice shedding from the windshield of the aircraft. The obtained results show that the minor different in the length of two above mentioned aircraft does not have a significant influence on the ice ingestion risk of the downstream engines.

A 4-DOF simulation model has been used by Kohlman and Winn (Kohlman, 2001) to simulate the square plate ice trajectories in the uniform flow field. Lift and drag forces are assumed to be the main forces on the ice fragment and experimental data have been used to calculate the aerodynamic coefficients. The forces generated by the rotation of the ice piece are taken into account by calculating the angular velocity, aerodynamic damping and moment of inertia for

the plate. The results of the simulations emphasize the importance of the initial orientation of the ice piece and the aerodynamic damping coefficient on the trajectory of the ice piece. Furthermore, the thickness of the ice piece influences the vertical displacement of the particle and its area alter the horizontal displacement.

Shimoi (Shimoi, 2010) has studied the ice shedding and ice trajectory both experimentally and numerically. His 6-DOF model simulates the trajectory of square, rectangular plates, disks, upper surface horn and double horn ice pieces. The data base of Wichita state university (WSU) is used for the aerodynamic coefficients of ice particles and the flow field used in his research is obtained from a commercial Navier-Stock computer code. The trajectory of the different ice pieces is simulated in the flow field of a business jet with different angles of attack. The analyzes of the study shows the influence of the shedding location, initial orientation of the ice piece and the aircraft's angle of attack on the trajectory of the ice fragment. Monte-Carlo simulation is implemented to determine the probability of the ice piece strike with downstream components of the aircraft and the ice ingestion possibility by aft-mounted engines.

De Castro et al. (De Castro, 2003) have conducted a two-dimensional study on the 3-DOF trajectory of the square plate ice piece in a non-uniform flow field. The flow field used in the simulations belongs to a symmetric NACA airfoil. Monte-Carlo method has been used to statically analyze the trajectories of the ice piece due to the uncertainty of the initial conditions of the shedding. Initial angle of attack of the plate, angular velocity and the damping coefficient are the varying parameters of the initial conditions. The pass probability of the ice piece with the defined areas around the airfoil is presented as the result of the research.

Baruzzi et al. (Baruzzi, 2007) have considered 6-DOF trajectories in their research to simulate the movement of the ice piece. FENSAP-ICE computer code has been used to determine forces and moments on the ice particle in each time step and consequently, to calculate linear and angular acceleration of the shed ice.

The literature review conducted in this research emphasizes the importance of inflight icing, ice shedding and ice ingestion by engines in reducing the performance of the aircraft and engines. CFD models used in this field were introduced and their approaches to simulate the

ice trajectory were briefly reviewed. Although precious research and works have been carried out in this domain, farther researches are needed to fully understand the behavior of the ice pieces in uniform and non-uniform flow fields and aerodynamic coefficients for different ice shapes are remained to define more precisely.

1.3 Contributions

The contributions of the author in this research project are as follows:

1. **Developing a code for the flow field:** A Matlab code was developed to simulate the Joukowski airfoil and its flow field. The potential flow function and potential velocity of the flow field are computed to have the velocity of the flow at each point of the plane.
2. **Improving the code of ice trajectory:** The code of the 2D ice trajectory available in the university was improved to integrate with the code of Joukowski airfoil.
3. **Improving the Monte-Carlo code:** The code of the Monte-Carlo simulation was improved to make it compatible with other codes of the research.
4. **Developing a code to calculate the probability of ice passing:** A code is developed to estimate the pass probability of the ice piece through the defined areas around the airfoil.
5. **Studying ice trajectory in different conditions:** As the main objective of the research, the influence of the airfoil's geometry and its angle of attack as well as ice's shape and mass on the trajectory of the ice piece are studied.

CHAPTER 2

MATHEMATICAL MODEL AND SIMULATION METHODOLOGY

To simulate the ice trajectory in a flow field, the translational and angular movements of the ice piece generated by aerodynamic and gravitational forces on it should be calculated. The parameters acting in these calculations are the mass properties of the ice particle, the aerodynamic properties of the ice particle and the properties of the flow field. This chapter contains the mathematical models to calculate these physical properties of the ice trajectory simulation.

2.1 Flow fields

This section will introduce the flow fields used in the research project. The research is done to simulate 2D ice trajectories in uniform flow field and in the flow field of the Joukowski airfoil. To have the flow field around the Joukowski airfoil, the flow field around a circular cylinder is transformed using Joukowski transformation. The flow field around the circular cylinder is the result of the superposition of three basic flow fields. After presenting these basic flow fields, and their superposition, Joukowski transformation as a method of conformal mapping, will be the last part of this section.

2.1.1 Flow field around the circular cylinder

The flow field around a circular cylinder with circulation is fully understood (Pope, 1951). This knowledge about the circular circle can be transferred to an airfoil by using conformal mapping. By using such a transformation, the characteristics of the flow around the airfoil including pressure distribution and its lift can be defined (Pope, 1951).

To have the flow field around a circular cylinder, the first step is to simulate the circular cylinder and its flow filed by using the superposition of the three basic flows. This can be achieved by the superposition of the uniform, doublet and vortex flows (Kapania, 2008). The superposition of the doublet, uniform, and vortex flows yields a potential function and a stream function (Kapania, 2008).

2.1.1.1 Uniform, doublet and vortex flow fields

Complex potential flow for uniform flow field in a complex plane z, when it has a velocity of U_∞ and its direction makes an angle of α with the horizontal axis is (Panton, 2005):

$$F_{uniform} = U_\infty z\, e^{-i\alpha} \tag{2.1}$$

This equation describes the potential flow field in every point of the plane z. The velocity function is the derivative of the potential flow function in every point in the complex z plane. Following is the derivative of the uniform potential flow function with respect to z :

$$W_{uniform} = \frac{dF_{uniform}}{dz} = U_\infty\, e^{-i\alpha} \tag{2.2}$$

According to this equation, in the uniform flow field, the velocity of the flow is not a function of the location of the complex z plane. This means that the velocity is constant in a uniform flow field and does not change from point to point.

Doublet potential flow function is the superposition of the source and sink flow fields (Panton, 2005). The complex potential flow function for a Doublet flow field in the distance of R from the center of the Doublet and the flow velocity of $U_\infty$is:

$$F_{Doublet} = \frac{U_\infty R^2}{z}\, e^{i\alpha} \tag{2.3}$$

Following the same method as potential uniform flow, doublet potential velocity function can be obtained by derivation of its potential flow function:

$$W_{Doublet} = -\frac{U_\infty R^2}{z^2}\, e^{i\alpha} \tag{2.4}$$

According to this equation the velocity in a doublet flow field is a function of z and is different in each point of z plane.

The steady cylinder without circulation does not generate any lift force. Generation of the lift is due to the circulation of the cylinder (Panton, 2005). The superposition of the uniform flow field and doublet flow field represents the flow field around a steady cylinder in uniform flow. To generate the lift force, vortex flow field is added to these two flow fields. Complex potential function for Vortex flow field with a radius of R is (Panton, 2005):

$$F_{vortex} = k_{vortex} iLn(\frac{z}{R}) \tag{2.5}$$

In this equation k_{vortex} is the vortex strength and is defined as following:

$$k_{vortex} = \frac{\Gamma}{2\pi} \tag{2.6}$$

Γ is the circulation, being the line integral of the velocity field over the closed curve of the cylinder. Circulation is a conceptual tool that relates the lift force of an object to the nature of the fluid flow around it (Kapania, 2008) and is equal to:

$$\Gamma = 4\pi U_\infty R\, sin(\alpha) \tag{2.7}$$

Angle α is the angle of the free stream velocity with respect to the horizontal axis. Kutta-Joukowski theorem is used to compute the lift force of a circular cylinder. This fundamental theorem of aerodynamics relates the lift per unit span of an airfoil to the velocity of the airfoil U_∞ through the fluid, the fluid density ρ and the circulation Γ. When Γ is known, the lift per unit span L becomes (Kapania, 2008):

$$L = \rho U_{\infty} \Gamma \tag{2.8}$$

By derivation of the potential flow function of the vortex, the potential velocity function of the vortex flow field will be:

$$W_{vortex} = \frac{ik_{vortex}}{z} \tag{2.9}$$

By defining three simple flow fields, in the next section, the superposition of these flow fields will be presented.

2.1.1.2 Superposition of the flow fields

The superposition method is used to compute a complex potential flow field by summing up some simple potential flow fields. To obtain the complex potential flow function around a circular cylinder in a uniform flow, potential functions of uniform, doublet and vortex flow fields are put together, by which potential flow function is:

$$F_Z = Uz\, e^{-i\alpha} + \frac{UR^2}{z}\, e^{i\alpha} + ik_{vortex} Ln(\frac{z}{R}) \tag{2.10}$$

Also, superposition of the potential velocity functions of these three flow fields, yields the potential velocity function of the circular cylinder in a uniform flow field by which potential velocity function will be:

$$W_Z = U\, e^{-i\alpha} - \frac{Ua^2}{z^2}\, e^{i\alpha} + \frac{ik_{vortex}}{z} \tag{2.11}$$

In this section the potential flow field function and potential velocity function of the flow field around a circular cylinder in a uniform flow field were presented in detail. To have the flow field around an airfoil, the flow field around the circular cylinder can be transformed by using conformal mapping. In the next section using the conformal mapping to the circular cylinder flow field through Joukowski transformation, the flow field around the Joukowski airfoil will be computed.

2.1.1.3 Joukowski transformation

By using conformal mapping, both geometry of the circular cylinder and its peripheral flow filed can be transformed. This function is possible because of the angle preserving feature of the conformal mapping. To use this function, airfoil shape, potential and velocity function of the flow field should be expressed in complex variables (Pope, 1951). The transformed circulation Γ of the airfoil and its consequent lift power is the same as the circulation and lift power of the original circular cylinder (Pope, 1951).

One of the conformal mapping methods is the Joukowski transformation. This research has used Joukowski transformation to define a Joukowski airfoil and its pertaining flow field. The basic equation of the Joukowski transformation is:

$$Z = \zeta + \frac{\lambda^2}{\zeta} \tag{2.12}$$

By using this equation a circular cylinder and its pertaining flow filed in plane ζ can be transformed to an airfoil in plane Z. This circular cylinder should be well defined to get the desired results. Not every circular cylinder will be transformed in a proper Joukowski airfoil. In this regard the coordinate of the center of the circular cylinder plays an important rule (Pope, 1951). λ, the transformation parameter, depends on the radius and the origin of the circular cylinder. This factor determines the resulting shape of the Joukowski airfoil. To have an airfoil which meets the desired aerodynamic properties, transformation parameter, λ, should be properly employed (Pope, 1951). Figure 2.1 shows the original cylinder and resulted Joukowski airfoil. According to this figure, when X and Y are the coordinates of the center of the cylinder, parameter λ is:

$$\lambda = \left(\frac{Y}{tan(\beta)}\right) - |X| \tag{2.13}$$

Where angle β can be found as following:

$$\beta = arcsin(\frac{Y}{R}) \tag{2.14}$$

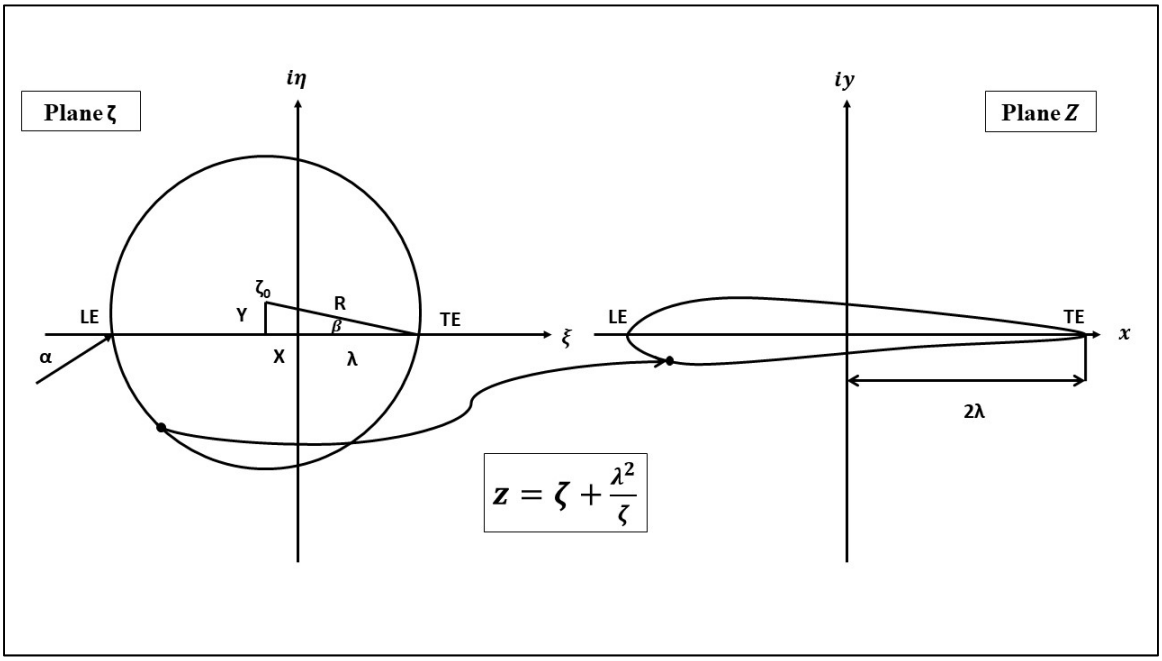

Figure 2.1 Joukowski transformation

The other important point in Joukowski transformation is that all points on the x axis of the plane ζ will be transformed to the points on the horizontal axis in plane Z. These points are correspondents with leading and trailing edge of the airfoil. Since the rear stagnation point of the airfoil should be located on the trailing edge of the airfoil, a special care should be applied to these points. Stagnation points of a cylinder without circulation are on the x axis of the ζ plane. Such a flow filed is not a desired one, due to this fact that, because of symmetry, it will not generate any lift power. To have lift power, vortex should be added to the flow field which can be obtained by the circulation of the cylinder. Circulation moves down the stagnation points of the circular cylinder. To compensate for this effect, the circle should move upward, to establish the stagnation points on the horizontal axis of the plane ζ (Pope, 1951). To have a reasonable airfoil the center of the original circle cannot be on the vertical axis of the plane

ζ .Thus, these conditions require to define a special circle to transform to an airfoil (Pope, 1951).

The flow field around a circular cylinder was elaborated as the first step to define the flow field around the Joukowski airfoil. By presenting conformal mapping and Joukowski transformation, next section will discuss the parameters of the Joukowski transformation.

2.1.2 Joukowski airfoil and its flow field

In this research, a Matlab code was developed to simulate the Joukowski airfoil and its flow field in a two-dimensional plane. To develop this code, the equations and nomenclature of Panton (Panton, 2005) are used. It is tried to use identical nomenclature in the transcript of the Matlab code.

To have a Joukowski airfoil with desired properties regarding its size and lift coefficient the parameters of the original circular cylinder should be defined properly. The main steps to design the Joukowski airfoil and its parameters will be presented in following sections.

2.1.2.1 Parameters to design a Joukowski airfoil

Radius and the center of the circle:

The initial step for Joukowski transformation is defining a cylinder which is going to be transformed to the Joukowski airfoil. The main parameters of the cylinder, which have an important role in the shape of the produced airfoil, are the center of the cylinder and its radius. Other parameters are driven using these variables. Figure 2.1 from previous section will be used to define the parameters.

According to figure 2.1, the center of the cylinder is point $[X, Y]$ in plane ζ. The thickness of the Joukowski airfoil is governed by the value of X (horizontal axis) and the camber of the Joukowski airfoil is controlled by the value of the Y (vertical axis). In our code the center of

the original cylinder is defined as a complex number ζ_0. By entering the values of $[X, Y]$, the center of the circle ζ_0 is defined in the complex plane ζ as following:

$$\zeta_0 = X + iY \tag{2.15}$$

The flow in the plane is from left to right, so the direction of the airfoil should be chosen in a way that corresponds with the flow direction. That is, the leading edge of the airfoil should be on the left side, to let the flow leave the airfoil in the trailing edge on the right side. Also, to have a desired flow field, the camber of the airfoil should be upward in a wing of an aircraft.

The quadrant in which the origin of the cylinder is located should be well adapted to fulfill these conditions. By giving negative or positive values for X and Y the location of the center of the cylinder will change. By using Joukowski transformation, to get desired results, the center of the cylinder should be in the second quadrant of the complex plane ζ . In this case the leading edge of the produced airfoil is on the left and its camber is upward.

Beside the sign of X and Y components of ζ_0, their magnitudes and proportions with the radius of the cylinder are other key points to have a desired airfoil. By increasing the absolute value of the Y , the camber of the airfoil increases and vice versa. This parameter should be proportionally defined to have a smooth flow field in both up and down surfaces of the airfoil.

The horizontal coordinate of the center of the cylinder which is the real part of the complex number ζ_0 , defines the thickness of the airfoil. By increasing the absolute magnitude of the X thicker Joukowski airfoil will be obtained and vice versa. To have a desired airfoil this value should be defined proportionally with the radius of the cylinder.

The magnitude of X and Y should be proportional to the radius of the cylinder. The radius of the cylinder should be selected according to our desired cord length for the Joukowski airfoil.

Kutta condition:

The Kutta condition is exposed to an airfoil to avoid separation of the flow from the surface of the airfoil (Kapania, 2008). To provide such a condition, for the generation of the lift power, two neighbouring particles which separate in the stagnation point of the leading edge should

meet each other in the stagnation point situated in the trailing edge. In general, it means that the fluid flowing over the upper and lower surfaces of the airfoil should meet at the trailing edge of the airfoil (Kapania, 2008). The Kutta condition is achieved because of the friction between the boundary of the airfoil and the fluid (Jahnson, 2013). Due to this fact that, in a reasonable airfoil for a wing the length of the upper surface is longer than the lower surface, to fulfill the Kutta condition, the flow particles in the upper flow have to travel more distance for a limited time, which means increasing the flow velocity. Based on Bernoulli's principle, this increased velocity of the flow will decrease the pressure on the upper surface of the airfoil. Thus, unbalanced pressure in upper and lower surface of the airfoil will generate the lift power (Johnson, 2013). According to Kutta condition, the angle of attack of the airfoil must not exceed a critical angle known as the stall angle. As the angle of attack increases beyond this angle, the flow around the airfoil loses its smooth and continuous trajectory (Kapania, 2008).

Angle of Attack and Lift Power:

Angle α is the angle between the chord of the airfoil and the stream lines of the free stream. This angle is called angle of attack (AOA) of the airfoil. For having ideal flow, Kutta condition is applied and there is circulation directly related to angle β in equation 2.14. According to the Kutta-Joukowski theorem and figure 2.1, the circulation Γ for a circular cylinder with α angle of attack is (Panton, 2005):

$$\Gamma = 4\pi\, UR\, sin(\alpha + \beta) \tag{2.16}$$

The circulation of the cylinder will generate a lift power even with zero angle of attack. By ignoring Kutta condition for the Joukowski airfoil the circulation of the cylinder is computed only with the angle of α and circulation will be:

$$\Gamma = 4\pi\, UR\, sin(\alpha) \tag{2.17}$$

In this equation, angle of β caused by the circulation of the cylinder is not included, and for a zero angle of attack ($\alpha = 0°$) , according to equation 2.8 the cylinder and transformed airfoil will not generate any lift power.

Z and ζ planes:

By choosing complex plane Z for the airfoil as the physical and real plane, mesh grid should be defined in this plane. Complex plane Z is defined as:

$$Z = x + iy \tag{2.18}$$

As shown in Figure 2.1 the airfoil is in the physical complex plane Z and the circle is in complex plane ζ. The Joukowski equation 2.12 , transfers the circle in ζ plane to the Joukowski airfoil in Z plane. The potential flow is defined around the circular cylinder which is in ζ plane. Therefore, to have the ζ plane, inverse Joukowski transformation is used. Following is the equation of the inverse Joukowski transformation (Panton, 2005):

$$\zeta = \frac{1}{2}\, Z \pm \sqrt[2]{\left(\frac{1}{2}\, Z\right)^2 - \lambda^2} = \frac{1}{2}\,(Z \pm \sqrt[2]{Z^2 - 4\lambda^2}) \tag{2.19}$$

Inverse Joukowski transformation transforms the mesh grid in the plane Z plane to a mesh grid in the plane ζ .

Potential Flow function and Velocity function:

The potential flow function around the circular cylinder was presented in previous sections. This function is the product of the superposition of three basic flows around the circle. This flow field is in plane ζ . For a circular cylinder which its center is located on ζ_0, potential flow function is:

$$F_\zeta = U_\infty(\zeta - \zeta_0)e^{-i\alpha} + \frac{U_\infty R^2}{(\zeta - \zeta_0)}\, e^{i\alpha} + ik_{vortex} Ln(\frac{(\zeta - \zeta_0)}{R}) \tag{2.20}$$

In the same manner, the velocity function of the circular cylinder in plane ζ will be:

$$W_\zeta = \frac{dF_\zeta}{d\zeta} \tag{2.21}$$

$$W_\zeta = U_\infty e^{-i\alpha} - \frac{U_\infty R^2}{(\zeta - \zeta_0)^2} e^{i\alpha} + \frac{ik_{vortex}}{(\zeta - \zeta_0)} \quad (2.22)$$

By using these equations and Joukowski transformation, potential flow function and velocity function around the Joukowski airfoil is calculated.

Leading and Trailing Edges:

As indicated in Figure 2.1, leading edge and trailing edge of the airfoil are located on the x axis in plane Z and on ξ axis in plane ζ . For these points, the magnitudes of iy and $i\eta$ (imaginary part of the complex number) are zero but the magnitude of x and ξ (real part of the complex number) remains to be calculated. According to Figure 2.1, trailing and leading edge in the plane ζ for the cylinder are:

$$TE_\zeta = \lambda + 0i \quad (2.23)$$

$$LE_\zeta = -(|X| + R\,cos(\beta)) + 0i \quad (2.24)$$

These leading and trailing edges are in plane ζ , so Joukowski transformation should be used to find these points in the plane Z for the Joukowski airfoil. Trailing edge is always:

$$TE_z = \lambda + \frac{\lambda^2}{\lambda} = 2\lambda \quad (2.25)$$

For the leading edge, the equation is not simple like trailing edge and Joukowski transformation should be used to find this point on the airfoil. Velocity in these two points is calculated to verify the code and as expected, velocity in leading and trailing edge are zero.

Minimum and Maximum Speed:

The two other points which are important to spot on the plane are those that minimum and maximum speed occurs. As expected the maximum speed is on the upper side of the airfoil and near the surface of the airfoil and the minimum speed is located on the stagnation points.

2.2 Two dimensional ice particle trajectory simulation model

The trajectory of the ice piece and its acceleration in the flow field are the results of the aerodynamic and gravitational forces on the ice piece. The aerodynamic forces give the acceleration to the mass of the ice piece (second law of Newton) which make the ice piece move in the plane of the flow field. To determine the force components on the ice piece relative velocity of the ice piece and its angle with the referencing axis should be known. The moment brings about the rotational movement of the ice piece which changes the ice piece's angle of orientation, which is the key parameter to compute lift, drag and moment coefficients. These coefficients are used to compute the aerodynamic force components. The mathematical method to compute all these aerodynamic coefficients, forces and the moment will be presented in this section.

2.2.1 Relative velocity of the ice piece and its orientation

To calculate the relative velocity of the ice piece with referencing the flow field, the velocity is decomposed to its vertical and horizontal components in a 2D flow field plane. Relative velocity components in horizontal and vertical axis are defined as following:

$$u_{relative} = U_{flow} - u_{ice} \tag{2.26}$$

$$w_{relative} = W_{flow} - w_{ice} \tag{2.27}$$

Here, U_{flow} and W_{flow} are the velocity components of the flow stream and $u_{ice}\ and\ w_{ice}$ are the velocity components of the ice piece. As in coordinate system, the positive direction for the horizontal axis is rightward and for vertical axis is upward, the signs of the velocity components will be positive in this direction and vice versa. These relative velocity components are used to compute the angle of the relative velocity, and the absolute value of the relative velocity is used to obtain the aerodynamic forces on the ice piece.

The α angle of the relative velocity is defined as the angle between the relative velocity and horizontal axis and is computed as following:

$$\alpha = Arctan\left(\frac{w_{relative}}{u_{relative}}\right) \tag{2.28}$$

Figure 2.2 (a) shows the coordinate system and also, the relative velocity with two positive components. The angle α has a positive value and is in the first quadrant. In Figure 2.2 (b) relative velocity with a negative angle is illustrated. The horizontal component is still positive but the vertical component is downward and negative. Angle α is in forth quadrant and has a negative value. The sign of the angle α is important to calculate the components of the forces on the ice piece in x and z direction.

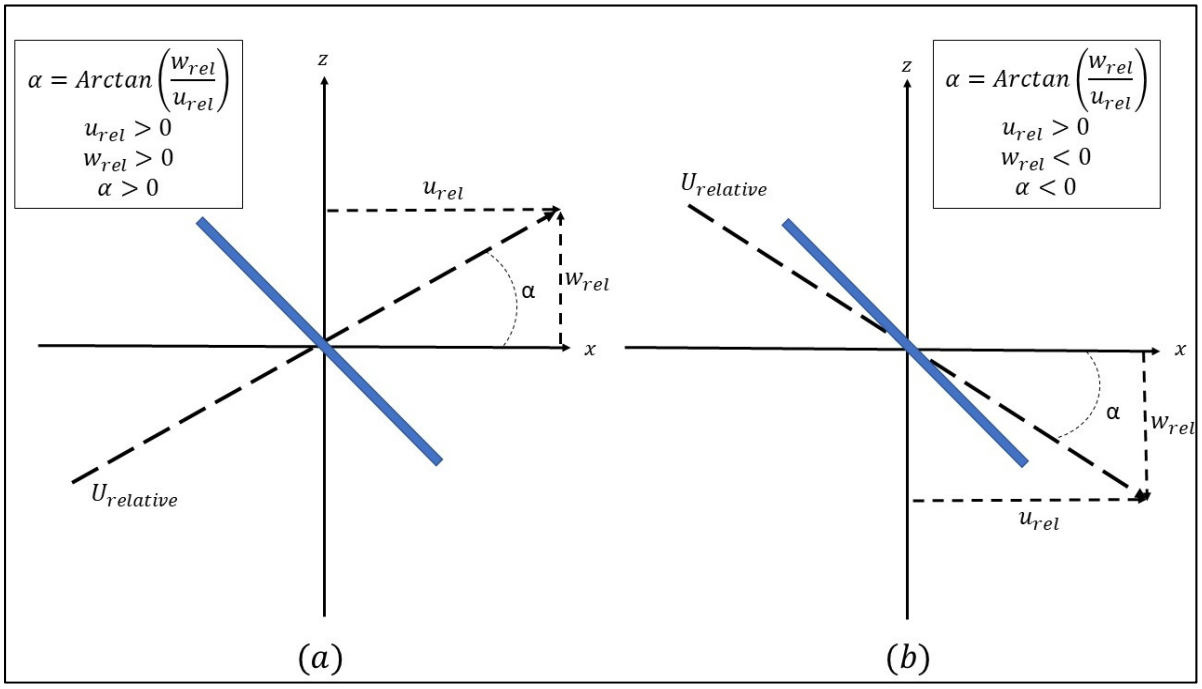

Figure 2.2 Angle of the relative velocity (α)

2.2.2 2D force components on the ice piece

To compute the vertical and horizontal force components on the ice piece, first the lift and drag forces (aerodynamic forces) on the ice piece should be obtained. Drag force is aligned with the relative velocity and the lift force is perpendicular to the drag force. To have the force components in x and z directions, the sine and cosine of the α will be applied to the drag and lift forces. All these force components are presented in Figure 2.3.

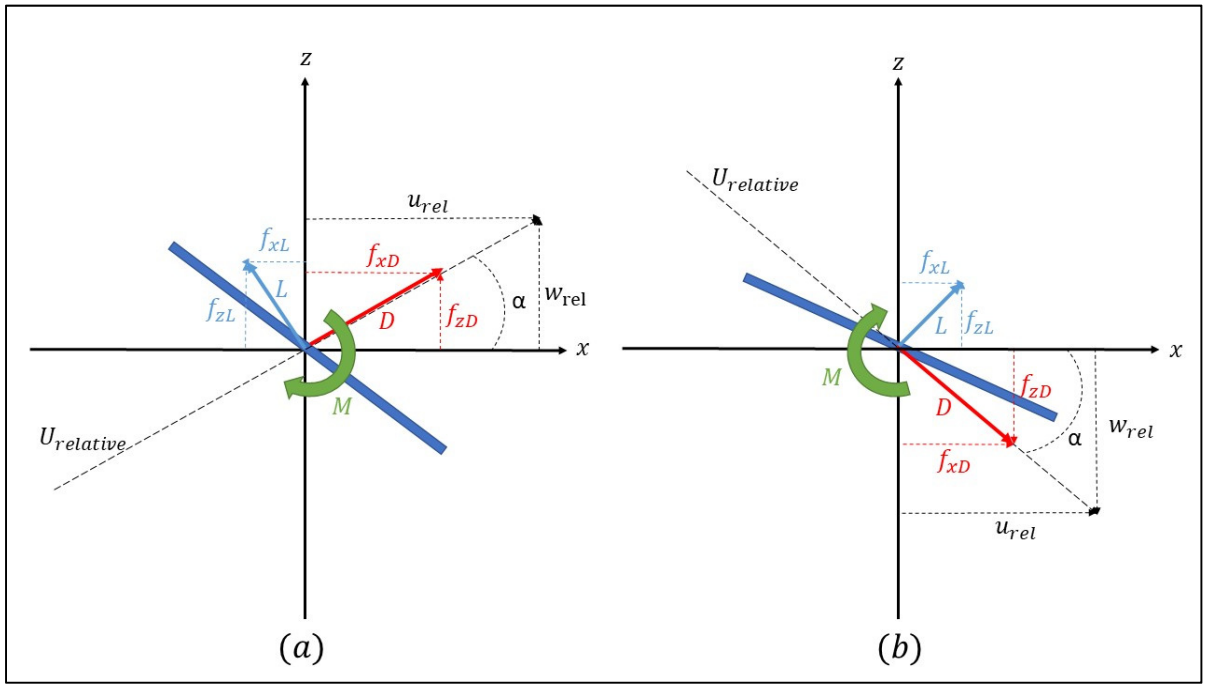

Figure 2.3 Aerodynamic force components on the ice piece

According to figure 2.3 (a), horizontal force (F_x) and vertical force (F_z) on the ice piece can be calculated as following:

$$F_x = f_{xD} - f_{xL} \tag{2.29}$$

$$F_z = f_{zD} + f_{zL} \tag{2.30}$$

In these equations f_{xD} , f_{xL} are the horizontal components of the drag and lift forces and f_{zD}, f_{zL} are the vertical components of the drag and lift forces.

Lift (L) and Drag (D) forces on an ice piece with a reference area of S and the relative velocity of U_{rel} in a flow with a density of ρ are:

$$L = 0.5\rho U_{rel}^2 S C_L \tag{2.31}$$

$$D = 0.5\rho U_{rel}^2 S C_D \tag{2.32}$$

By having the lift and drag forces, their horizontal and vertical components are:

$$f_{xD} = D \times cos\alpha,\ f_{xL} = L \times\ sin\alpha \tag{2.33}$$

$$f_{zD} = D \times sin\alpha,\ f_{zL} = L \times cos\alpha \tag{2.34}$$

Putting together all these equations gives:

$$F_x = Dcos\alpha - Lsin\alpha = 0.5\rho U_{rel}^2 S\ (C_D cos\alpha - C_L sin\alpha) \tag{2.35}$$

$$F_z = Dsin\alpha + Lcos\alpha = 0.5\rho U_{rel}^2 S\ (C_D sin\alpha + C_L cos\alpha) \tag{2.36}$$

These last two equations are used in the Matlab code to compute the force components on the ice piece and the sign and magnitude of the α governs the sign of the vertical and horizontal force components. In Figure 2.3 (b) sine of the α is negative and its cosine is positive so force components are:

$$F_x = f_{xD} + f_{xL} \tag{2.37}$$

$$F_z = -f_{zD} + f_{zL} \tag{2.38}$$

For a square plate ice with a dimension of $l \times l \times e$, the moment force around the y axis is:

$$M = 0.5\rho U_{rel}^2 l^3 C_M \tag{2.39}$$

In these equations, $C_L, C_D \; and \; C_M$ are lift, drag and moment coefficients. By illustrating both two cases for the angle of the relative velocity in figure 2.3, the accuracy of the calculation of the angle of the relative velocity α is verified. This angle is very important to calculate the vertical and horizontal components of drag and lift forces and consequently the horizontal and vertical forces on the ice piece.

The angle of the ice piece with the relative velocity γ (angle of attack) is used to determine lift, drag and moment coefficients. In the next section this angle will be discussed.

2.2.3 Ice piece's angle of attack γ:

Angle γ is the angle between the relative velocity and the ice piece. This angle is called the angle of attack of the ice piece. Figure 2.4 shows this angle in two cases when the angle of the relative velocity is positive and when this angle is negative.

According to Figure 2.4 in both cases γ will be:

$$\gamma = \theta + \alpha \tag{2.40}$$

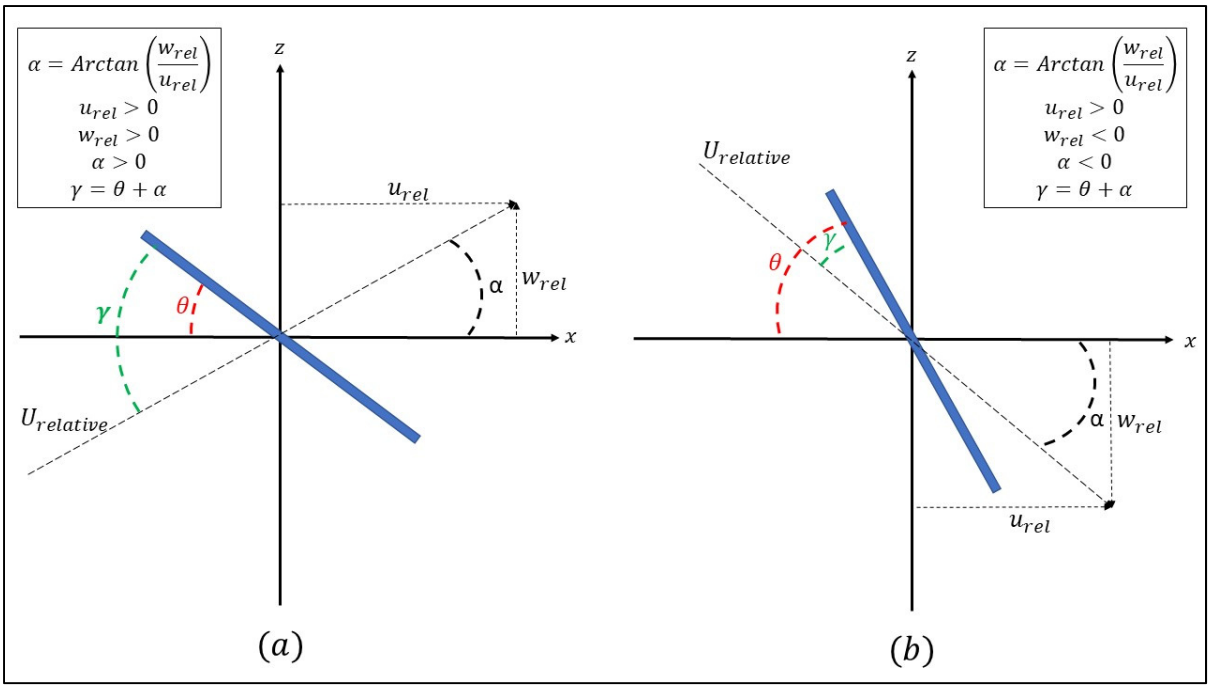

Figure 2.4 The angle between the relative velocity and the ice piece (γ)

Angle θ is the angle between the plate and horizontal axis and angle α is the angle of the relative velocity. Angle γ is a module of 180° and can have values from zero to 180 degrees and is used to calculate the pressure center of the plate ice piece ($\frac{c}{l}$) and normal coefficient C_N (Vedie, 2016). Next section is dedicated to the calculation of these two parameters and aerodynamic coefficients.

2.2.4 Lift, drag and moment coefficients

As discussed in the section 2.2.2 to have the lift, drag and moment forces on the ice piece, aerodynamic coefficients for these three forces are needed. The static lift, drag and moment coefficients using the normal coefficient C_N are as follows (Holmes, 2006):

$$C_{Ds} = 0.1 + C_N \, sin(\gamma) \tag{2.41}$$

$$C_{Ls} = C_N \cos(\gamma) \tag{2.42}$$

$$C_{Ms} = C_N \left(\frac{c}{l}\right) \tag{2.43}$$

The distance between the pressure center location and the center of the plate ice piece is c and C_N is the normal coefficient. The $\left(\frac{c}{l}\right)$ parameter and normal coefficient C_N are defined as a function of the angle of attack(γ):

$$\left(\frac{c}{l}\right) = \begin{cases} 0.3 - 0.22\left(\frac{\gamma}{38}\right) & if \quad 0° \le \gamma \le 38° \\ 0.08\cos\left(2(\gamma - 38°)\right) & if\ 38° \le \gamma \le 82.5° \\ 0 & if\ 82.5° \le \gamma \le 97.5° \\ -0.08\cos\left(2(142° - \gamma)\right) & if\ 97.5° \le \gamma \le 142° \\ -0.3 + 0.22\left(\frac{180° - \gamma}{38}\right) & if\ 142° \le \gamma \le 180° \end{cases} \tag{2.44}$$

$$C_N = \begin{cases} 1.7\left(\frac{\gamma}{40°}\right) & if \quad 0° \le \gamma \le 40° \\ 1.15 & if \quad 40° \le \gamma \le 140° \\ 1.7\left(\frac{180° - \gamma}{40°}\right) & if \quad 140° \le \gamma \le 180° \end{cases} \tag{2.45}$$

Figure 2.5 shows the static coefficients of the lift, drag and moment forces in different angles of attack for the ice piece. These coefficients are used in the equations of the forces and moment. To consider the forces caused by rotation of the ice piece three other coefficients should be added to these static coefficients. Angular velocity of the ice piece is used to determine these coefficients.

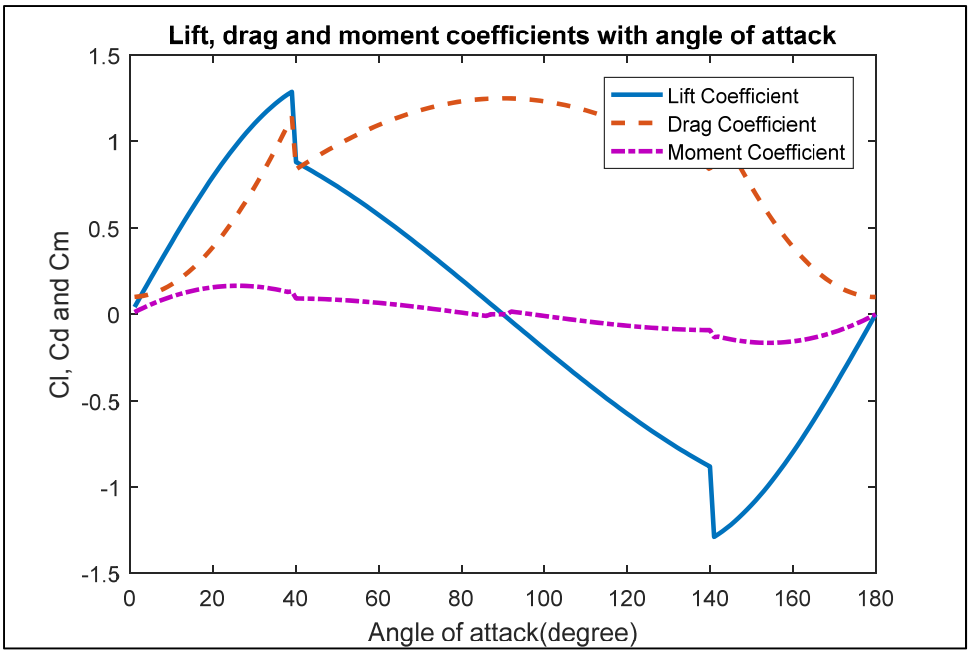

Figure 2.5 Lift, drag and moment coefficients

By adding these coefficients to the static coefficients, Magnus effect is included in the trajectories. The Magnus effect is not considered in all research and there are several methods to calculate this value. In this research, coefficients of the Magnus effect will be added to the static aerodynamic coefficients. Next section is the presentation of the Magnus effect.

2.2.5 Magnus effect

To compute the trajectory of the ice piece, the rotation of the ice piece should be taken into account. The steady coefficients of the aerodynamic forces, treat the ice piece as a steady object in every time-step of the trajectory with different angles of attack, while in fact, the Magnus effect generated by rotational movement of the piece should be considered. To consider the effect of the angular velocity of the ice piece, the coefficient of the aerodynamic forces related to Magnus effect should be added.

Magnus effect is not used in the majority of the research. In some references this effect is completely neglected and in some research Magnus effect is used only for the lift force (Holmes, 2006). The coefficients used in this research for Magnus effect are the same as used

by Kordi (Kordi, 2009). These Coefficients are introduced by Iversen (Iversen, 1979) and uses the ratio of the speed of the tip of the ice piece (S) and the speed of the ice's tip at the stable auto rotational point (S_0) (Vedie, 2016). Based on Iversen, if the plate's non-dimensional moment of inertia is greater than one ($I^* = 32I/\left(\pi\rho_{air}lL\right) > 1$):

$$S_0 = \left(0.329\,ln\left(\frac{l}{e}\right) - 0.0246\,ln\left(\frac{l}{e}\right)^2\right)\left(\left(\frac{AR}{2+(4+(AR)^2)^{0.5}}\right)\left(2-\left(\frac{AR}{AR+0.595}\right)^{0.76}\right)\right)^{2/3} \tag{2.46}$$

Where:

$$AR = \frac{l}{L} \tag{2.47}$$

l and L are the length and width of the ice plate. The speed of the plate's tip can be found as following:

$$S = \frac{\omega l}{2U_{rel}} \tag{2.48}$$

Where ω is the angular velocity of the ice piece and U_{rel} is the relative velocity of the ice piece and is equal to:

$$U_{rel} = \left((U_{flow} - u_{ice})^2 + (W_{flow} - w_{ice})^2\right)^{0.5} \tag{2.49}$$

Using these parameters, aerodynamic coefficients generated by Magnus effect can be obtained. Rotational lift coefficient (C_{LR}), rotational drag coefficient (C_{DR}) and rotational moment coefficients are:

$$C_{DR} = \begin{cases} 0.66\left|\frac{S}{S_0}\right| & if\ \left|\frac{S}{S_0}\right| \leq 0.4 \\ 0.12 + 0.36\left|\frac{S}{S_0}\right| & if\ 0.4 < \left|\frac{S}{S_0}\right| \leq 1.0 \\ 0.48 & if\ \left|\frac{S}{S_0}\right| > 1.0 \end{cases} \quad (2.50)$$

$$C_{LR} = \begin{cases} -1.575 + 0.2625\frac{S}{S_0} & if\ \frac{S}{S_0} \leq -0.2 \\ 1.05\frac{S}{S_0} & if\ -0.2 < \frac{S}{S_0} \leq 0.2 \\ 1.575 + 0.2625\frac{S}{S_0} & if\ \frac{S}{S_0} > 0.2 \end{cases} \quad (2.51)$$

$$C_{MR} = \begin{cases} -0.12\left(1 + \frac{S}{S_0}\right) & if\ \frac{S}{S_0} < -1.0 \\ -0.12\left(1 - \left|\frac{S}{S_0}\right|\right)\frac{S}{S_0} & if\ -1.0 \leq \frac{S}{S_0} \leq 1.0 \\ 0.12\left(1 - \frac{S}{S_0}\right) & if\ \frac{S}{S_0} > 1.0 \end{cases} \quad (2.52)$$

These coefficients will be added to the static coefficients of the aerodynamic forces and moments in the trajectories which Magnus effect is included.

2.2.6 2D lift, drag and moment coefficients

In this research the trajectory of the square plate ice with a finite dimension of $l \times l \times e$ in a two-dimension flow field is studied. It is assumed that the movement of the ice piece as a three-dimensional particle will be on a plane and the degree of freedom (DOF) for the movement of the ice particle is three. The ice piece can have two linear movements in two directions of x and z axes and an angular movement around the y axis. Also the movement of the ice piece is

confined to the movements in a plane but the ice piece is considered as a 3D object. It means that 3D lift, drag and moment coefficients are used to compute the forces on the ice particle.

The aerodynamic coefficients for a two-dimensional ice particle are different than those for 3D aerodynamic coefficients. A 2D dimensional ice piece has an infinite width, parallel to the y axis. By considering such an ice piece, 2D lift, drag and moment coefficients should be used to compute the forces and moments on the rectangular ice piece. Figure 2.6 shows the graphs of the 2D and 3D aerodynamic coefficients.

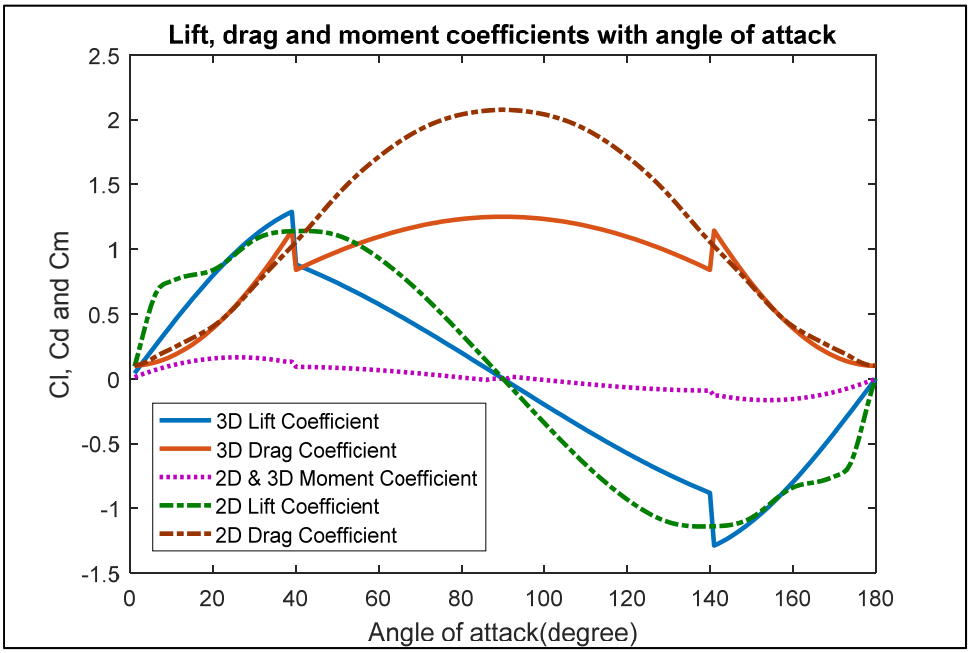

Figure 2.6 2D & 3D lift, drag and moment coefficients

The relation between the static aerodynamic coefficients and normal coefficient for 2D plate is the same as for 3D coefficients and equations 2.41, 2.42 and 2.43 are used to obtain these values. The normal coefficients (C_N) for 2D plate is introduced by Hoerner (Hoerner, 1965). Figure 2.7 shows the values of the normal coefficient for 2D plate in the function of the angle of attack of the plate.

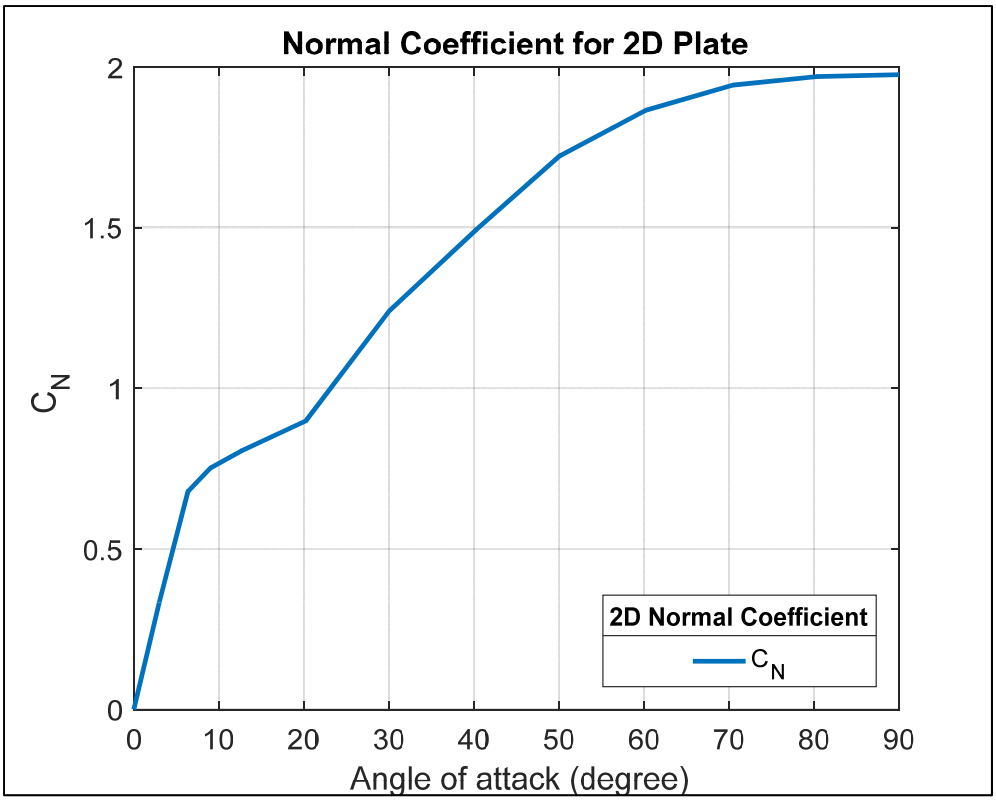

Figure 2.7 Normal coefficient for 2D rectangular plate ice piece

The Magnus effect for 2D plate is calculated as following (Hargreaves, 2014):

$$C_{LR} = \begin{cases} C_{LR0}\left(\left(\frac{S}{S_0}+1\right)\right)-1 & if\ \frac{S}{S_0} \le -0.6 \\ C_{LR0}\left(0.5\left(\frac{S}{S_0}+0.6\right)-0.6\right) & if\ -0.6 < \frac{S}{S_0} \le -0.1 \\ 3.5C_{LR0}\left(\frac{S}{S_0}\right) & if\ -0.1 < \frac{S}{S_0} \le -0.1 \\ C_{LR0}\left(0.5\left(\frac{S}{S_0}-1\right)+1\right) & if\ -0.1 < \frac{S}{S_0} \le 0.6 \\ C_{LR0}\left(\left(\frac{S}{S_0}-0.6\right)+0.6\right) & if\ \frac{S}{S_0} \ge 0.6 \end{cases} \quad (2.53)$$

$$C_{DR} = \begin{cases} C_{DR0}\left|\frac{S}{S_0}\right| + 0.6 & if\ \left|\frac{S}{S_0}\right| \leq 0.35 \\ 0.0769\, C_{DR0}\left(\left|\frac{S}{S_0}\right| - 0.35\right) + 0.95 & if\ 0.35 < \left|\frac{S}{S_0}\right| < 1.0 \\ C_{DR0} & if\ \left|\frac{S}{S_0}\right| \geq 1.0 \end{cases} \quad (2.54)$$

$$C_{MR} = \begin{cases} sign(S)0.3\left|\frac{S}{S_0}\right| - 0.04 & if\ \left|\frac{S}{S_0}\right| \leq 0.40 \\ sign(S)0.08 & if\ 0.40 < \left|\frac{S}{S_0}\right| \leq 0.70 \\ sign(S)\left(-0.2667\left(\left|\frac{S}{S_0}\right| - 0.7\right) + 0.08\right) & if\ \left|\frac{S}{S_0}\right| > 0.70 \end{cases} \quad (2.55)$$

C_{DR0} and C_{LR0} are the steady-state drag and lift coefficients and are equal to 1.28 and 0.76 respectively.

2.2.7 Coefficients for Sphere ice piece

In order to investigate the influence of the ice shape on the trajectory of the ice piece, simulations for a sphere ice piece with the same mass as the square plate ice are conducted. Lift, drag and moment coefficients for a sphere ice piece used in the calculations are borrowed from Grace and Weber (Grace & Weber, 1978) and are as following:

$$C_L = 0 \quad (2.56)$$

$$C_M = 0 \quad (2.57)$$

$$C_D = \begin{cases} \frac{3}{16} + \frac{24}{Re + 1e - 12} & if\ Re < 0.01 \\ \frac{24}{Re(1 + 0.1315Re^{(0.82 - 0.05\log_{10} Re)})} & if\ Re \leq 20 \\ \frac{24}{Re(1 + 0.1935Re^{0.6305})} & if\ Re \leq 260 \\ 10^{(1.6435 - 1.1242\log_{10} Re + 0.1558(\log_{10} Re)^2)} & if\ Re \leq 1500 \\ 10^{(-2.4571 + 2.5558\log_{10} Re - 0.9295(\log_{10} Re)^2 + 0.1049(\log_{10} Re)^3)} & if Re \leq 1.2e4 \\ 10^{(-1.9181 + 0.6370\log_{10} Re - 0.0636(\log_{10} Re)^2)} & if\ Re \leq 4.4e4 \\ 10^{(-4.3390 + 1.5809\log_{10} Re - 0.1546(\log_{10} Re)^2} & if\ Re \leq 3.38e5 \\ 29.78 + 5.3\log_{10} Re & if\ Re \leq 4e5 \\ 0.1\log_{10} Re - 0.49 & if\ Re \leq 1e6 \\ 0.19 - \frac{8e4}{Re} & if\ Re > 1e6 \end{cases} \quad (2.58)$$

Re is the Reynolds number being equal to:

$$Re = \frac{\rho_{air} D U_{rel}}{\mu_{air}} \quad (2.59)$$

Where μ_{air} is the air dynamic viscosity and D is the diameter of the sphere ice particle. To calculate the force components on the sphere ice particle, equations 2.35 and 2.36 will be used. Reference area for the sphere in these equations is:

$$S = \frac{\pi D^2}{4} \quad (2.60)$$

In the next section differential equations of the movement will be presented.

2.2.8 2D differential equations of motion

The ice trajectory is computed by integrating the differential movement equations. The aerodynamic forces of the flow accelerate the ice piece. The integration of the linear (translational) acceleration of the ice piece, computes the linear velocity of the ice piece and

the integration of the velocity of the ice piece computes the translational movement of the ice piece. On the other hand, the integration of the angular acceleration yields the angular velocity and consequently angular movement of the ice piece. 2D differential equations of the movement are as following (Holmes, 2006):

$$\frac{dx}{dt} = u_{ice} \tag{2.61}$$

$$\frac{du_{ice}}{dt} = \frac{F_x}{m_{ice}} \tag{2.62}$$

$$\frac{dz}{dt} = w_{ice} \tag{2.63}$$

$$\frac{dw_{ice}}{dt} = \frac{F_z}{m_{ice}} - g \tag{2.64}$$

$$\frac{d\theta}{dt} = \omega \tag{2.65}$$

$$\frac{d\omega}{dt} = \frac{M}{I_{yy}} \tag{2.66}$$

For a square plate ice with a dimension of $l \times l \times e$ moment of inertia is:

$$I_{yy} = m_{ice}\left(\frac{l^2}{12} + \frac{e^2}{12}\right) \tag{2.67}$$

These equations are used to compute the acceleration, velocity and the movement of the ice piece in every time-step of the trajectory.

2.2.9 Ice piece samples and their properties

In this research, the plate samples are similar to those found in the literature. The trajectories have been validated with the trajectories of Holmes (Holmes, 2006), Kordi (Kordi, 2009), Suares (Suares, 2005) and Shimoi (Shimoi, 2010), therefore the properties of their square plate pieces are used in the simulations of this research. The dimension and the density of the plates are needed to compute the forces and the moment on the plate. In the literature the dimension of the plate samples is clearly mentioned but in some cases the density of the ice pieces is not directly stated and their density will be extracted by using their other parameters.

The dimension of the ice piece is defined by l, l and e which represent the length, width and thickness of the plate respectively. Figure 2.8 is an illustration of these values on the plate sample.

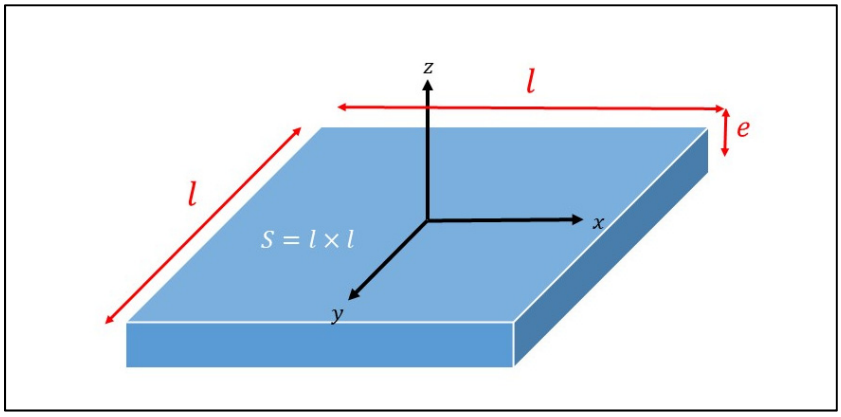

Figure 2.8 Dimensions of square plate ice piece

In some references the ice piece has been introduced by its Tachikava number (Tachikava, 1983). Using the Tachikava number (K) and having the other known values, the density of the ice piece can be found by following equation:

$$K = \frac{\rho_{air} U^2 l^2}{2mg} = \frac{\rho_{air} U^2}{2\rho_m hg} \tag{2.68}$$

Table 2.1 has categorized the plate samples used in simulations. The dimensions are in millimeters and the unit of mass density is kilograms per cubic meter. This table introduces the general properties of the plate samples and more detailed properties of the trajectories will be mentioned in each simulation.

Table 2.1 Properties of the square plate ice pieces used in the simulations

Ice shape	**Reference**	**Material**	**Density** (kg/m^3)	**Dimension**(mm)
Square flat plate	Holmes	Plastic	1163	$40 \times 40 \times 2$
		Basswood	570	$75 \times 75 \times 9$
		Plywood	847	$75 \times 75 \times 3$
Square flat plate	Kordi	Plastic	1120	$40 \times 40 \times 2$
Square flat plate	Suares	-	917	$130 \times 130 \times 36$
Square flat plate	Shimoi	Polyethylene	941	$152 \times 152 \times 10$

In the section of Monte-Carlo study, the impact of the ice shape on the trajectories and its pass possibility through defined areas is investigated. A sphere ice particle and a rectangular plate with following properties are used to compare with square plate ice particles. All three samples have the same mass but their dimension differs.

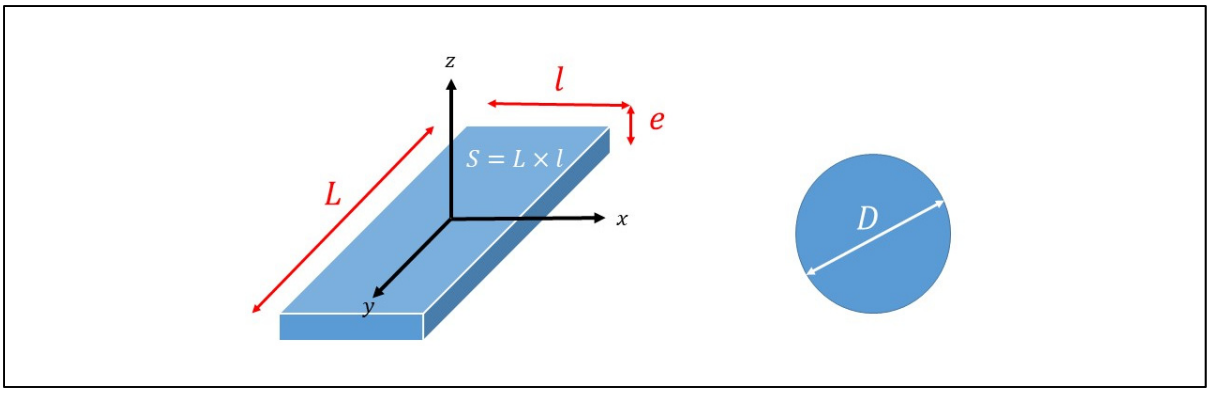

Figure 2.9 Dimensions of the sphere and rectangular ice particles

Table 2.2 Contains the properties of the plate samples used in our Monte-Carlo simulations.

Table 2.2 Properties of the ice particles used in Monte-Carlo simulations

Ice shape	**Reference**	**Density (kg/m^3)**	**Dimension (mm)**
Square flat plate	Suares	917	$130 \times 130 \times 36$
Rectangular flat plate	-	458.5	$130 \times 260 \times 36$
Sphere	-	917	106

2.3 Monte-Carlo statistical study

Simulation of the ice piece trajectory starts with defining the initial conditions of the ice piece to the ice trajectory code. Ice piece shedding can happen with many different initial conditions which bring about different trajectories for each set of initial conditions. Monte-Carlo method is widely used in the domain of ice trajectory simulations to consider the uncertainties of the initial condition of the shedding (Suares, 2005), (Shimoi, 2010).

The set of the initial condition for ice shedding can be the combination of several conditions. These variable parameters can be the size and the shape of the ice piece, the initial linear and

angular velocity of the ice piece, the location of the ice piece on the wing or in the flow field and the orientation of the ice piece with respect to the axis of the plane. In this research a code has been developed to run the ice trajectory simulation for a large number (60,000) of initial condition sets by using a random number generator.

The variable parameters that are included in the research are the location of the ice piece, the initial linear and angular velocity and the orientation of the ice piece with respect to the horizontal axis. To generate this initial conditions for the velocity and the orientation of the ice piece, following equation is used (Shimoi, 2010):

$$P = P_{min} + \left|P_{range}\right| \times rand \tag{2.69}$$

In this equation P_{min} is the minimum value of the parameter, P_{range} is the range of variation of the parameter and $rand$ is a uniform random number between zero and one. For the initial linear velocity of the ice piece, it is assumed that the ice piece can have three percent of the flow velocity either in the direction of the flow or opposite to its direction. Velocity components of the ice piece will be:

$$u_{ice_0} = -0.03 \times U_\infty + |2 \times 0.03 \times U_\infty| \times rand \tag{2.70}$$

$$w_{ice_0} = -0.03 \times U_\infty + |2 \times 0.03 \times U_\infty| \times rand \tag{2.71}$$

For the angular velocity a variation of $0.5\, rad/s$ either clockwise or counter clockwise is considered. According to equation 2.69 the random angular velocity for the initial condition of the trajectory can be achieved as following:

$$\omega_0 = -0.5 + |2 \times 0.5| \times rand \tag{2.72}$$

The orientation of the ice piece can change from $-180°$ to $+180°$, therefore the random value for this parameter can be calculated as following:

$$\theta_0 = -180 + |2 \times 180| \times rand \tag{2.73}$$

The combination of these parameters creates the initial condition set for each run of the ice trajectory simulation. Table 2.3 shows these variable parameters briefly.

Table 2.3 Variation of initial parameters for square plate ice piece trajectories around the Joukowski airfoil

Parameters	**Limits of variation**
Ice piece linear velocity	± 0.03 U_∞
Ice piece angular velocity	± 0.5 rad/s
Ice piece orientation angle with horizon	± 180°
Location of ice piece	40 locations on the upper side of the leading edge
	40 locations on the down side of the leading edge

The location of the ice piece in a uniform flow does not have influence on the ice trajectory because the velocity vector is equal in all points of the plane. The flow field around an airfoil is not a uniform flow field and the velocity vector is different in each point of the plane, so the location of the ice piece at the moment of the shedding is considered as a variable for initial conditions of the trajectories.

In the Monte-Carlo methodology, the uncertainty of the location of the ice piece is not considered as a random point on the plane and instead, the locations of the ice particle are defined on the airfoil's geometry in which the ice shedding can occur. The number and the locations of the ice pieces are defined before running the Monte-Carlo simulation. As ice accretion is mostly built on the leading edge of the airfoil, this research has studied the trajectories initiated from this area on the airfoil. These locations are limited to 10% of the cord's length of the airfoil starting from the stagnation point on the leading edge. The total number of random initial condition sets are divided between these locations of the ice pieces on the airfoil

As mentioned in table 2.3, Monte-Carlo simulations for Joukowski airfoil simulate ice shedding from 40 locations on the upside and 40 locations on the downside surface of the leading edge. To find these 40 locations following approach is used:

$$\theta_{stagnation} = \pi + \beta \tag{2.56}$$

$$\theta_n = \theta_{stagnation} \pm (n-1) \tag{2.75}$$

Here. $\theta_{stagnation}$ is the angle of the stagnation point on the original cylinder of the Joukowski airfoil and θ_n is the angle of other shedding locations on the cylinder which differ by one degree from each other (n is the number of the shedding location which is from one to 40). In equation 2.75, plus sign is used for upper side of the stagnation point and minus sign is used for downside of the stagnation point. By using Joukowski transformation the locations of ice shedding can be found on the Joukowski airfoil.

To compare the results of Monte-Carlo simulations, the mean trajectory $\tilde{g}$ is calculated using the following equation (Vedie, 2016):

$$\tilde{g} = \frac{1}{N}\sum_{i=1}^{N} g(x_i, t) \tag{2.57}$$

Principally, in this research, uniform random numbers are used to generate initial conditions for ice trajectories in Monte-Carlo simulations. In addition, normal random number distribution as another method to generate random numbers will be used to compare the results of these two different methods and their influences on the ice trajectories.

To generate normal random numbers, the mean, standard deviation and variation for each parameter are defined. Following is the general equation of the normal random numbers used in the Monte-Carlo simulation:

$$P_n = \mu + \sqrt{\sigma^2} \times randn \tag{2.77}$$

In this equation P_n is a normal random parameter of the initial condition. μ is the mean value of the parameter and σ^2 is the variation of the parameter and σ is the standard deviation of the parameter. Using this equation, initial normal values for the angle of the ice piece and its velocities are:

$$u_{ice_0} = 0 + \sqrt{0.03 \times U_\infty} \times randn \tag{2.78}$$

$$w_{ice_0} = 0 + \sqrt{0.03 \times U_\infty} \times randn \tag{2.79}$$

$$\omega_0 = 0 + \sqrt{0.5} \times randn \tag{2.80}$$

$$\theta_0 = 0 + \sqrt{180} \times randn \tag{2.81}$$

The mean values for the initial angle and velocities of the ice piece are zero and the variations are as the same as uniform distribution.

Figure 2.10 is an illustration of the general functions of the Matlab code for Monte-Carlo simulations. Since for some set of the initial conditions, the ice piece hits the airfoil itself, a function is developed to separate these trajectories from the matrix of the trajectories. Another function is developed for pass probability estimation of the objects downstream or around the airfoil and computes the pass probability of the ice piece around the airfoil and the results are plotted as a footprint map around the airfoil.

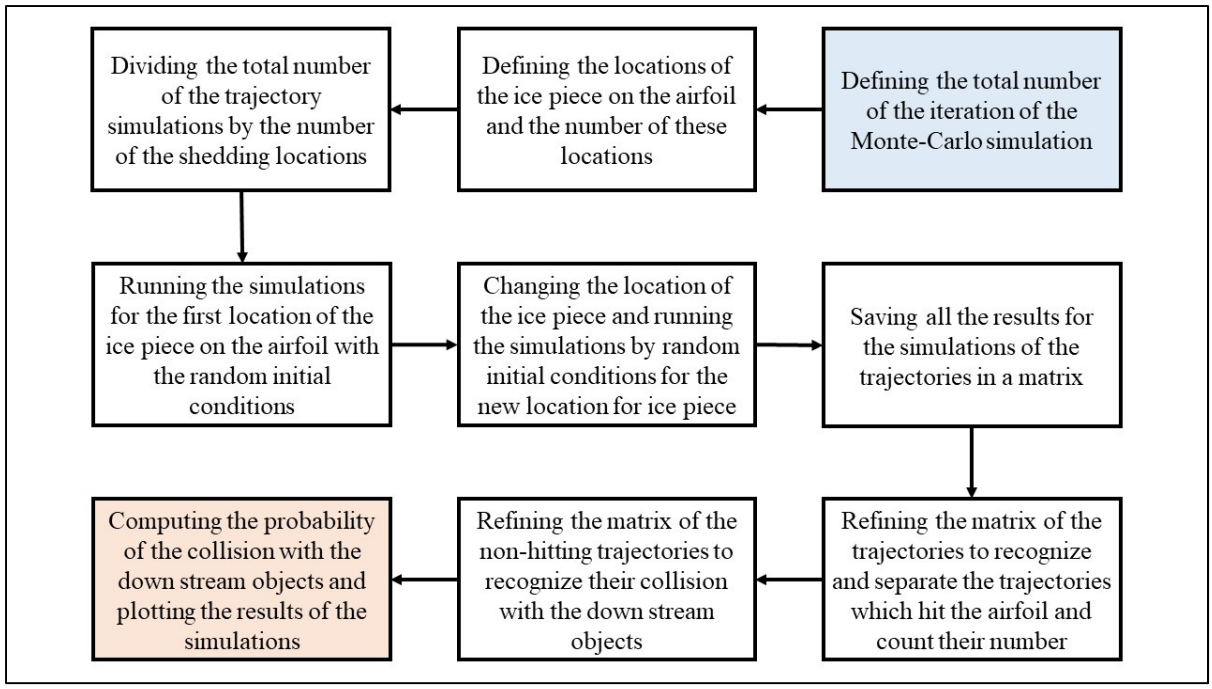

Figure 2.10 Diagram of the Matlab code for Monte-Carlo simulations

Next chapter will discuss the results of the research for Joukowski airfoil, single trajectories and Monte-Carlo simulations.

CHAPTER 3

RESULTS AND DISCUSSION

By implementing the methodology of the research in the simulation codes, the results of the research project are obtained. In this chapter these results will be verified, validated and discussed in different sections for Joukowski airfoil, ice trajectory in horizontal uniform flow, ice trajectory in non-horizontal uniform flow, ice trajectory in the flow field of Joukowski airfoil and Monte-Carlo statistical study of the trajectories.

3.1 Joukowski airfoil

Following are the results for the Joukowski airfoil simulation code. The resulted figures will show how different parameters of the cylinder influence the shape of the Joukowski airfoil and its generated lift force. Also the results will compare the lift generation capability of the Joukowski airfoil with different angles of attack.

3.1.1 Graphical result of the Joukowski code

The code designed for the simulation of the Joukowski airfoil and its peripheral flow field generates four figures. Two of the figures plot the stream lines and velocity field around the circular cylinder and two other plot the stream lines and the velocity field around the Joukowski airfoil. Figure 3.1 shows these four figures for a sample cylinder and Joukowski airfoil generated by Joukowski code. These shapes are for a cylinder with a radius of $1\ m$ which its center is located at $\zeta_0 = [-0.1, 0.04]$.

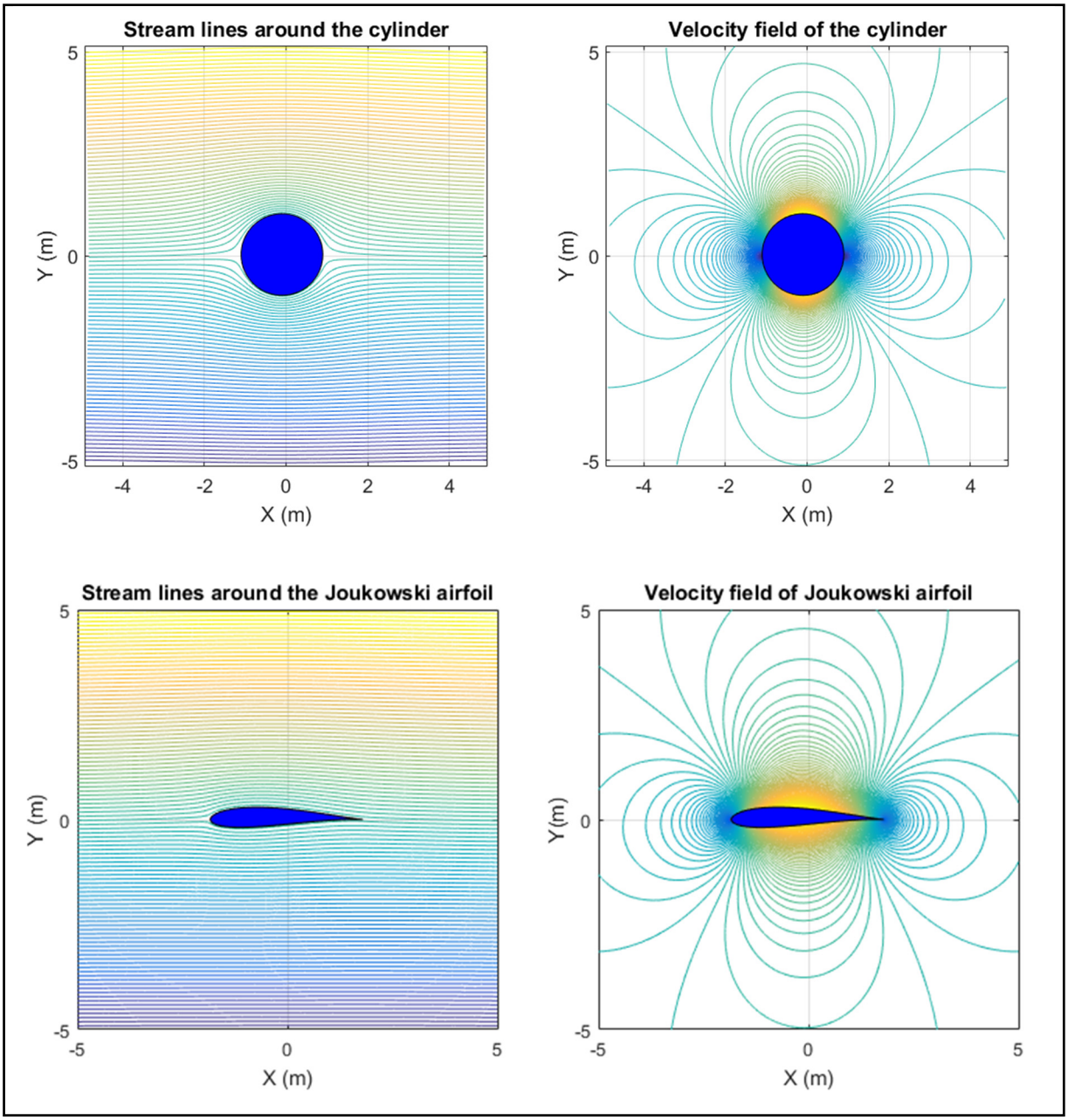

Figure 3.1 Graphical results of the Joukowski airfoil Matlab code

In the following subsections the results of the Joukowski code will be verified based on the mathematical equations of the Joukowski transformation to see if the code yields the expected results of the mathematical equations of the transformation.

3.1.2 Center of the circle in different quadrants

As mentioned before in the section (2.1.2), the center of the cylinder plays a key rule to determine the shape of the transformed Joukowski airfoil. According to the sign of the real and imaginary part of this point, center of the cylinder is located in different quadrant of the plane ζ. Figure 3.2 illustrates the resulted airfoils in different quadrants.

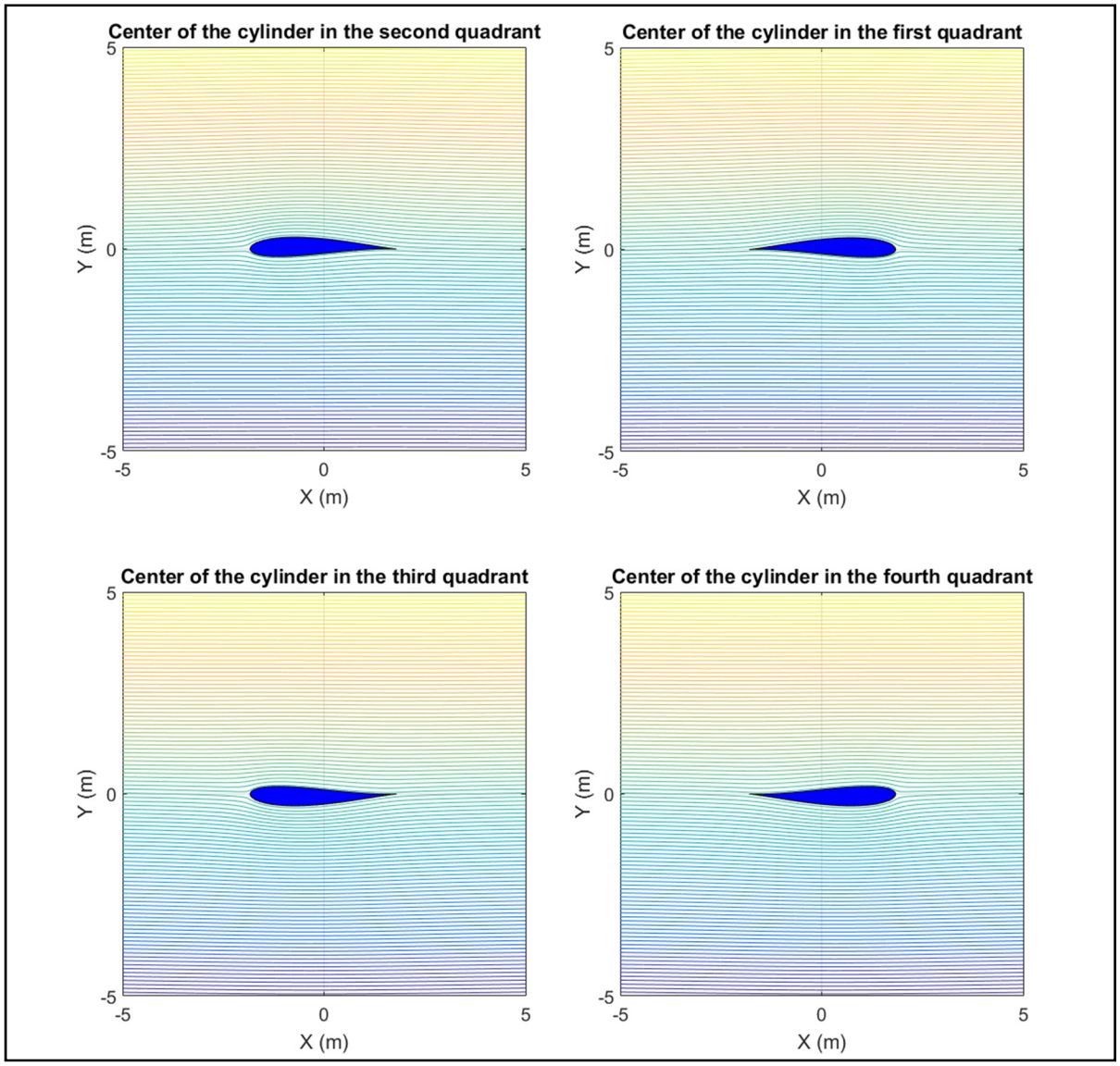

Figure 3.2 Joukowski airfoil with center of the cylinder in different quadrants of plane ζ

As the flow is from left to right (as the coordinate system is from left to right) and the lift force should be upward for a wing, the center of the cylinder (ζ_0) is defined in the second quadrant of the plane ζ. In this case the leading edge of the airfoil is in front of the flow stream and its camber is upward.

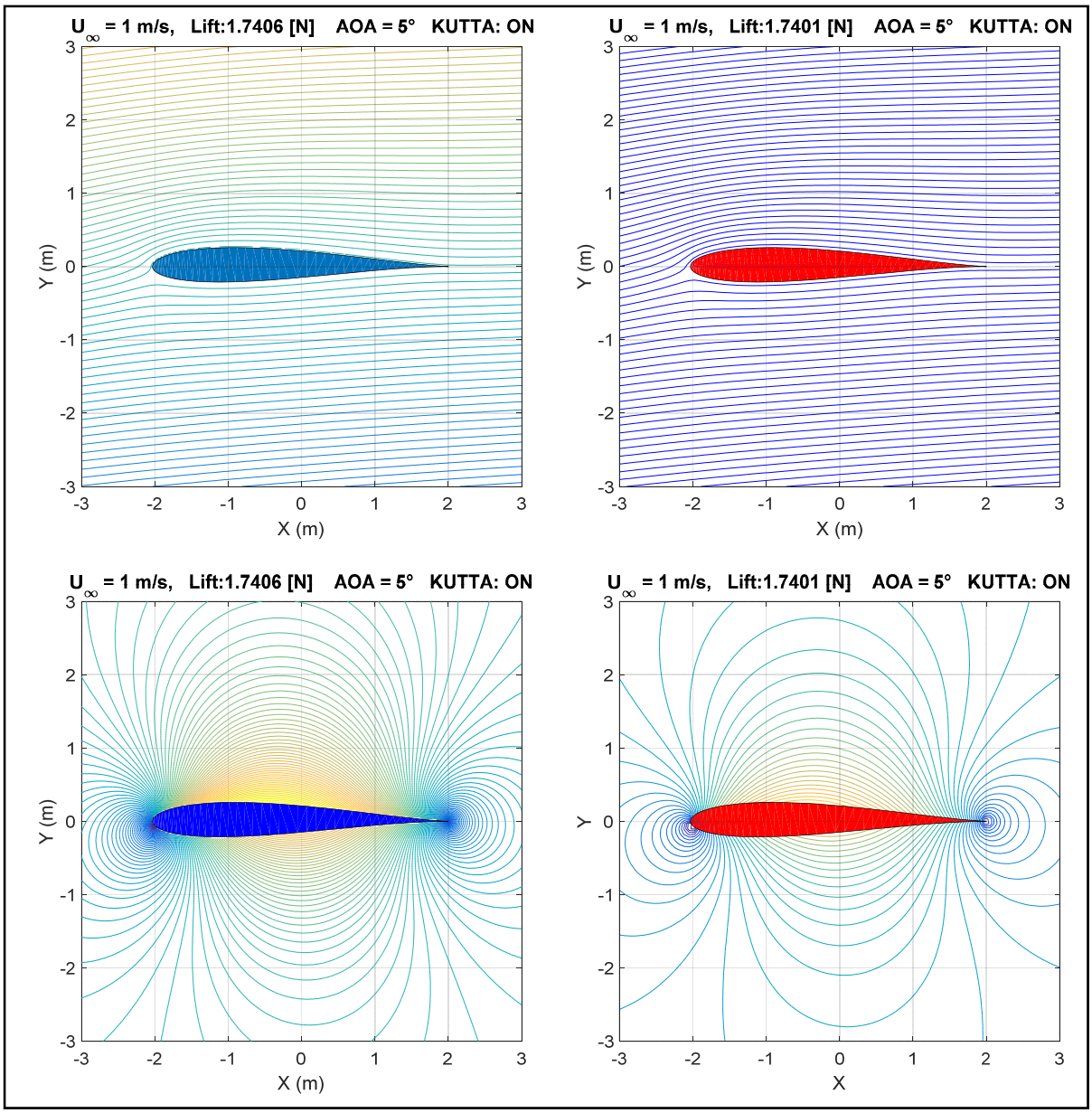

Figure 3.3 Comparison between the results of the Matlab code (left) and the results of Newman (right), up: Joukowski airfoil and stream lines, down: velocity field

To validate the code for Joukowski airfoil, graphical results are compared with those found in the literature. Figure 3.3 compares the obtained results with the result of Newman (Newman, 2011). The results are identical by using the same parameters for the flow field and original cylinder (radius and center of the cylinder).

3.1.3 Thickness of the airfoil and lift force

One of the characteristics of the airfoil is its thickness. The thickness of the Joukowski airfoil is a function of the real part (X) of the center of the cylinder (ζ_0). By increasing the absolute magnitude of this parameter thicker airfoil are generated and vice versa. In figure 3.4 the lift forces of two Joukowski airfoils with different thicknesses are compared. Both the airfoils are moving with a velocity of 70 m/s in the air and their angle of attack is 0°.

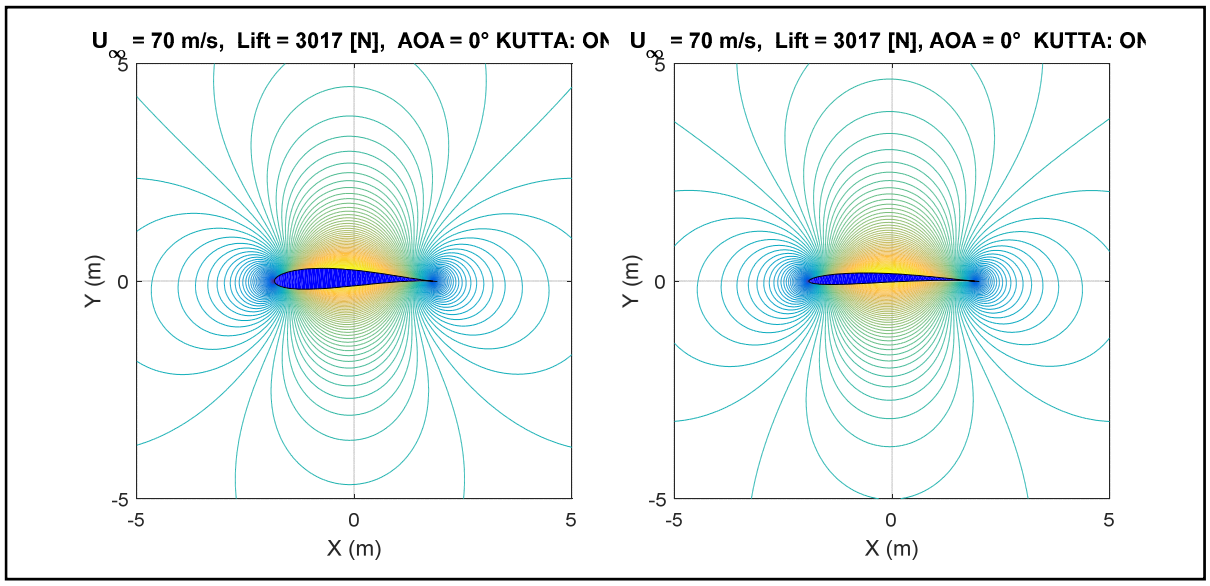

Figure 3.4 Two Joukowski airfoils with different thicknesses: left: $\zeta_0 = -0.1 + 0.04i$, right: $\zeta_0 = -0.05 + 0.04i$, the radius of the circle for both airfoils is $R = 1\ m$.

According to figure 3.4, the lift forces for both of the airfoils are equal. According to Kutta-Joukowski theorem, the lift force is related to the circulation of the flow field around the airfoil.

As Kutta condition is exposed on the airfoils, the circulation around the airfoil is obtained using equation 2.16.

The flow velocity, cylinder radius and angle of attack α is the same for both the airfoils, so remains to investigate the influence of the angle β on the circulation around the airfoil. According to equation 2.14 angle β is a function of the imaginary part of the ζ_0 and the radius of the circle. As these two values for both these airfoils are equal, the circulation around them and their lift force will be of the same magnitude.

Although based on the Kutta –Joukowski theorem, the thickness of the Joukowski airfoil does not have any influence on the lift force of the Joukowski airfoil, a proportional value for the real part of the ζ_0 should be used. The ratio of the airfoil's thickness influence the drag coefficient of the airfoil, therefore the thickness of the airfoil is important in the design of the airfoil. In the next section the influence of the Joukowski airfoil's camber on the lift force will be discussed.

3.1.4 Camber of the airfoil and lift force

Camber of the Joukowski airfoil is a function of the imaginary part (Y) of the center of the cylinder ζ_0 . Increasing the value of the Y will increase the camber of the airfoil and decreasing these value results in more symmetric Joukowski airfoil. By presenting four Joukowski airfoils with different values for Y, the impact of the camber on the lift force of the airfoil is shown in figure 3.5. The velocity of the airfoils is 70 m/s and their cords are parallel to the airstream.

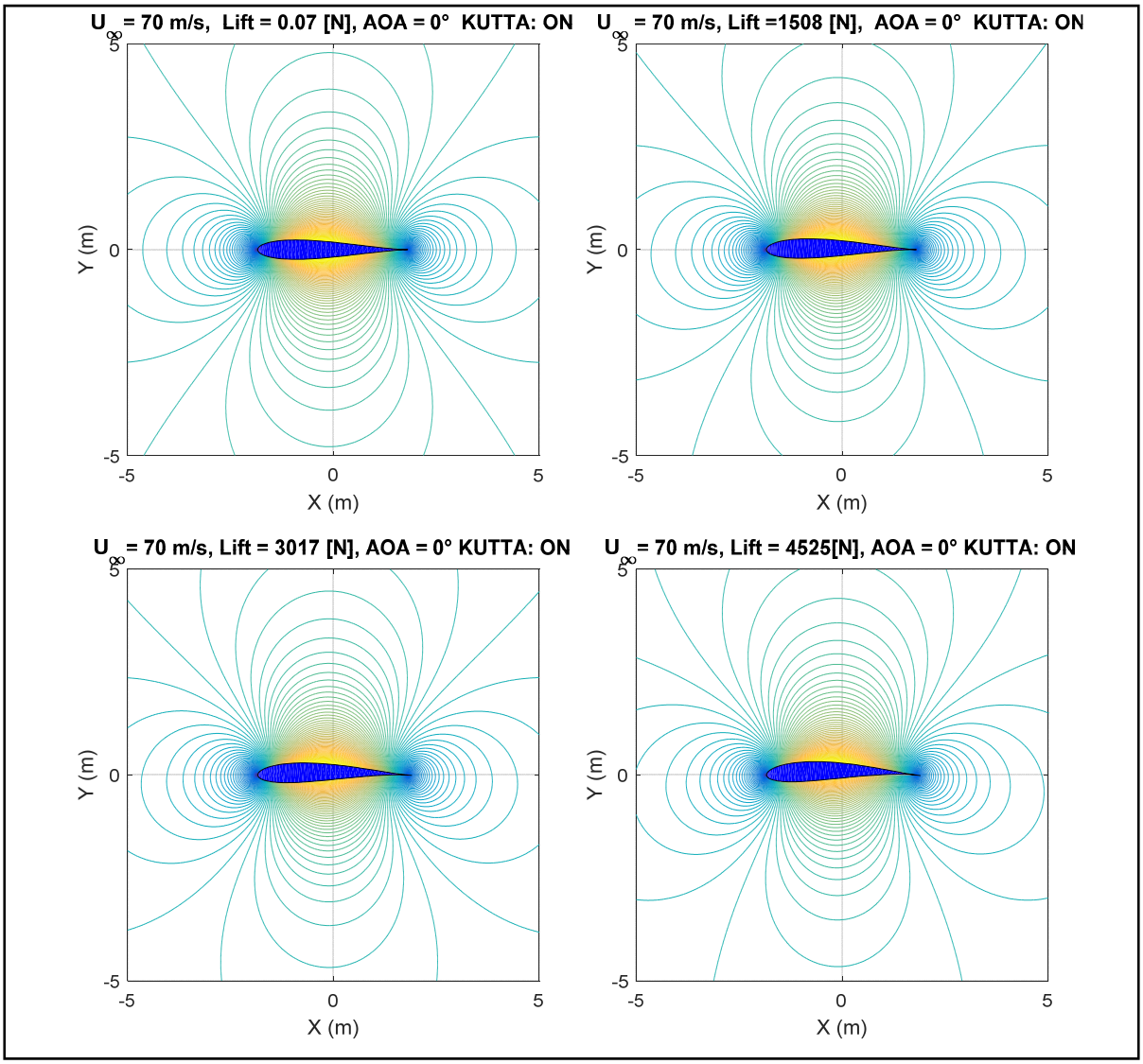

Figure 3.5 Four Joukowski airfoils with different cambers, up-left: $\zeta_0 = -0.1 + 0.000001i$, up-right: $\zeta_0 = -0.1 + 0.02i$, down-left: $\zeta_0 = -0.1 + 0.04i$, down-right: $\zeta_0 = -0.1 + 0.06i$, radius of the circles is $R = 1\ m$.

Unlike the thickness of the Joukowski airfoil, its camber has a direct influence on generated lift force. The magnitude of the Y (imagenary part of the ζ_0) alters the angle β which influences the circulation Γ. A symmetric Joukowski airfoil when its angle of attack is zero does not generate any lift force. To have a smooth flow field around the airfoil, without seperation of the fluid and with an acceptable drag to lift ratio, a proportional value for the vertical position

of the center of the cylinder should be selected. In the next section, lift force generation of the Joukowski airfoil with different angles of attacks will be elaborated.

3.1.5 Airfoil's angel of attack and lift force

The lift force of an airfoil is directly a function of its angle of attack. An aircraft gains more upward lift force with increasing its angle of attack. In figure 2.1 this angle is indicated by α. According to equation 2.16 , circulation around the airfoil is related to its angle of attack. By increasing the magnitude of the circulation, the airfoil will generate more lift force. Figure 3.5 is the comparison of four Joukowski airfoils with different angles of attack. All these airfoils experience a flight with 70 m/s velocity and the air has a density of 1.225 kg/m^3.

The lift force is mentioned in each plot of the figure 3.6. It is observed that the lift force generation has direct relation with the angle of attack and lift force increases as the angle of attack increases. In the figures it can be seen that in an elevated angle of attack the velocity field around the airfoil is more unsymmetric and there is a velocity difference between the upside and downside of the airfoil. According to Bernoulli equation when the airfoil has positive angle of attack, there is less pressure on the upper side of the airfoil. The pressure difference between the two sides of the airfoil generates an upward force on the airfoil. when the angle of attack is negative, the velocity of the downside surface of the airfoil is greater, so force will be downward.

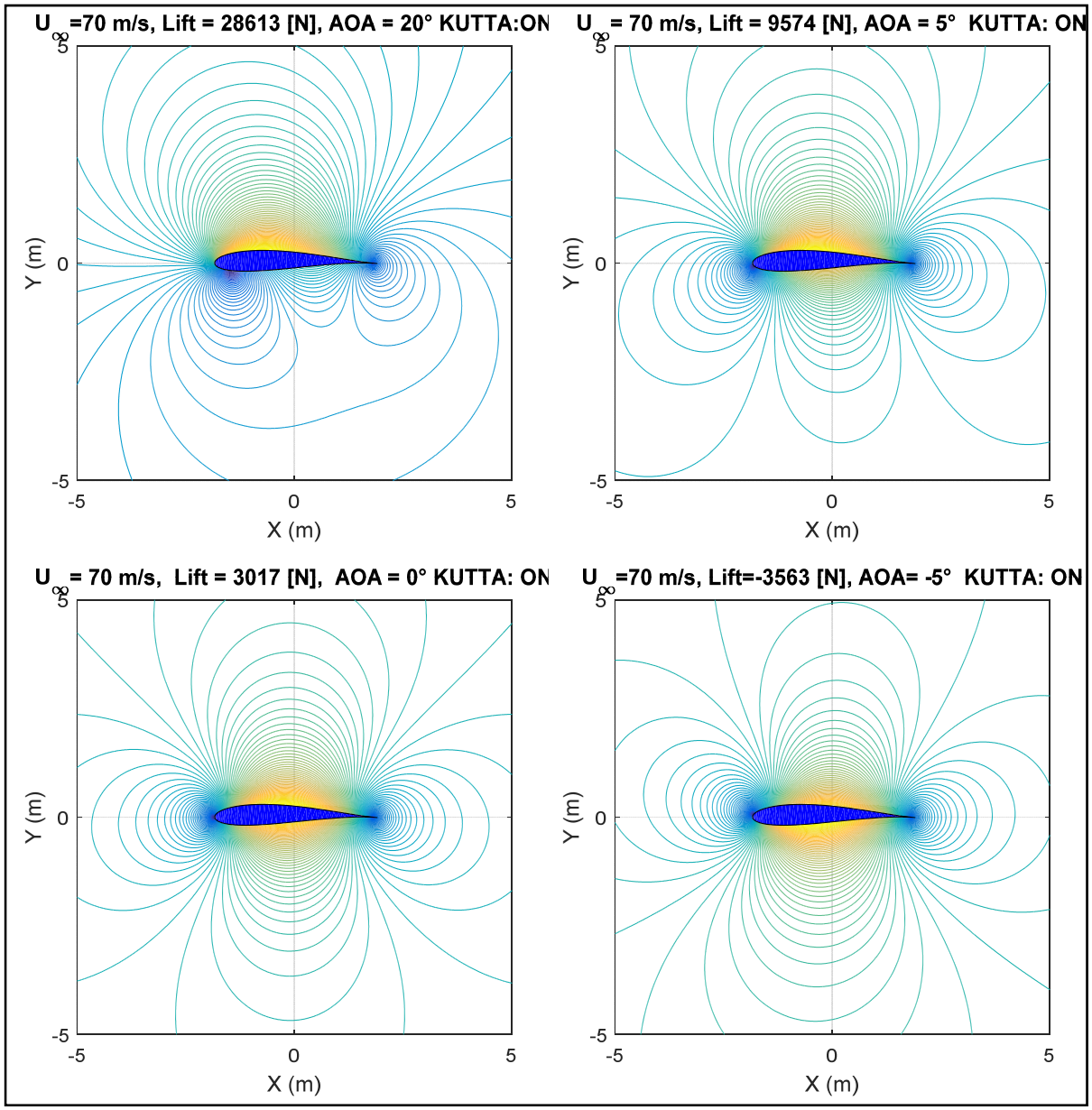

Figure 3.6 Joukowski airfoils with different angles of attack

In the next section, the results for the simulation of the ice piece in a uniform flow field will be presented.

3.2 2D ice trajectory in horizontal uniform flow field

In this section single ice trajectories in a horizontal uniform flow will be presented. The trajectory of the ice piece, as its position on the plane in each time step of the simulation, will be compared with those found in the literature. The references used to validate the simulation code in this section (Holmes, 2006), (Kordi, 2009), have investigated the trajectory of the wind-borne plate-type debris in the uniform wind. Since the physical and mathematical models used in these researches are the same as the model of ice trajectory simulations, these references are used to study the trajectory of the ice piece in the uniform flow. The validation of the trajectories will be divided in two sections. First the trajectories in which the Magnus effect is not included will be validated and later trajectories with Magnus effect will be considered. Plate samples, flow velocity, flow density and initial orientation of the plate will be different in each case studies. The properties of each validation case will be mentioned in pertaining figures.

3.2.1 Trajectories without Magnus effect

Holmes (Holmes, 2006) has conducted experimental and numerical trajectories to study the trajectory of the plate-type windborne debris in uniform wind. Holmes's steady coefficients for lift, drag and moment are used in this research project. The queasy-steady model to calculate the forces and moments on the plate ice is the same used in Holmes's research. Holmes has published his result for trajectories with and without Magnus effect. This section will compare the trajectories with the trajectories of Holmes without Magnus effect. The plate samples simulated in these cases are of different sizes and materials. Although the density of the pieces is not directly mentioned in the test cases of Holmes but can be obtained using Tachikava number.

Figure 3.7 illustrates the trajectories for a $40 \times 40 \times 2\ mm$ square plastic plate with mass density of $1163\ kg/m^3$ in a horizontal uniform flow with a velocity of $9.2\ m/s$. The initial

angle between the plate and the horizontal axes are 15 and 45 degrees. The air density is 1.24 kg/m^3 and gravity acceleration is 9.81 m/s^2.

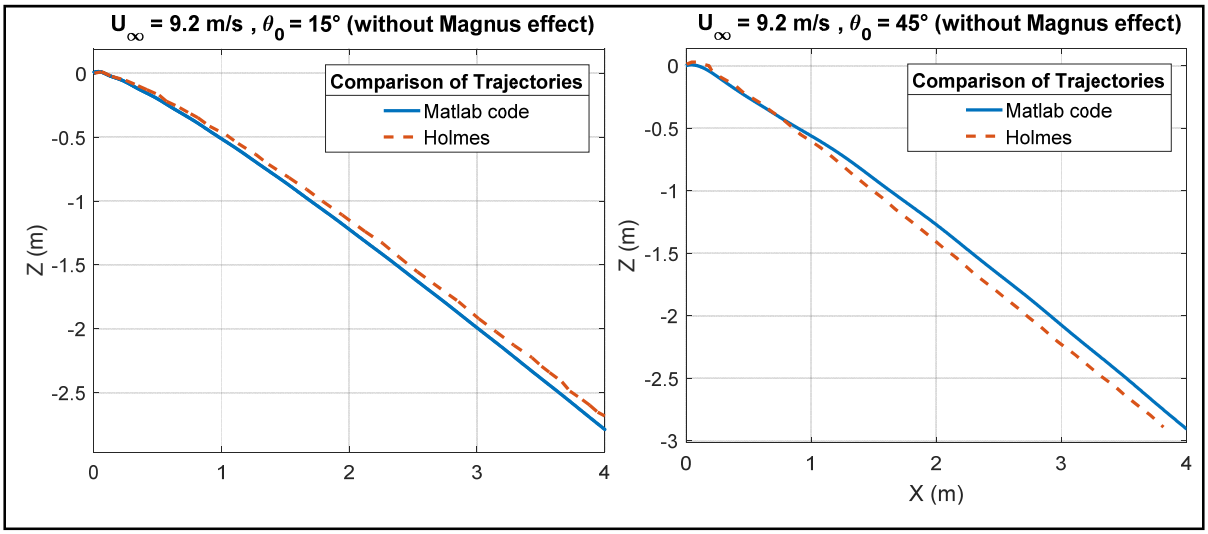

Figure 3.7 Comparison of trajectories between Holmes's results and computed trajectories - square plastic plate ($40 \times 40 \times 2$ mm) with a density of 1163 kg/m^3

Holmes has also done experimental and numerical trajectory simulations on the square plate samples made of basswood. These trajectories are compared with the result of the research in figure 3.8. A $75 \times 75 \times 9$ mm basswood square plate is released in three uniform airflow with different velocities. In all three cases the initial angle of the plate is 0 degree. The flow velocity for each trajectory is written in each figure. The air density for all these cases is 1.24 kg/m^3 . These trajectories are run without taking into account the Magnus effect.

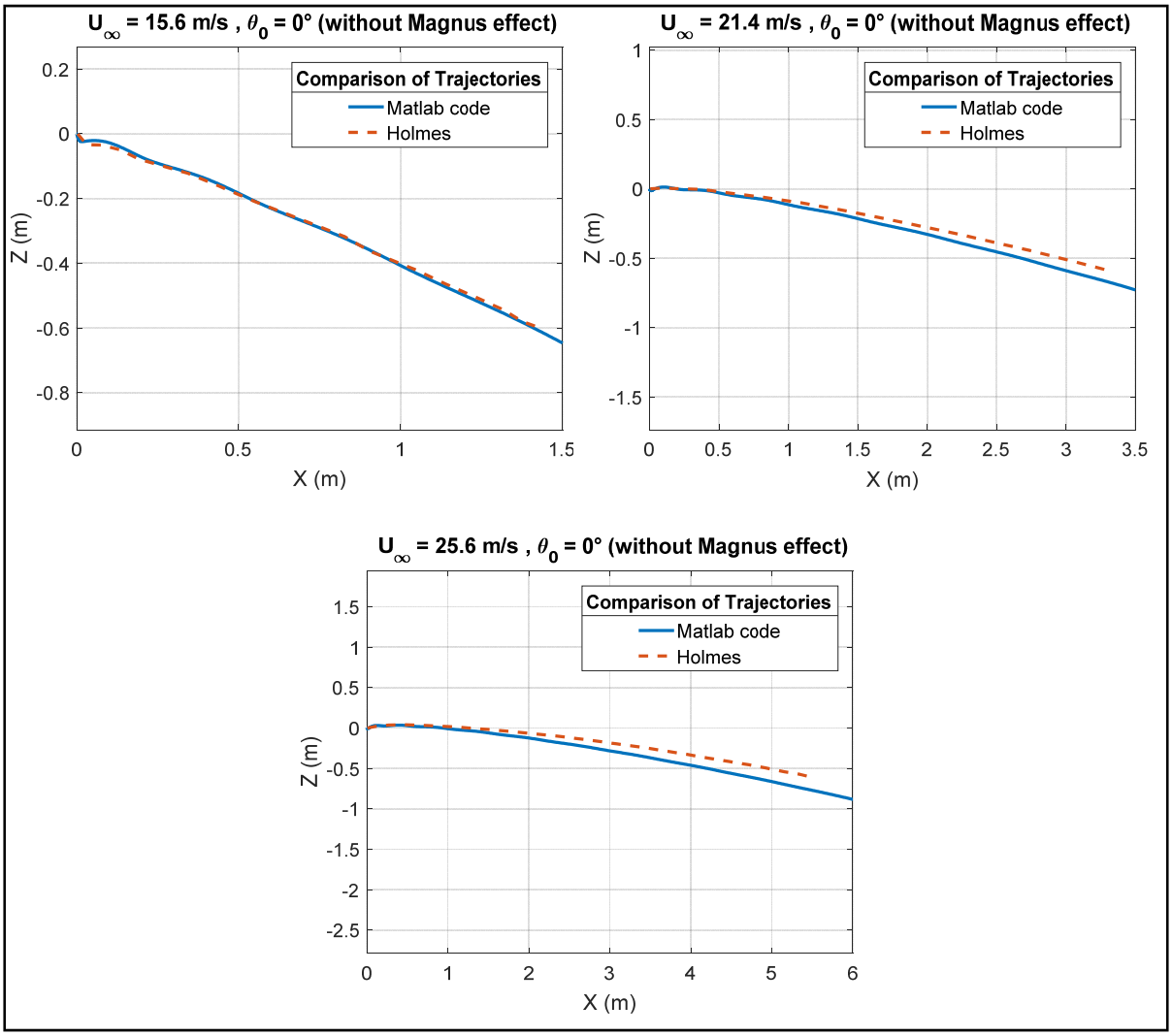

Figure 3.8 Comparison of trajectories between Holmes's results and computed trajectories - basswood square plate ($75 \times 75 \times 9\ mm$)

Comparison of the trajectories of Holmes without Magnus effect and the result of the simulation code proves a good agreement between two simulations. The same numerical model to calculate the forces and moments on the square plate pieces and the same static coefficients for lift, drag and moment as Holmes are used in this research. The reason for slightly different result for the trajectories can be due to unclear values given in the literature. The air density is not given explicitly in Holmes's article and the mass density of the plate sample is extracted by using Tachikava number. The Tachikava numbers are only given in one decimal numbers

which seem to be imprecise. In the next section other test cases which the Magnus effect is included will be validated.

3.2.2 Trajectories with Magnus effect

Pervious section compared the results for single square plate trajectories in horizontal uniform flow without Magnus effect. In these section simulation code is validated by comparing the results of the research with the results of Holmes (Holmes, 2006) and Kordi (Kordi, 2009) with Magnus effect.

Comparison of two trajectories for basswood square plate samples with $L = l = 75\ mm$ and $e = 3\ mm$ simulated with two different initial angle of attack and two different velocities for the horizontal uniform airflow are presented in figure 3.9. Holmes has included the Magnus effect for these trajectories, so the simulations of the trajectories will be run both with static lift, drag and moment coefficients and the coefficients caused by auto rotation of the plate (Magnus effect). The auto rotational aerodynamic coefficients used in the research of Holmes are not the same as the Magnus coefficients used in this research. Although in these two cases trajectories are not very similar, but still there is a good agreement in general form of the trajectories between two references. Notice the different parameters for initial angle of attack, the mass density and airflow velocity for each trajectory.

The physical model used by Kordi (Kordi, 2009) to calculate the force components and moments on the square plate particles are the same as this research. Kordi has published her results taking into account the Magnus effect. Since the trajectories of this research uses the same coefficients for auto rotational forces and moment, it would be prudent to expect the same results for trajectories with the same parameters for the square plate particles and the same flow filed.

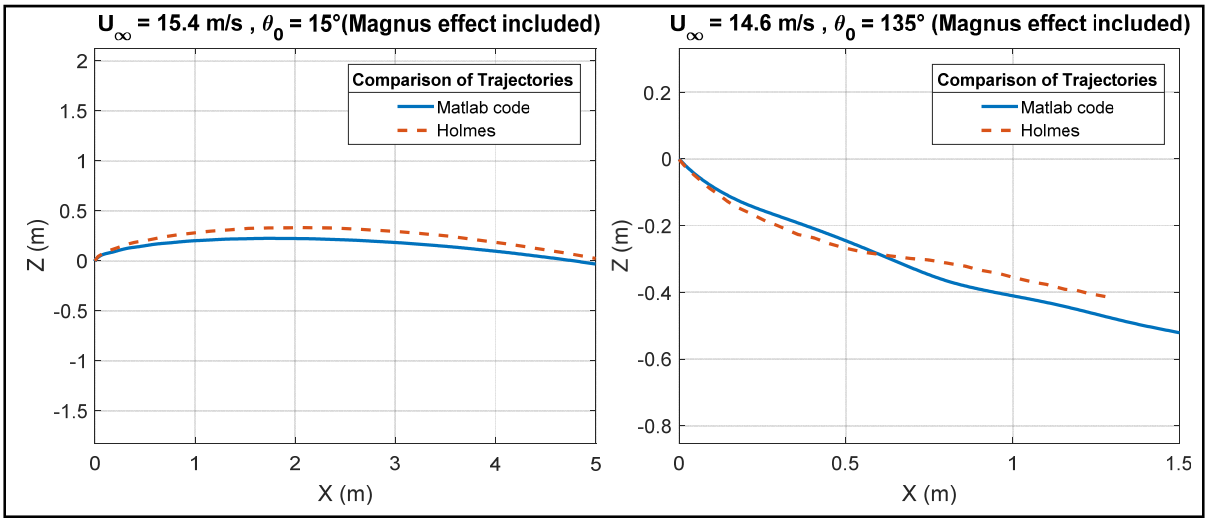

Figure 3.9 Comparison of trajectories between Holmes's results and computed trajectories with Magnus effect- plywood square plate ($75 \times 75 \times 3\ mm$) with a density of 847 kg/m^3

Figure 3.10 presents the trajectories for a square plastic plate with a dimension of $L = l = 40\ mm$ and $e = 2\ mm$. These square plastic plates which have $1120\ kg/m^3$ mass density experiences two trajectories in a horizontal uniform airflow with a velocity of $9.18\ m/s$. The influence of the initial parameters such as the angle of attack, on the trajectories of the plate in the same flow fields are obvious in this figure. The influence of the initial parameters on the trajectories will be discussed in next sections.

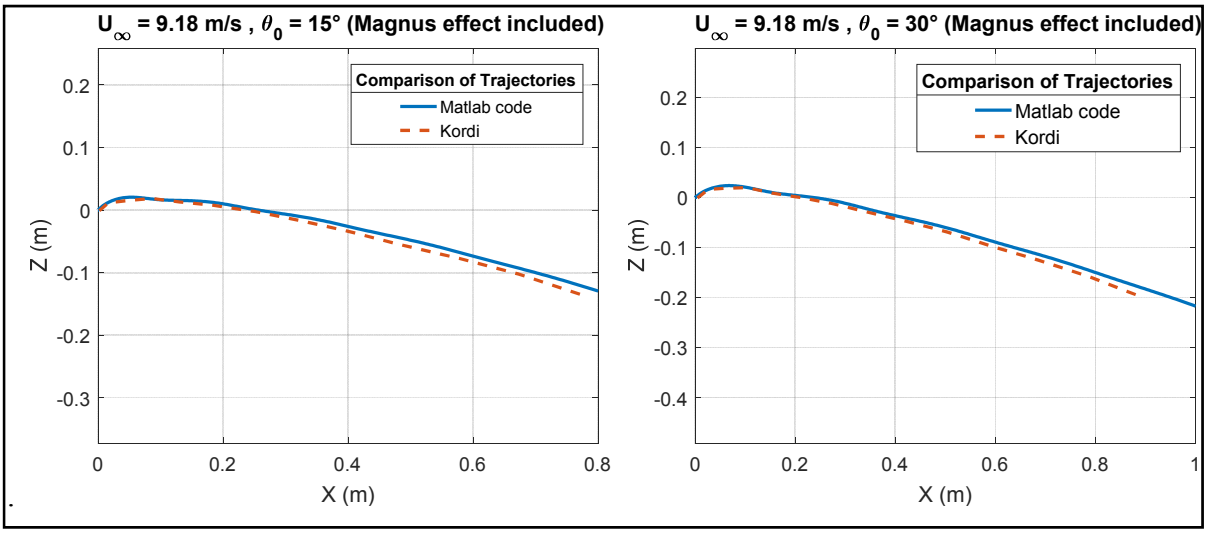

Figure 3.10 Comparison of the trajectories between Kordi's results and computed trajectories with Magnus effect - square plastic plate ($40 \times 40 \times 2\ mm$) with a density of $1120\ kg/m^3$

Three test cases in figure 3.11, simulate the trajectories for basswood square plate sample with a dimension of $75 \times 75 \times 9\ mm$. In each case the horizontal uniform airflow has different velocities but the ice plate will begin its trajectory with the same initial angle of attack. Kordi has used the data of Tachikawa (Tachikawa, 1983) for ice pieces (the same as Holmes's data). The parameters of each trajectory are mentioned under the figures. Each trajectory is associated with the comparison of its velocity development during the trajectory. Comparing the results confirms a good agreement between two numerical simulations and except for the first two cases, obtained trajectories are almost identical.

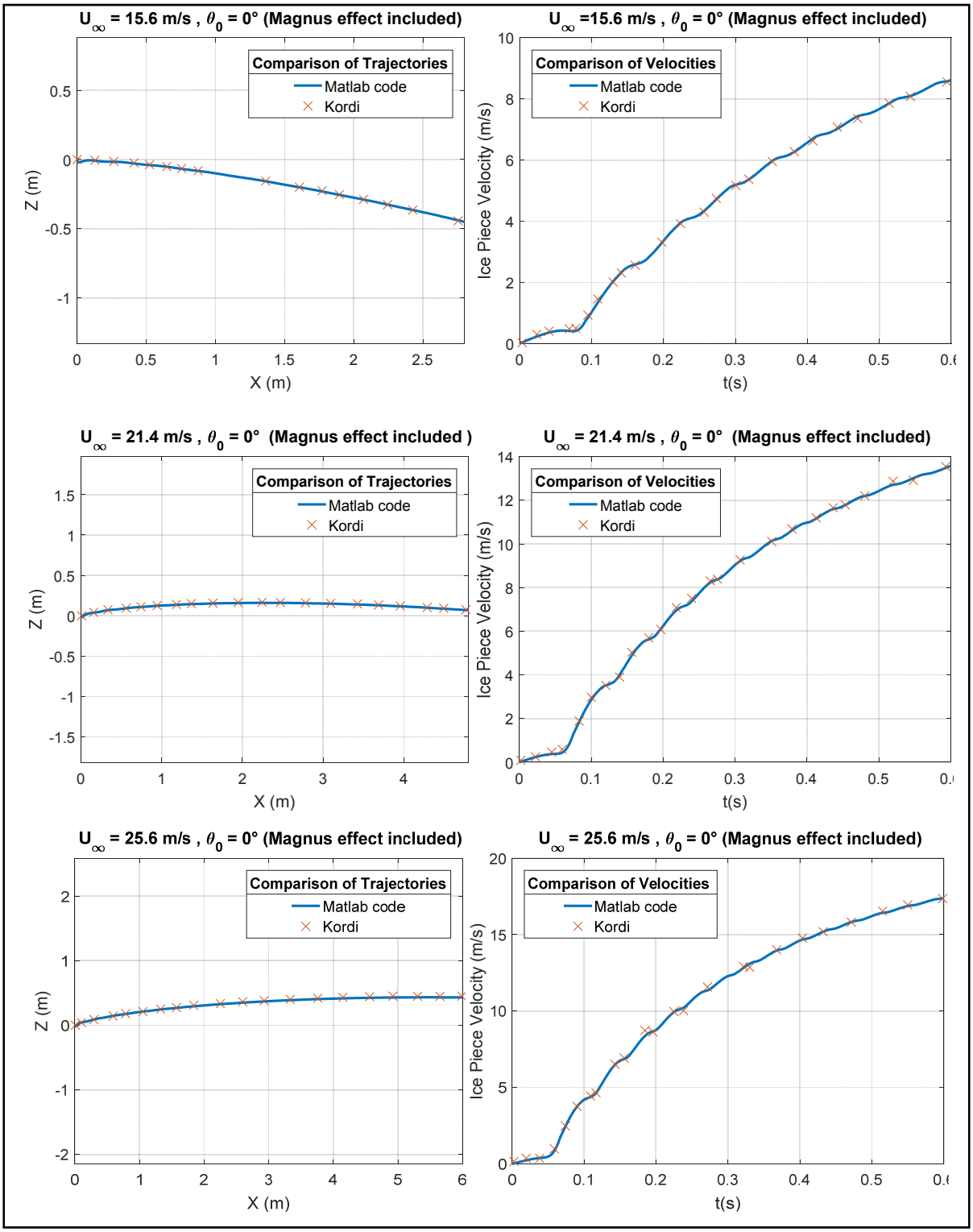

Figure 3.11 Comparison of trajectories and Velocities between Kordi's results and computed trajectories with Magnus effect- basswood square plate ($75 \times 75 \times 9\ mm$) with a density of $575\ kg/m^3$

Based on the validation of the code results in previous sections it is safe to say that the Matlab code delivers correct results according to the numerical method to compute the relative velocity, angle of attack of the ice plate, static lift, drag and moment coefficient as well as the auto rotational coefficients of lift, drag and moment. These values are used to compute the force components and moments on the ice piece which make the ice piece move in a 2D horizontal uniform flow.

All the validations presented in this section were related to trajectories in completely horizontal uniform flow fields due to this fact that trajectories available in the literature are conducted in horizontal uniform flow fields. The simulation code in this research is developed to make it able to simulate the trajectory of the ice piece in non-horizontal uniform flow fields. In the next section results for non-horizontal uniform flow field will be presented and verified.

3.3 2D Ice trajectory in Non-horizontal uniform flow

To obtain the velocity components of the flow field, the flow field is defined by a complex potential function. In this order, a function is added to the Matlab code to calculate the potential flow and the potential velocity in the uniform flow and trajectories of the square plate ice pieces in a non-horizontal uniform flow are simulated. Figure 3.12 shows two set of test cases with different angles of the flow with the horizontal axis.

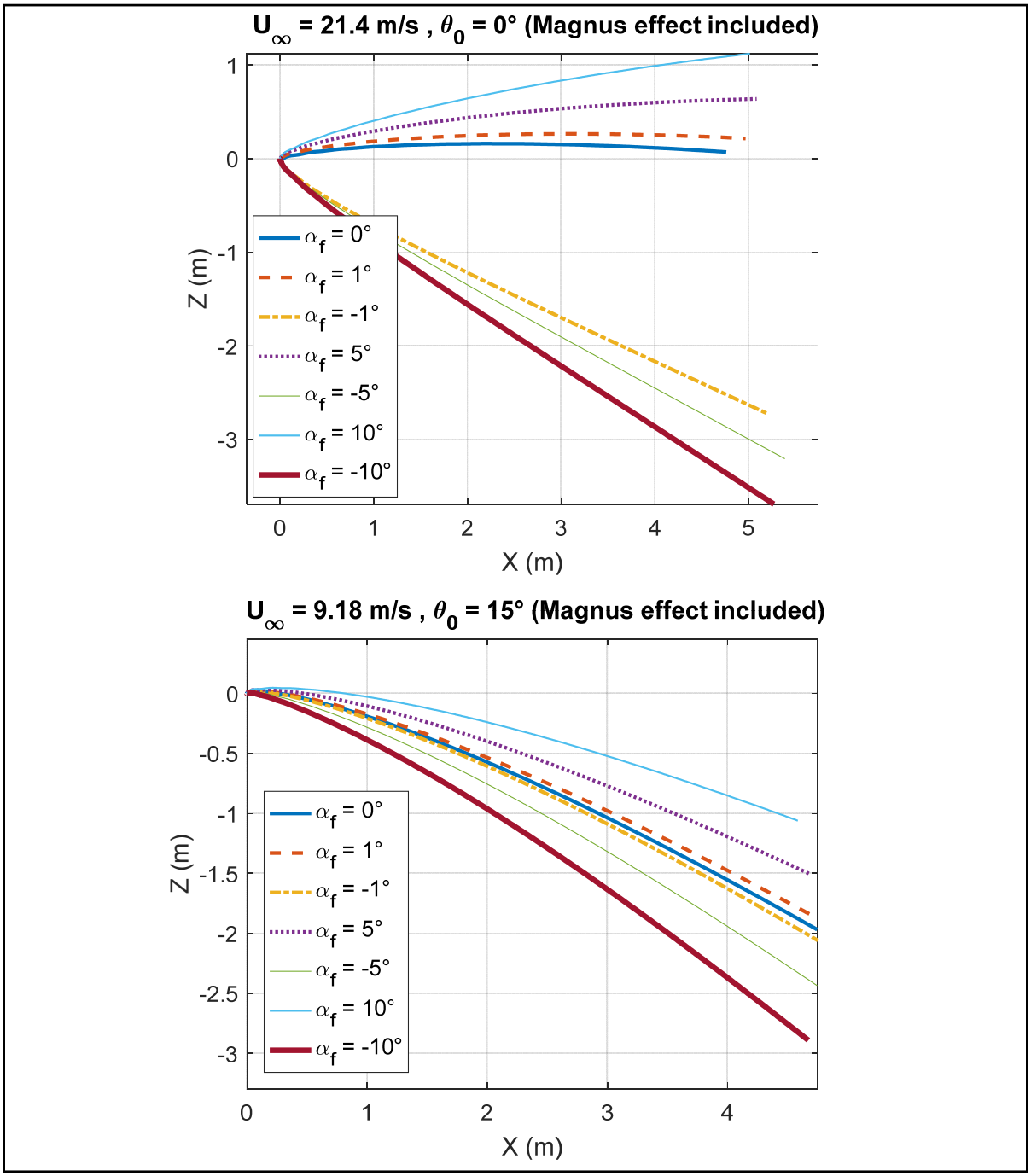

Figure 3.12 Comparison of trajectories in Non-horizontal uniform flow field with different angles of the flow with the horizontal axis - Magnus effect included – up: plastic square plate ($40 \times 40 \times 2\ mm$) with a density of 1120 kg/m^3 - down: basswood square plate ($75 \times 75 \times 9\ mm$) with a density of 575 kg/m^3, $\rho_{air} = 1.24\ kg/m^3$.

Although the Matlab code used for both horizontal and non-horizontal uniform flow fields are the same, but to verify the code in non-horizontal flow field, several trajectories by trivial differences in the angle of the uniform flow filed are simulated. As can be seen in figure 3.12 the trajectory of the ice piece changes logically by increasing and decreasing the angle of the uniform flow. The ice piece has more vertical displacement when the flow field has greater vertical velocity component and vice versa.

In some cases, extreme changes in the trajectories occur as the angle of the uniform flow changes. This is due to this fact that initial conditions of the trajectory are important factors to determine the trajectory of the ice piece. In figure 3.12 (up) there is a big different between the trajectory for the flow with an angle of $1°$ and the flow with an angle of $-1°$. In this trajectory case, the initial angle of the ice piece is zero (parallel with the horizontal axis). When the flow is upward, the initial vertical component force of the flow field on the ice piece is positive (upward) but when the flow is downward the initial vertical force component of the flow is negative (downward). This initial condition brings about two completely different trajectories. In the trajectories of the figure 3.12 (down) the initial angle of the ice piece is $15°$, so there is not a big gap between the trajectories of the flows with an angle of $1°$ and $-1°$.

The validation of the code in the horizontal uniform flow field and its verification in non-horizontal uniform flow field were presented. In the next section the trajectories of the square plate ice in the flow field of a Joukowski airfoil will be presented.

3.4 2D ice trajectory in Joukowski airfoil's flow field

Suares (Suares, 2005) has conducted several 2D and 3D ice trajectory simulations in the uniform horizontal flow field and also in the flow field of airfoil. His mathematical approach to compute the trajectories is different than this research and he has used different lift, drag and moment coefficients in his force and moment calculations, Magnus effect has been neglected as a factor influencing the trajectory of the ice piece, therefore Magnus effect will not be included in the simulations of validation. For his flow field around the airfoil he has

used clean and iced NACA 23012 airfoil with a cord length of 7.3 ft (2.22 m) with different angle of attack.

The ice piece of Suares's simulations is a $0.1303m \times 0.1303m \times 0.0365\ m$ square plate with a mass of $0.5715\ kg$. The trajectory of this ice piece will be simulated when the airfoil has a velocity of $113\ m/s$, flying 15000 ft above sea level. For this altitude, 0.770 kg/m^3 is used for the value of the air density. The initial angle of the ice piece with the positive direction of the $X\ axis$ is introduced by Suares which is 145.63°.

In mathematical method of this research, for the calculation of aerodynamic forces, the angle of the ice piece is calculated with respect to the negative direction of X axis, therefore 34.37° will be used for initial value of the ice piece angle with the horizontal axis.

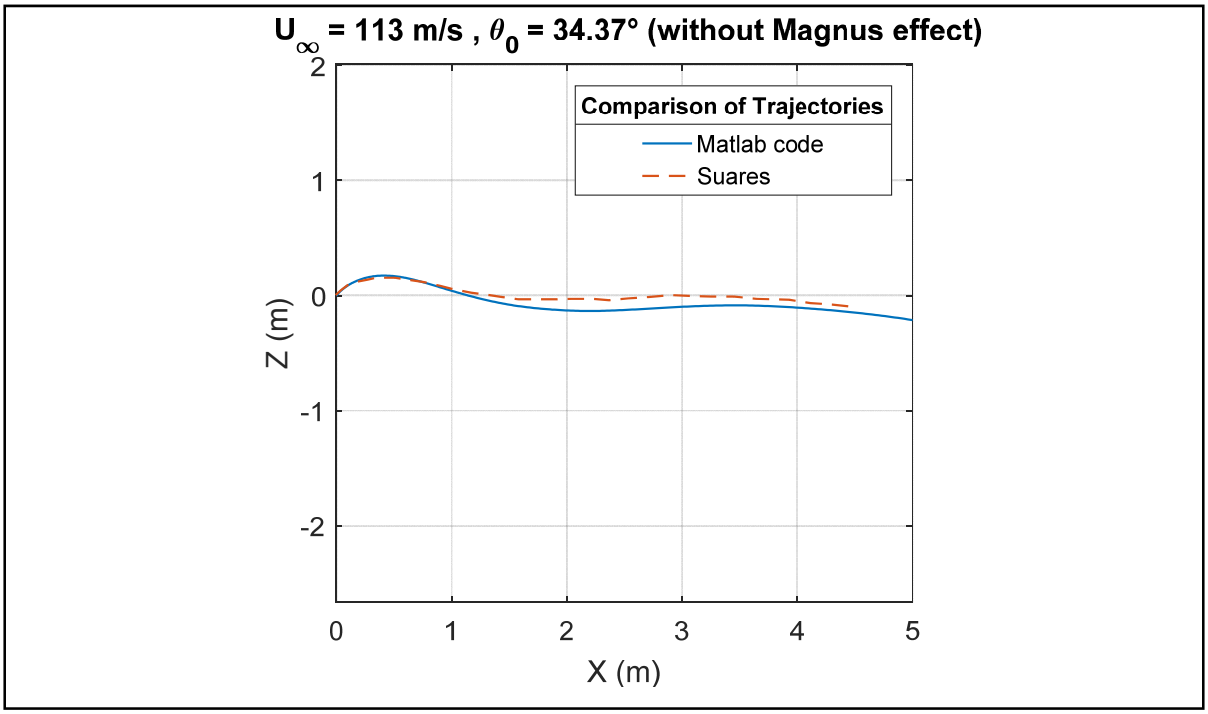

Figure 3.13 Comparison of the trajectories in a uniform flow field without Magnus effect – square plate ice piece with a dimension of $0.1303\ m \times 0.1303\ m \times 0.0365\ m$ and a mass of 0.5715 kg.

Figure 3.13 is the comparison between resulted trajectory and the trajectory of Suares for square plate ice in the horizontal uniform flow field. A good agreement between two trajectories is shown despite this fact that the mathematical approach and the aerodynamic coefficients are different in two simulations.

The flow fields used by Suares (Suares, 2005) to simulate trajectories around the airfoil and the flow field around the Joukowski airfoil are different due to different geometries of the airfoils. Same results are not expected from comparison between trajectories in these two flow fields. Size of the Joukowski airfoil is adjusted to resemble the airfoil used in the Suares's research.

In this set of simulations the cord of the Joukowski airfoil has $2.23\ m$ length. This Joukowski airfoil is generated from a cylinder with a radius of $0.615\ m$ which its center is located at $\zeta_0 = -0.0615 + 0.0246i$. The dimension of the ice piece, its orientation, airflow velocity and its density is the same as the uniform flow field case.

The trajectories around the Joukowski airfoil are compared with the trajectories of Suares for clean NACA 23012 airfoil with $AOA = 0°$ and $AOA = 4°$. The ice piece will start its trajectory $0.09\ m$ ahead and $0.122\ m$ above the leading edge of the airfoil (Suares, 2005).

Figure 3.14 presents the comparison of simulated trajectories with those of Suares (Suares, 2005) in the flow fields of the airfoils. As expected, results are not very similar trajectories for these two different flow fields but yet, it can be seen that the general behaviour of the ice pieces are somehow similar, especially in the case of 4° angle of attack of the airfoils.

The difference between the trajectories may be due to this fact that the geometries of the two airfoils are different. For two different airfoils, airflow velocity and its direction at every given point in the plane are not the same. In such a condition initial parameters for two trajectories are not the same (which are very influential in the trajectory of the ice piece). Beside the different initial conditions, having different velocity components in the plane of the trajectory results in different forces on the ice pieces which leads to different trajectories.

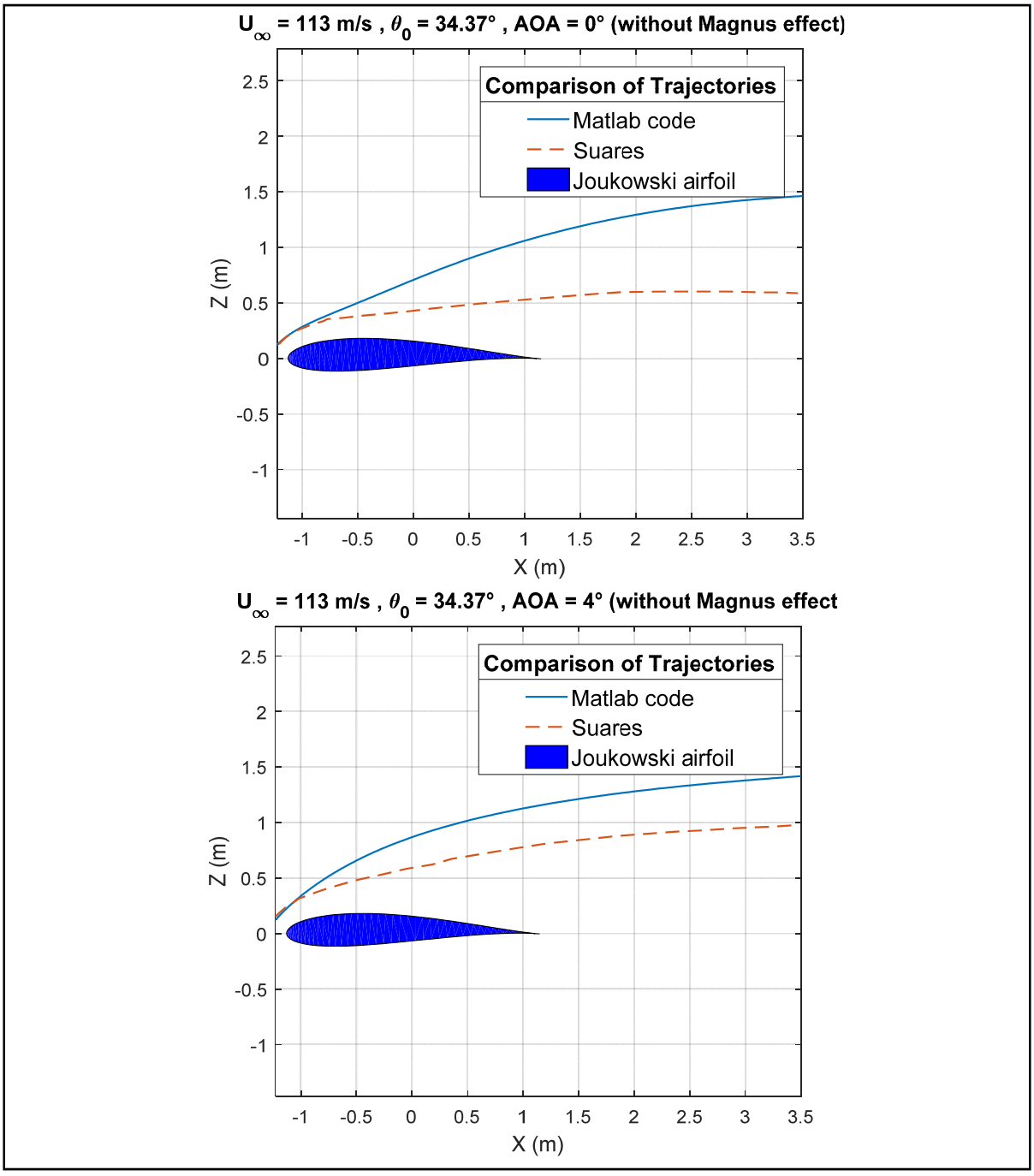

Figure 3.14 Comparison of the trajectories in the flow field of two airfoils (Joukowski airfoil and NACA 23012) without Magnus effect- square plate ice piece with a dimension of $0.1303\ m \times 0.1303\ m \times 0.0365\ m$ and a mass of 0.5715 kg.

Comparing the results of the research with the results of the Suares (Suares, 2005) in the uniform flow validated the Matlab code further. This comparison confirmed that the

calculation of the initial angle of the ice piece is correct in the code developed in the research. Although the Matlab code uses a different approach to calculate this angle, it yields similar results as Suares (Suares, 2005) when adjustment of this angle is done to simulate the initial parameters of the ice piece of his simulations.

Comparison of the trajectories in two different airflow fields pertaining to two different airfoils makes it necessary to investigate the impact of the geometry of the airfoil and its angle of attack on the trajectories of the ice piece. Next section will discuss the results of the trajectories when the Joukowski airfoils have different angle of attack, different thicknesses and different cambers. Also it will show how much important is the density of the air on the trajectories.

3.4.1 Airfoil's angle of attack and trajectories

The test case of Suares (Suares, 2005) has been used to investigate the influence of the angle of attack of Joukowski airfoil on the trajectories of an ice piece. Five trajectory simulations were conducted with the exact same set of initial parameters and the same ice piece properties. The airflow velocity in all trajectory cases are the same but the angle of attack of the airfoil differs in each case.

Figure 3.15 depicts these five trajectories and shows the behavior of the ice piece in different angles of attack. As the ice piece is located ahead and above the leading edge, it can be seen that with the AOA of 4° and 10° the ice piece has more acceleration along the vertical axis of the plane. With a negative AOA, ice piece initially is pushed downward, toward the airfoil but due to higher upward velocity component of the airflow around the airfoil, the aerodynamic forces make the ice piece change its direction and to follow the stream lines of the flow field around the airfoil.

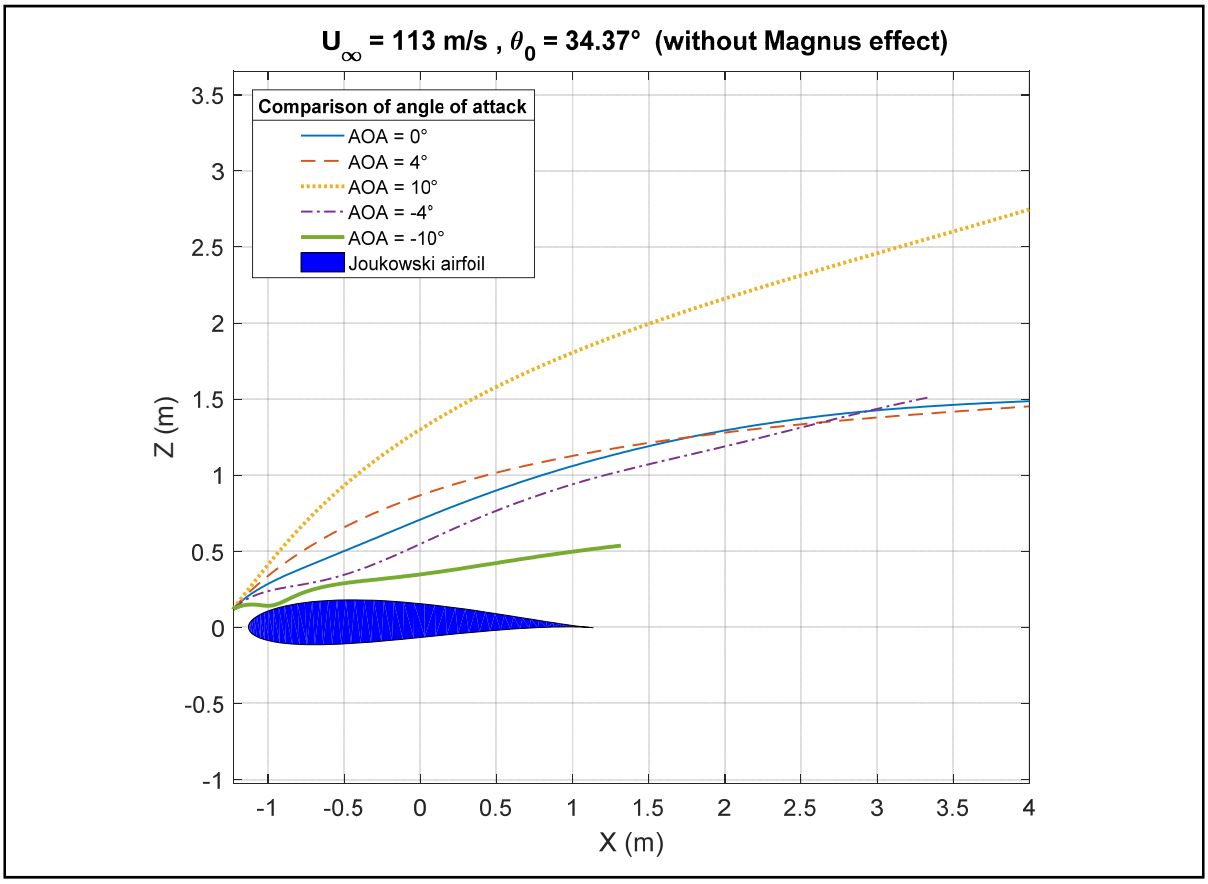

Figure 3.15 Comparison of the trajectories in the flow field of Joukowski airfoil with different angles of attack for the airfoil- without Magnus effect - square plate ice piece with a dimension of $0.1303\ m \times 0.1303\ m \times 0.0365\ m$ and a mass of 0.5715 kg.

These single trajectories are presented to further validate the simulation of the Matlab code and to examine if the trajectories in different AOA are as expected and logical. According to figure 3.15 the ice piece trajectories are proportional to the magnitude of horizontal and vertical components of the velocity vector in the plane. The influence of the AOA on the trajectories will be elaborated in the section of the Monte-Carlo method to see how the pass probability of an ice piece with an object can change due to the change of AOA of the airfoil.

3.4.2 Airfoil's thickness and trajectories

This section will show how the thickness of the airfoil can change the trajectory of the ice piece. Again the test set of Suares is used and the ice piece is located ahead and above the leading edge ($Z = -1.22 + 0.122i$) in airflow with a velocity of $113\ m/s$. The dimension of ice piece and its density are mentioned in figure 3.16. By keeping all parameters same and varying only the thickness of the airfoil five different ice trajectories are achieved.

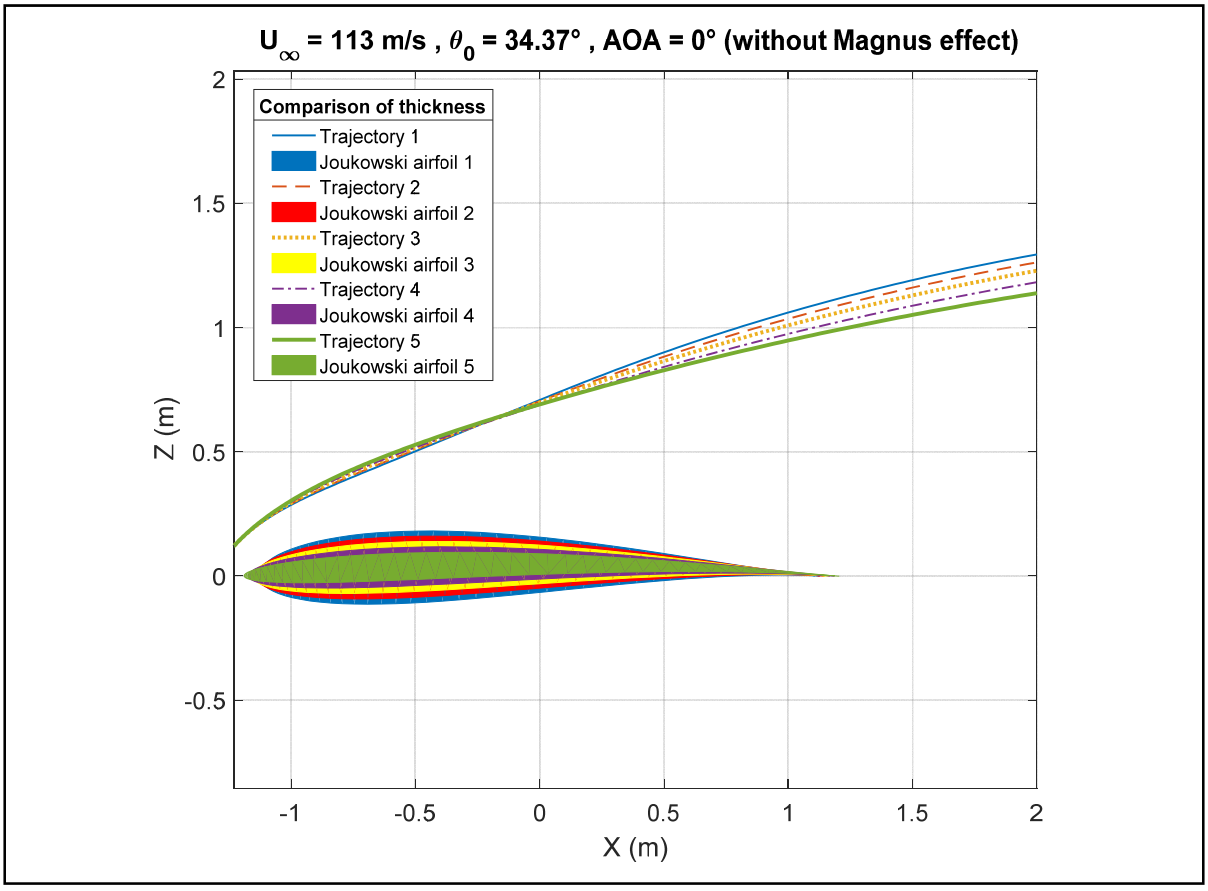

Figure 3.16 Comparison of the trajectories in the flow field of Joukowski airfoils with different thicknesses without Magnus effect - square plate ice piece with a dimension of $0.1303\ m \times 0.1303\ m \times 0.0365\ m$ and a mass of 0.5715 kg.

Figure 3.16 illustrates five trajectories in different colors which correspond to the airfoils with the same color. The blue trajectory is for the flow field of blue airfoil which is the thickest airfoil. The thicker airfoil generates higher vertical velocity component around its geometry. This higher vertical velocity component results in higher vertical aerodynamic force on the ice piece and the ice piece reaches higher altitude. The blue ice trajectory satisfies the expectation completely and flies above all other trajectories which are for thinner airfoils. The green path gets less vertical force component and has the less final altitude in our simulation. Three other trajectories place themselves between these two extreme trajectories.

By having studied the behavior of the ice piece around the airfoils with different thicknesses, the impact of other changes of the airfoil's geometry on the trajectory of the ice piece will be inspected. Next section presents the influence of the camber of the Joukowski airfoil on the trajectories.

3.4.3 Airfoil's camber and trajectories

The same approach as the previous section will be followed to verify the simulations of the Matlab code when the Joukowski airfoil have different cambers. Test set of the simulation is the same as the previous section but this time varying parameter of the airfoil will be its camber instead of its thickness. Higher altitude travel of the ice piece is expected when it is released in the upper side flow field of the airfoil with greater camber. Air particles will have more vertical velocities arriving in the flow field of a more curved airfoil. These upward redirected flow particles will deliver more vertical aerodynamic forces to the ice piece.

Figure 3.17 is dedicated to the trajectories of this simulation. Five selected Joukowski airfoil with different cambers generate five different flow fields and consequently result in different aerodynamic forces on the ice piece. Different colors pair trajectories with the corresponding airfoils. Green airfoil is the most curved airfoil and its trajectory is above all other four trajectories. Blue airfoil is a symmetric airfoil and thus its upward curve is less than other airfoils and its trajectory gains less altitude compared with other airfoils. Three other airfoils

are defined between these two airfoils and their trajectories follow the physical logic of the simulation.

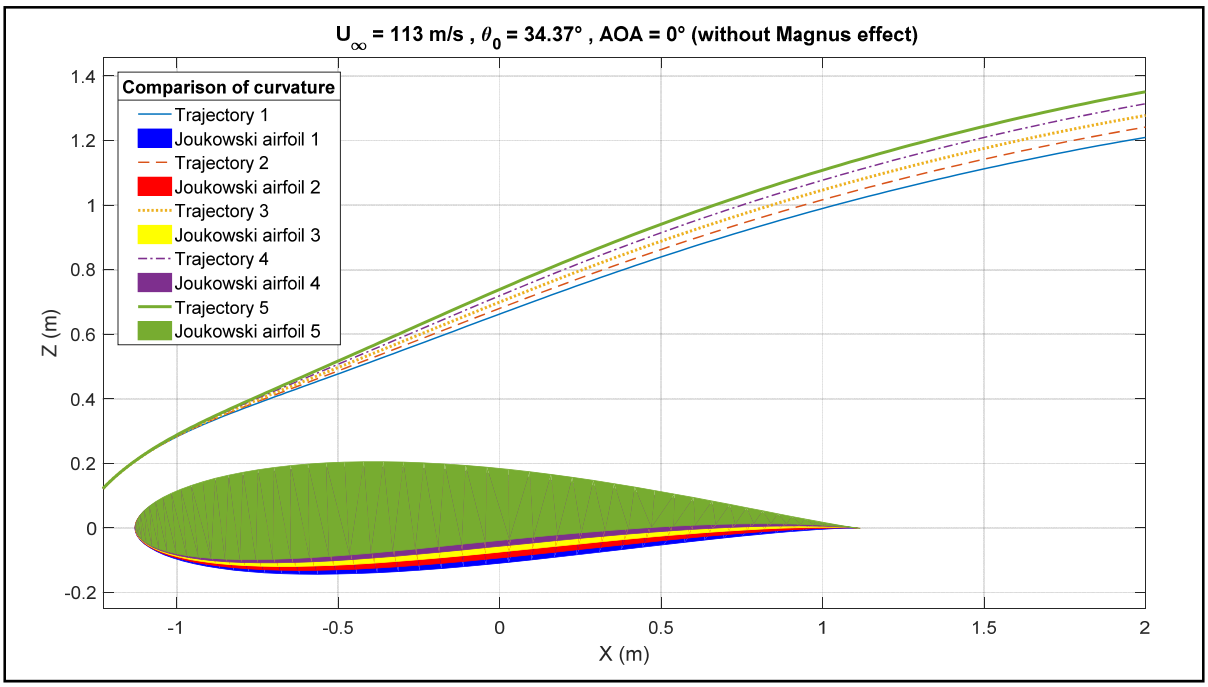

Figure 3.17 Comparison of the trajectories in the flow field of Joukowski airfoils with different cambers without Magnus effect - square plate ice piece with a dimension of $0.1303\ m \times 0.1303\ m \times 0.0365\ m$ and a mass of 0.5715 kg.

Beside the geometry of the airfoil the properties of the flow (air) can play a rule to alter the trajectories of the ice piece. The influence of the flow's properties will be discussing in next section.

3.4.4 Flight altitude and trajectories

The properties of the air flow change in different altitudes and different temperatures. The main factor acting on the aerodynamic forces on the ice piece is the density of the air. According to equations 2.35 and 2.36, air density has a direct influence on the force components. This means that in a flow filed with higher density, the ice piece will get more

aerodynamic forces and more acceleration. The air density decreases when altitude increases. Several trajectories are run for the same set of tests to see how much important is the magnitude of the air density on the trajectories of the ice piece.

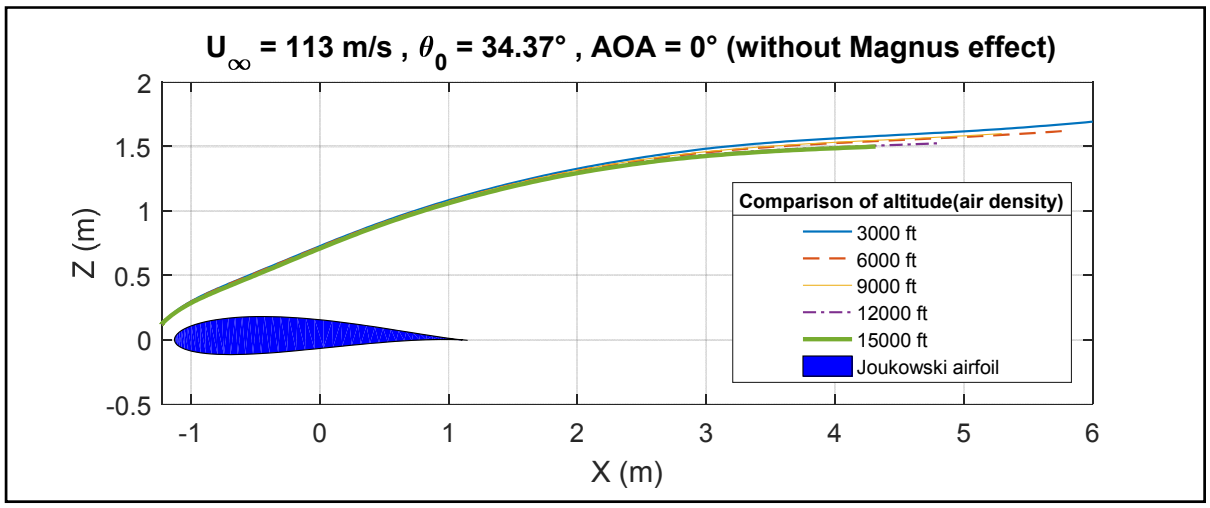

Figure 3.18 Comparison of the trajectories in the flow field of Joukowski airfoil in different altitudes (different air densities) - square plate ice piece with a dimension of $0.1303\ m \times 0.1303\ m \times 0.0365\ m$ and a mass of 0.5715 kg.

Figure 3.18 shows the trajectories simulated for the same ice piece in the same flow field of a Joukowski airfoil in different altitudes. As shown the influence of the air density is not very significant but still can alter the trajectory of the ice piece. The blue trajectory belongs to the simulation at lowest altitude and has more vertical displacement. This ice piece travels more horizontal distance due to its higher horizontal speed.

Although a considerable impact of the air density on the trajectories of the ice piece is not observed, simulations will be run with setting the air density for the $15000\ ft$ (Suares, 2005) to imitate the real condition of the inflight icing, which mostly happens in high altitude where the icing conditions exist.

3.5 Monte-Carlo simulations

Previous sections presented the results of the research for single trajectories. The Matlab code of the research was validated by comparing the results for square plates, in horizontal uniform flow field with the available trajectories in the literature. Later, it was verified for non-horizontal flow field and the flow field of Joukowski airfoil, with doing a comparative study on the trajectories in different flow field conditions.

This section will present the result of Monte-Carlo simulations. The pass probability of the ice piece around the Joukowski airfoil with different geometry and angles of attack will be depicted as footprint maps. Also, it will be shown how the shape of the ice piece can alter this probability maps. In this order the simulation code will simulate the trajectories of square plate, rectangular plate and sphere ice shapes with the same mass. Each section will study the shedding of the ice pieces from the upside and downside surface of the leading edge, separately.

The Joukowski airfoil used in this section is the same as section 3.4 and is generated from a cylinder with a radius of $0.615\ m$ which its center is located at $\zeta_0 = -0.0615 + 0.0246i$. The chord of this asymmetric Joukowski airfoil is $2.23\ m$ in length and its maximum thickness is $13\ \%$ at 22% of the chord. The research will use this airfoil as the standard airfoil to compare with other geometries of the Joukowski airfoil.

The locations of the ice shedding are defined as the 10% of the cord's length starting from the stagnation point of the leading edge. The starting positions of the ice trajectories are uniformly divided to 40 different coordinates on the upside and downside surface of the airfoil.

Probability map all around the airfoil in each case is plotted to compare the footprint of the ice particle in different test cases. However, to compare the impact of each parameters on the trajectory of the ice pieces, the research is more concerned with the areas in which the down stream components of the aircraft such as engines are located. In this order, it is assumed that the engine behind the airfoil is located at $4\ m$ downstream of the leading edge on the horizontal axis and the vertical interval of the engine's inlet is $1.5\ m$. In the figures, this area is presented by last two squares down stream, up and down of the horizontal axis.

3.5.1 Effect of the airfoil's angle of attack on the probability map

This section will compare the probability maps around the Joukowski airfoils with $AOA = 0°$, $AOA = 4°$ and $AOA = 15°$. The square plate ice piece has a dimension of 0.1303 m $\times$ 0.1303 m $\times$ 0.0365 m and a mass of 0.5715 kg. The airflow velocity is $113\ m/s$ and its density is $0.770\ kg/m^3$ (flight altitude is $15000\ ft$). The variation of the initial condition for Monte-Carlo simulation is presented in Table 2.1. The detailed properties of each simulation are mentioned in pertaining figures.

Figure 3.19 compares the results of Monte-Carlo simulation for two Joukowski airfoil with different angles of attack. The airfoil in the left side of the figure has $AOA = 0°$ and the airfoil in the right side of the figure has $AOA = 4°$. In this simulation the location of the ice shedding is upside surface of the leading edge.

As shown there is an upward increasing shift in the probability map when the airfoil has a positive AOA and the probability of the ice ingestion by the engine behind the airfoil decreases when the angle of attack increases.

Figure 3.20 depicts the result of the same simulation as previous case when the shedding occurs from the downside surface of the leading edge. Having the same upward increasing shift for the mean trajectory brings about greater probability for strike of the ice piece with an engine behind the airfoil.

These changes in the probability map are more obvious when the simulation increase the angle of attack to 15°. The greater strike probability with an angine behind the airfoil is possible when the ice sheds from downside surface of the leading edge with $AOA = 15°$.

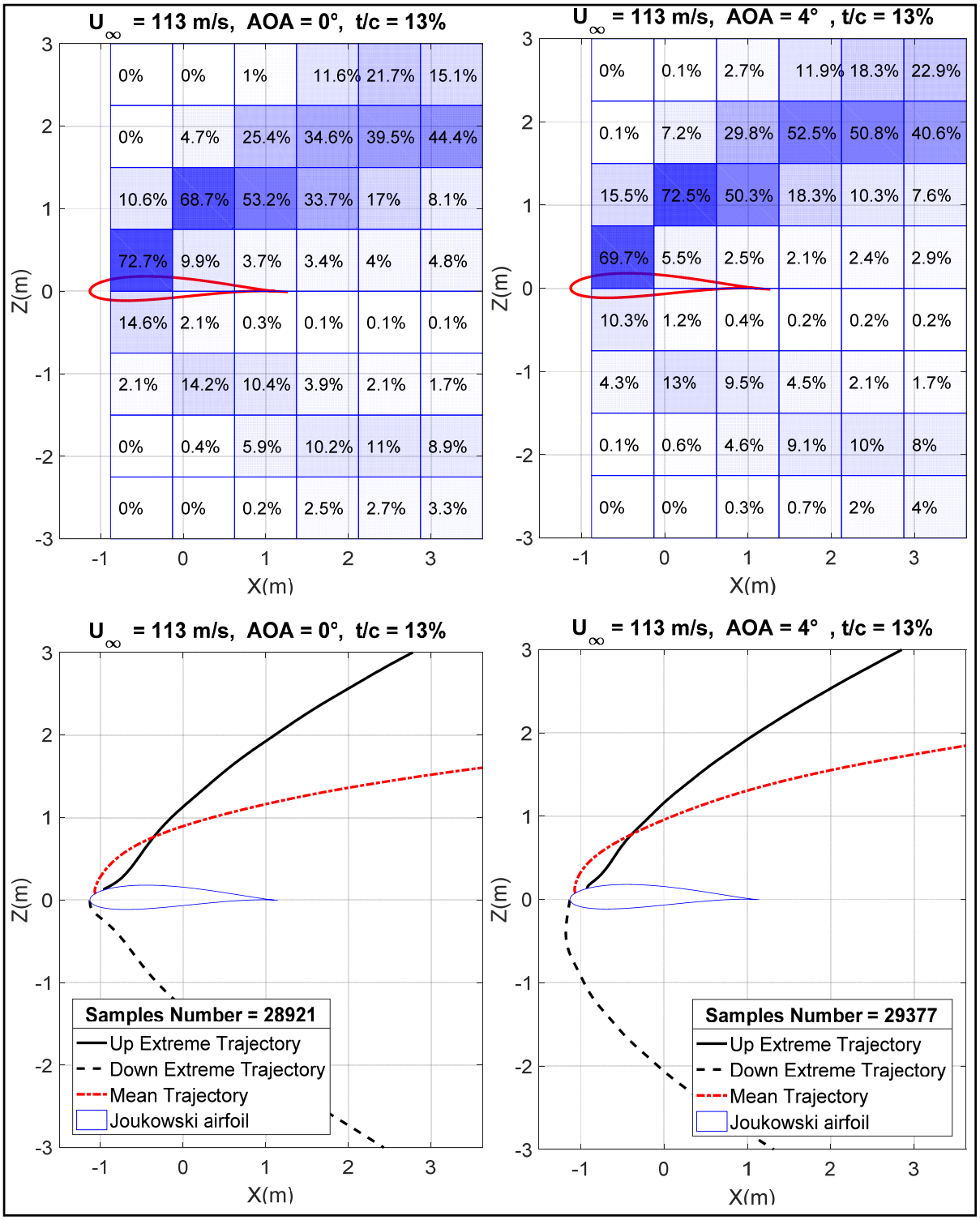

Figure 3.19 Monte-Carlo simulations for square plate ice around the Joukowski airfoil with AOA=0° (left) and AOA= 4° (right), Ice particle $0.1303 \times 0.1303 \times 0.0365\, m$, $m_{ice} = 0.5715\, kg$, $\rho_{air} = 0.770\, kg/m^3$, shedding is from the upside surface of the leading edge, Magnus effect included.

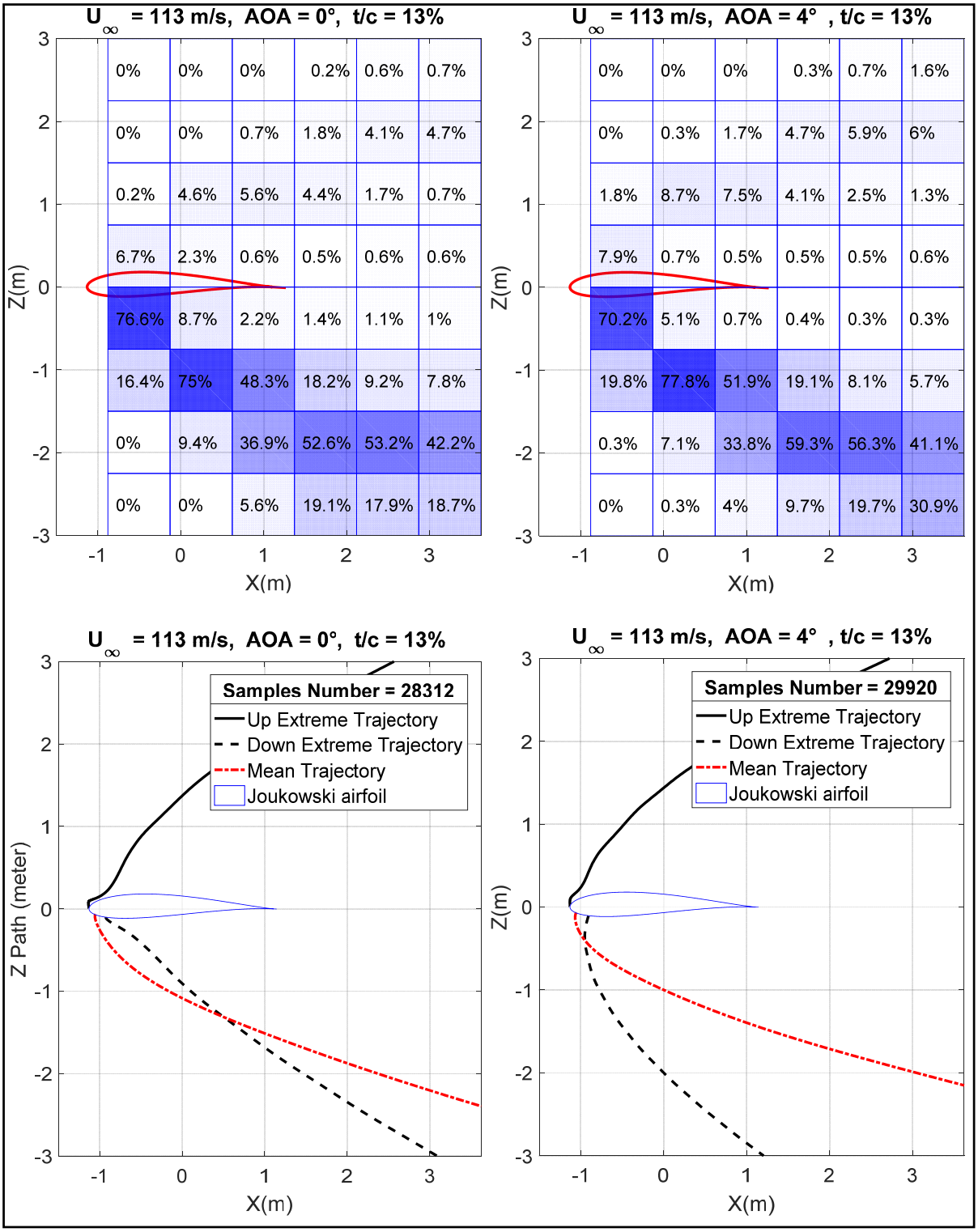

Figure 3.20 Monte-Carlo simulations for square plate ice around the Joukowski airfoil with AOA=0° (left) and AOA= 4° (right), Ice particle $0.1303 \times 0.1303 \times 0.0365\, m$, $m_{ice} = 0.5715\, kg$, $\rho_{air} = 0.770\, kg/m^3$, shedding is from the downside surface of the leading edge, Magnus effect included.

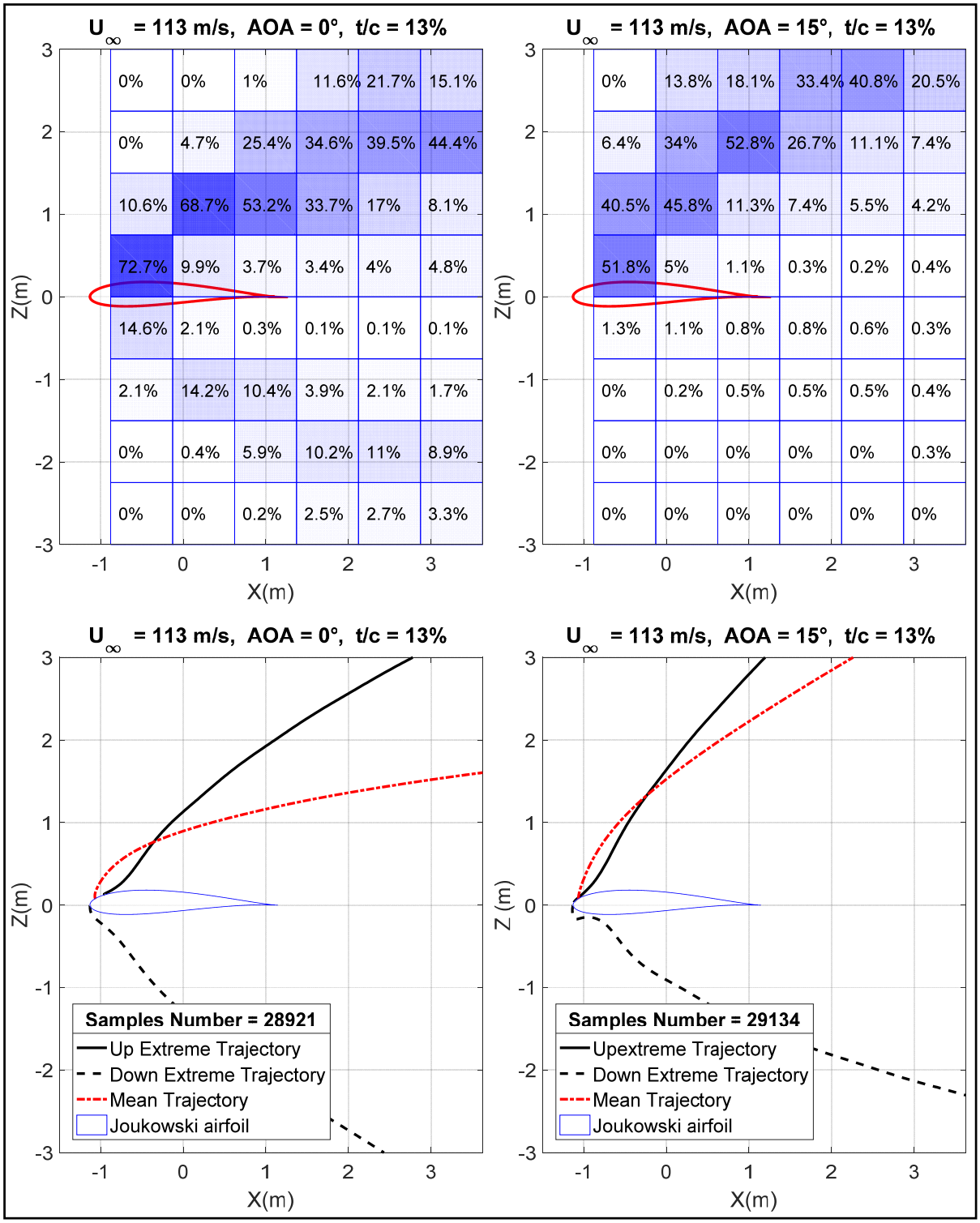

Figure 3.21 Monte-Carlo simulations for square plate ice around the Joukowski airfoil with AOA=0° (left) and AOA=15° (right), Ice particle $0.1303 \times 0.1303 \times 0.0365$ m, $m_{ice} = 0.5715$ kg, $\rho_{air} = 0.770$ kg/m^3, shedding is from the upside surface of the leading edge, Magnus effect included.

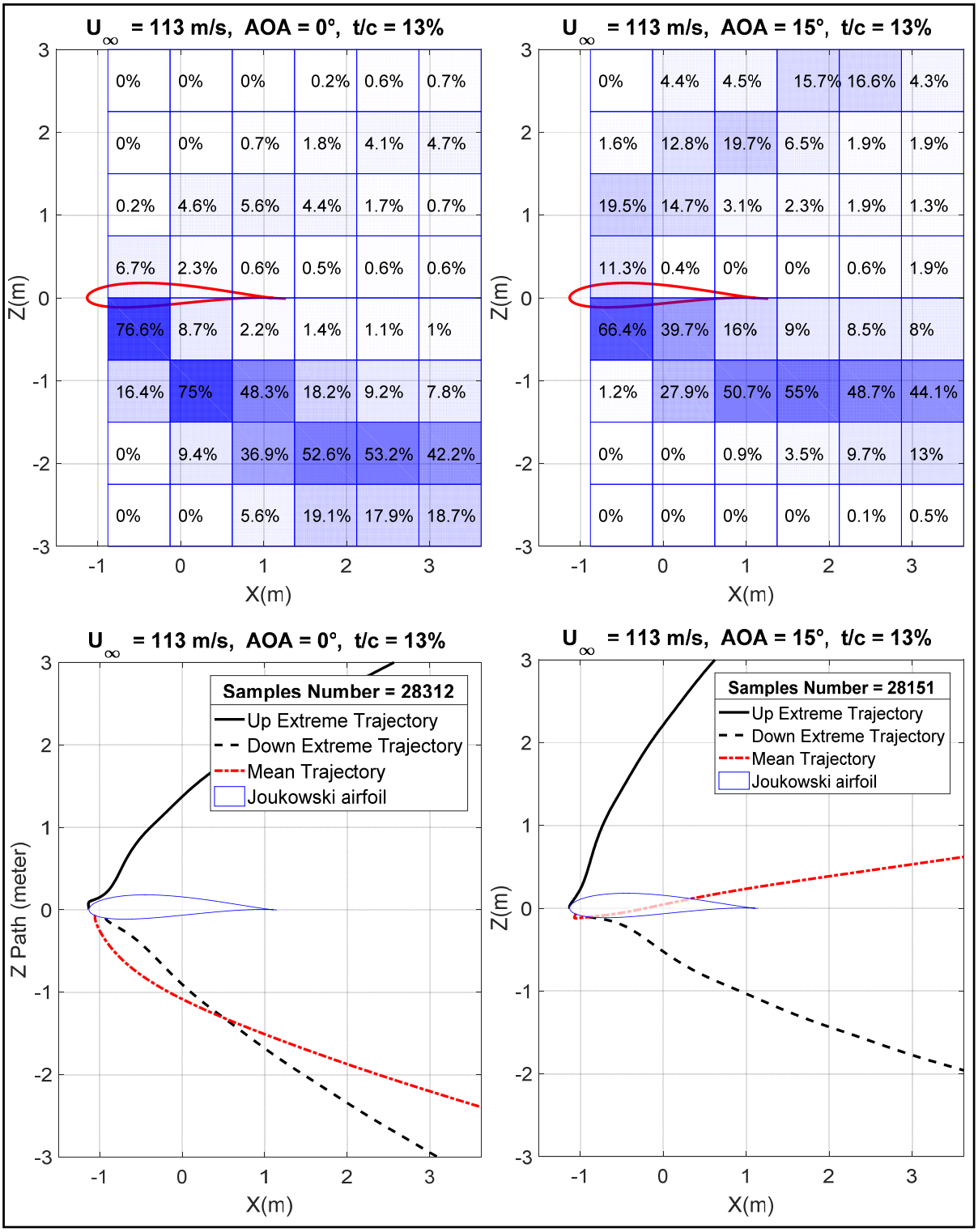

Figure 3.22 Monte-Carlo simulations for square plate ice around the Joukowski airfoil with AOA=0° (left) and AOA=15° (right), Ice particle is $0.1303 \times 0.1303 \times 0.0365\ m$ and $m_{ice} = 0.5715$, $\rho_{air} = 0.770\ kg/m^3$, shedding is from the downside surface of the leading edge, Magnus effect included.

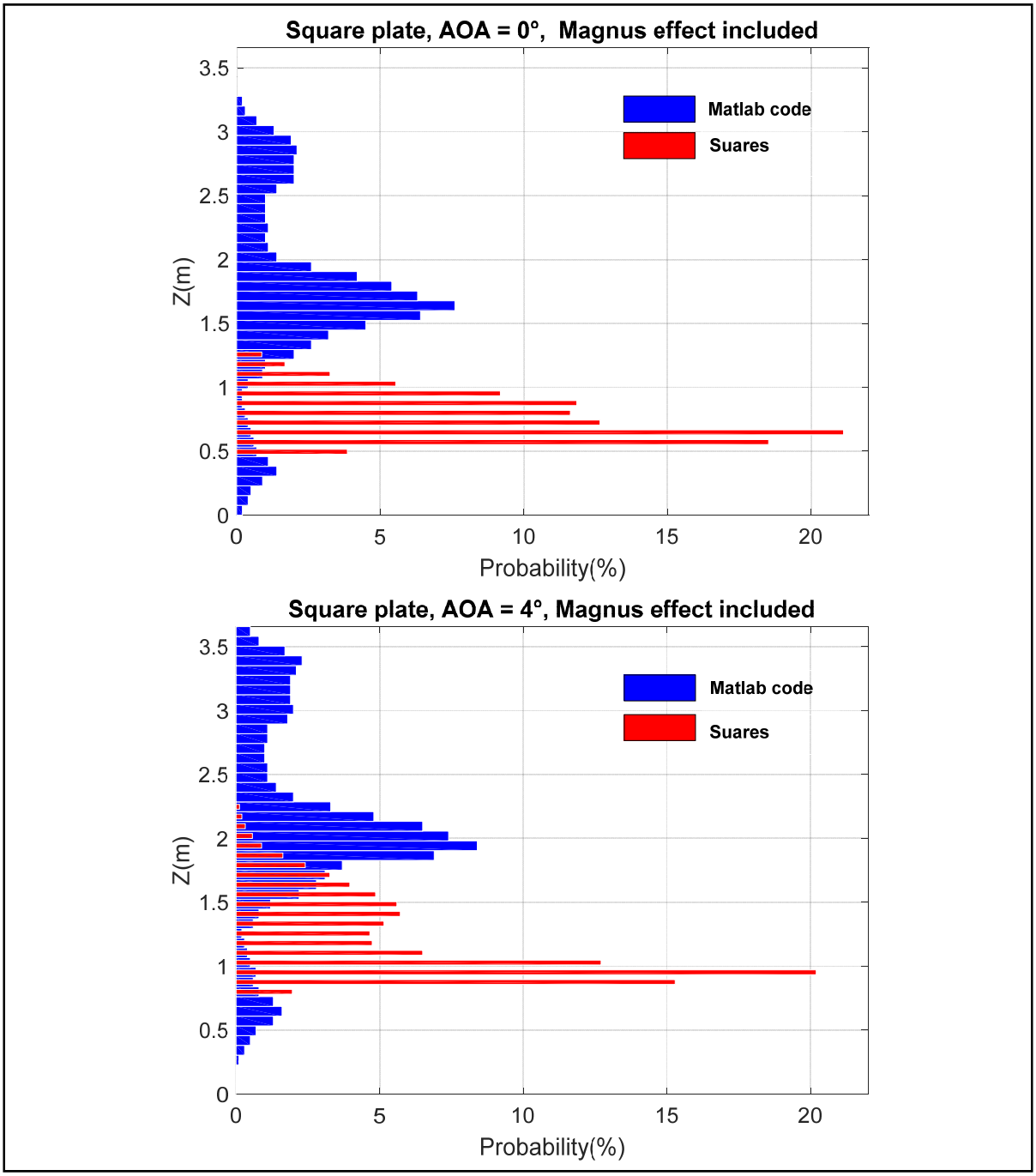

Figure 3.23 Comparison between the results of Suares for trajectories with different angles of attack of airfoils

Figure 3.23 compares the results of the research with those of Suares (Suares, 2005) for square plate ice in the flow field of the airfoils. The parameters of the airfoils, flow fields and ice pieces are the same as section 3.4. The figure compares Monte-Carlo simulations with the results of Suares for clean NACA 23012 airfoil with $AOA = 0°$ and $AOA = 4°$. The ice piece starts its trajectory $0.09\ m$ ahead and $0.122\ m$ above the leading edge of the airfoil. The pass probability of ice is computed at the engine inlet plane $4.45\ m$ downstream of the leading edge. The pass probability on this plane is calculated for intervals with $0.0762\ m$ width.

The varying initial parameters of the Monte-Carlo simulation in the research of Suares (Suares, 2005) are lift and drag coefficients, length and thickness of the ice particle and the initial orientation of the ice piece (between 0 and 90 degrees). The initial varying parameters used in this thesis are presented in section 2.3. The different flow fields and initial conditions have led to different results.

The result shows that parameters used in the research brings about more diverse trajectories regarding their vertical displacement. In the other word, initial linear and angular velocity of the ice piece and its angle of orientation is much more influential than the lift and drag coefficients and the dimension of the ice piece. Although Suares (Suares, 2005) has used the initial angle of the ice piece as an initial parameter in Monte-Carlo simulation but this variation is limited up to 90 degrees while in this research it can vary up to 180 degrees.

In this figure upper plot shows the pass probability when the airfoil's angle of attack is zero and the other plot shows the result of the airfoil with $AOA = 4°$. Although the result of two researches are different but both of them have upward shift in the case of $AOA = 4°$ which means, in this case, the ice particles have more upward vertical movement.

3.5.2 Effect of the thickness of the airfoil on the probability map

This section will present the investigation of the effect of the airfoil's thickness on the probability map of ice trajectory. Simulations will compare an airfoil with t/c = 13 % at 22 % of the cord and another airfoil with t/c = 6.5 % at 22% of the cord. These two airfoils are generated from two cylinders with the same radius but different coordinates for the center of

the cylinders. The center of the thicker airfoil is at $\zeta_0 = -0.0615 + 0.0246i$ and the other is located at $\zeta_0 = -0.03075 + 0.0246i$. The square plate ice piece has a dimension of $0.1303\ \text{m} \times 0.1303\ \text{m} \times 0.0365\ \text{m}$ and a mass of 0.5715 kg. The airflow velocity is $113\ m/s$ and its density is $0.770\ kg/m^3$ (flight altitude is $15000\ ft$).

Figure 3.24 shows the results of Monte-Carlo simulation for ice shedding from the upper side of the leading edge. The angle of attack in these sets of simulations are zero. According to this figure a downward shift for higher pass probability of the ice piece is resulted in narrower airfoil. The ice pieces tend to have less vertical movement in the flow field of the narrower airfoil. The ice ingestion probability by an engine behind the airfoil in this simulation has increased by 0.9%.

Comparing the mean trajectory for these two airfoils shows conflicting results. It can be seen that the mean trajectory has greater vertical movement in the airfoil with 6.5% of thickness. This is due to this fact that greater percentage of ice samples in thicker airfoil go below the airfoil. In thicker airfoil 16.4% of the ice samples go downward and in the narrower airfoil this percentage is 13.3.

Figure 3.25 shows the results when the shedding happens from the down side surface of the leading edge. Again results show closer trajectories to the horizontal axis of the plane. The ice ingestion probability with the engine behind the airfoil has increased (0.2%) but it is not as significant as the previous case when the ice shedding is from the upper surface of the leading edge. Studying the effect of the airfoil's thickness shows a trivial different between two different airfoils with different thicknesses. However, as a general conclusion, the flow filed around a thicker airfoil has greater vertical velocity component which pulls the ice particles more vertically.

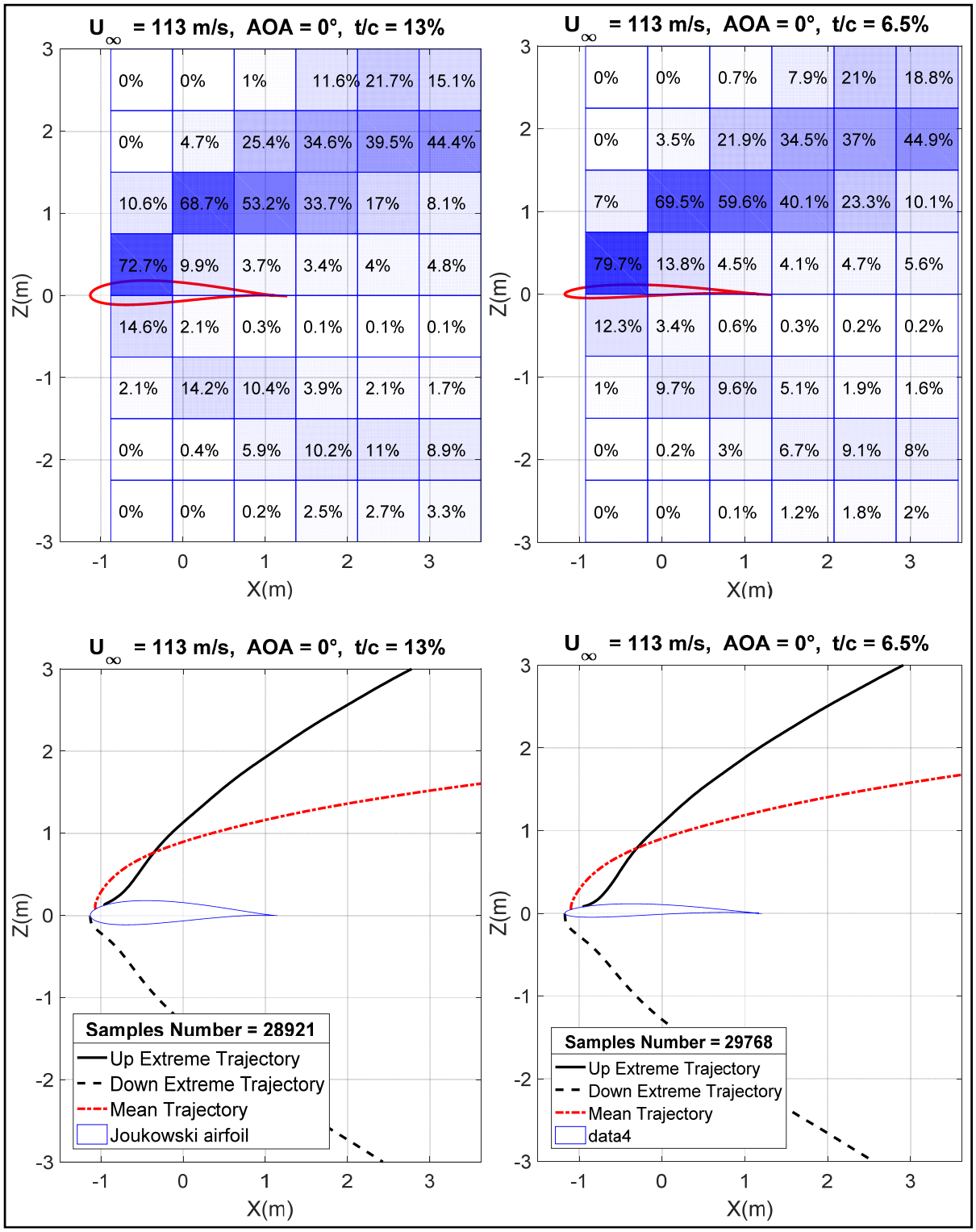

Figure 3.24 Monte-Carlo simulations for square plate ice around the Joukowski airfoil with thickness t/c= 13% (left) and thickness t/c=6.5% (right), Ice particle is $0.1303 \times 0.1303 \times 0.0365\ m$ and $m_{ice} = 0.5715$, $\rho_{air} = 0.770\ kg/m^3$, shedding is from the upside surface of the leading edge, Magnus effect included.

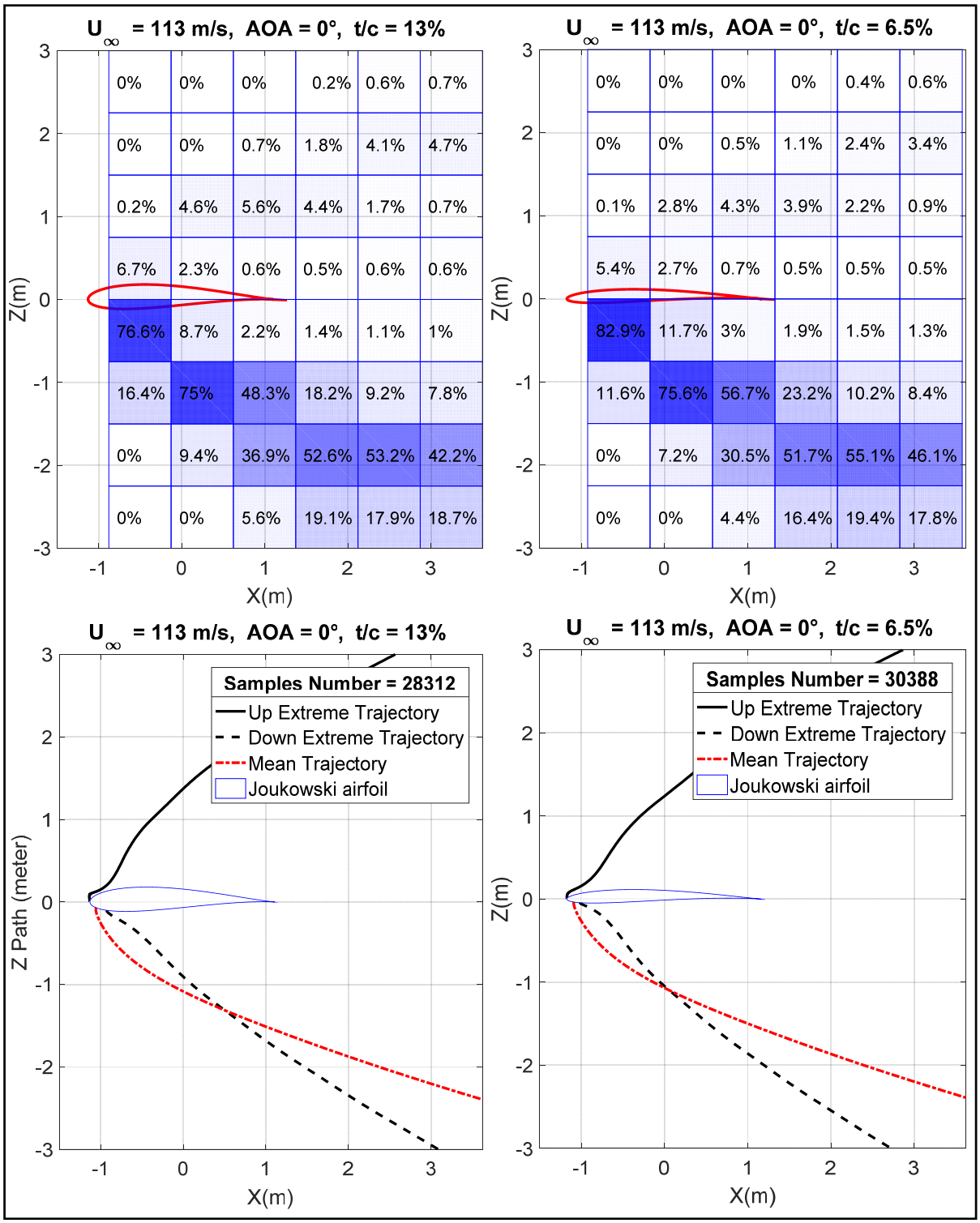

Figure 3.25 Monte-Carlo simulations for square plate ice around the Joukowski airfoil with thickness t/c= 13% (left) and thickness t/c=6.5% (right), Ice particle is $0.1303 \times 0.1303 \times 0.0365$ m and $m_{ice} = 0.5715$, $\rho_{air} = 0.770$ kg/m^3, shedding is from the downside surface of the leading edge, Magnus effect included.

3.5.3 Effect of the camber of the airfoil on the probability map

In section 3.4.3 the impact of the airfoil's camber on a single trajectory was inspected. In this section the results obtained from Monte-Carlo simulations for two airfoils with different cambers will be presented. In this order resulted figures will compare a curved airfoil with a symmetric airfoil. The square plate ice piece has a dimension of $0.1303\ \text{m} \times 0.1303\ \text{m} \times 0.0365\ \text{m}$ and a mass of 0.5715 kg. The airflow velocity is $113\ m/s$ and its density is $0.770\ kg/m^3$ (flight altitude is $15000\ ft$).

The curved airfoil is generated from a cylinder with $R = 0.615\ m$ and $\zeta_0 = -0.0615 + 0.246i$. The symmetric airfoil has the same radius but its center is located on $\zeta_0 = -0.0615 + 0.000001i$. The thickness for both airfoils is 13% at 22% of the airfoil's cord and the angle of attack for both cases is zero degree.

Based on the results of the section 3.4.3 for single trajectory a higher vertical displacement in the flow filed of a curved airfoil is expected. By comparing the results in figure 3.26 and 3.27 the same results for Monte-Carlo statistical method are obtained.

Figure 3.26 shows the probability map of two airfoils with different cambers when the ice shedding occurs from the upper surface of the leading edge. The probability map shows a greater percentage of ice pass probability in the areas closer to the horizontal axis. The ice ingestion by an engine behind the airfoil is 0.9% more likely in the flow field of a symmetric airfoil.

Figure 3.27 is an illustration for the results of ice trajectories when the ice pieces shed from the downside surface of the leading edge. In this case majority of the ice samples travel in the flow field, below the airfoil. as the camber of the symmetric airfoil is downward in the downside of the airfoil more downward vertical velocity component in this airfoil are resulted. Comparing the probability maps in this figure confirms that the ice samples tend to go farther from the horizontal axis when are shed from the downside surface of the symmetric airfoil which decreases the ice ingestion probability by an engine behind the airfoil. However, this effect is not significant and ice ingestion possibility decreases just by 0.4%.

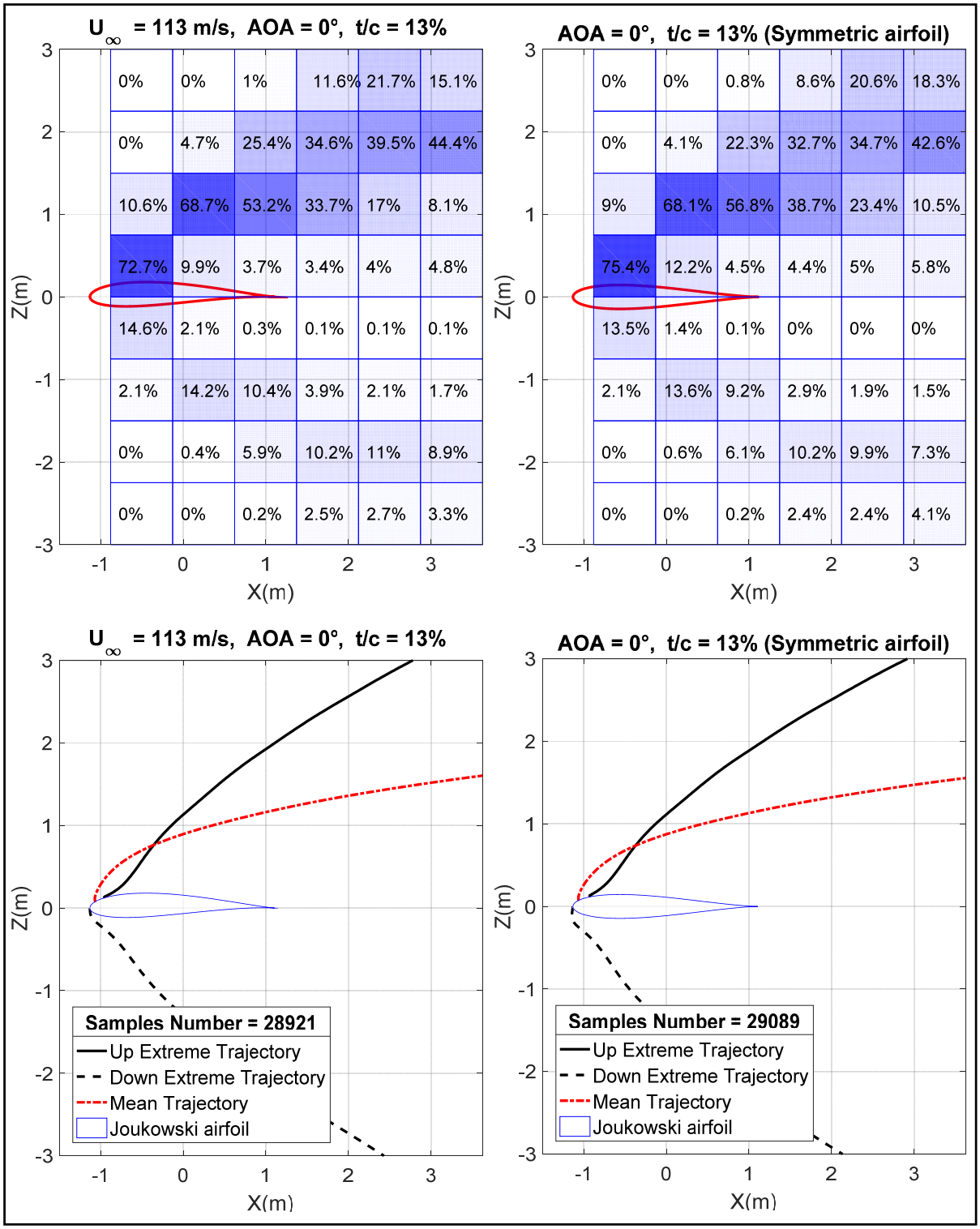

Figure 3.26 Monte-Carlo simulations for square plate ice around the curved (left) and symmetric (right) Joukowski airfoil, Ice particle is $0.1303 \times 0.1303 \times 0.0365\ m$ and $m_{ice} = 0.5715$, $\rho_{air} = 0.770\ kg/m^3$, shedding is from the upside surface of the leading edge, Magnus effect included.

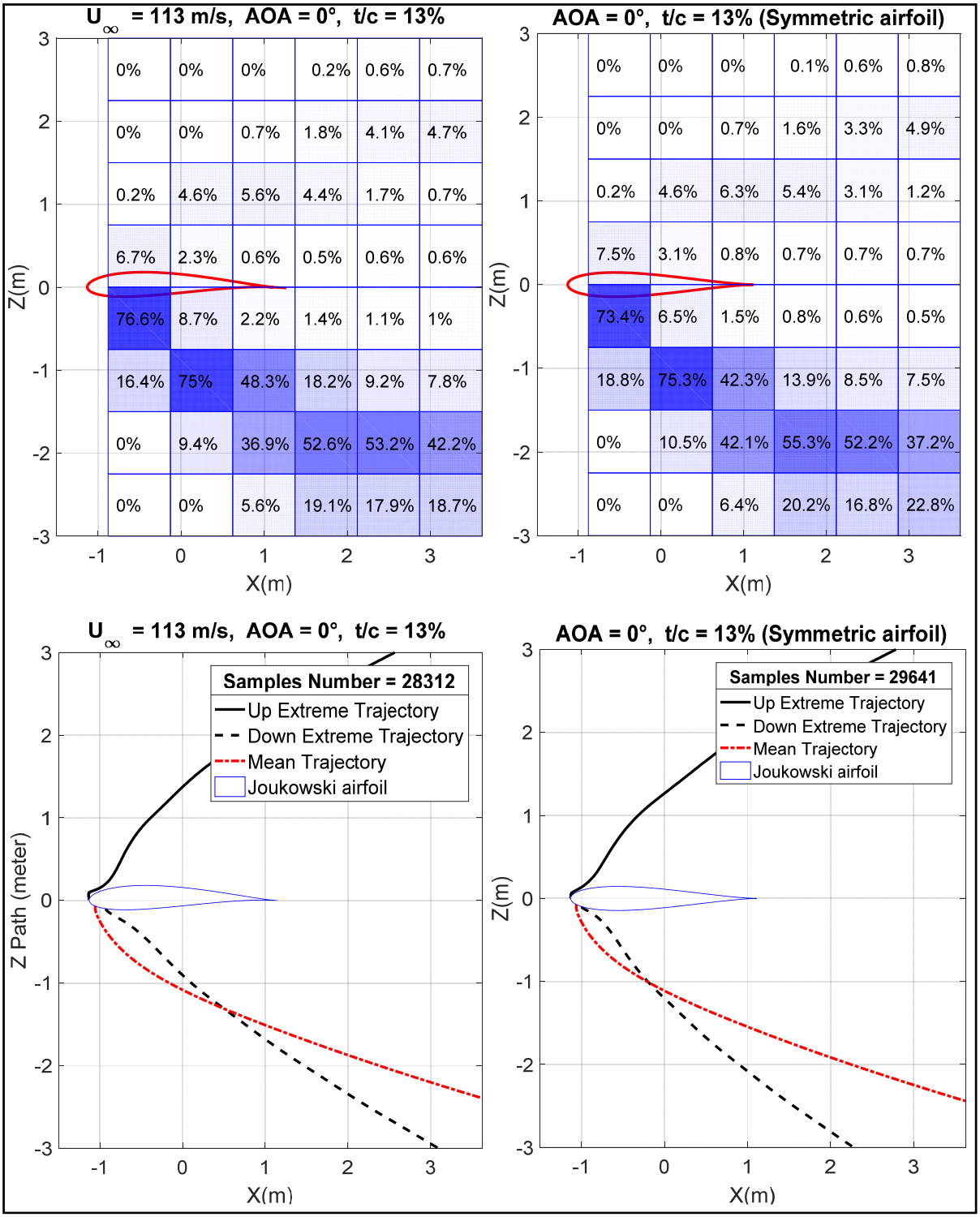

Figure 3.27 Monte-Carlo simulations for square plate ice around the curved (left) and symmetric (right) Joukowski airfoil, Ice particle is $0.1303 \times 0.1303 \times 0.0365\ m$ and $m_{ice} = 0.5715$, $\rho_{air} = 0.770\ kg/m^3$, shedding is from the downside surface of the leading edge, Magnus effect included.

3.5.4 Effect of the ice piece's size on the probability map

In previous three sections, the effect of the airfoil's geometry as well as its angle of attack on the ice pass probability map were studied. Next three sections will show how the shape and mass of the ice piece and Magnus effect can change the percentages in the probability map.

Figure 3.28 and 3.29 compare the results between Monte-Carlo simulations for two different ice pieces. These two ice pieces differ in mass and volume. The graphs on the left side of the figure are the results of a square plate with a dimension of $0.1303\ m \times 0.1303\ m \times 0.0365\ m$ and a mass of 0.5715 kg and the right side of the figure shows results for a square plate with half of this dimension and mass. The airflow velocity is $113\ m/s$ and its density is $0.770\ kg/m^3$ (flight altitude is $15000\ ft$).

According to figure 3.28 smaller ice particles shed from the upper surface of the leading edge have less vertical displacement in the same flow field. The pass probability in the regions near to the horizontal axis has raised. The strike probability with the engines behind the airfoil has increased by 1.2 %. The mean trajectory has a significant downward shift in the case of smaller ice piece.

Figure 3.29 shows the same comparison but for ice pieces shed from downside surface of the leading edge. The same differences in the force components on the ice piece cause less upward movement of the smaller ice piece. The smaller ice pieces lose their altitude more rapidly which brings about their divergence from the horizontal axis of the plane. The ice ingestion probability by an engine behind the airfoil drops by 0.8%. The comparison of the mean trajectory shows a downward shift for the smaller ice piece.

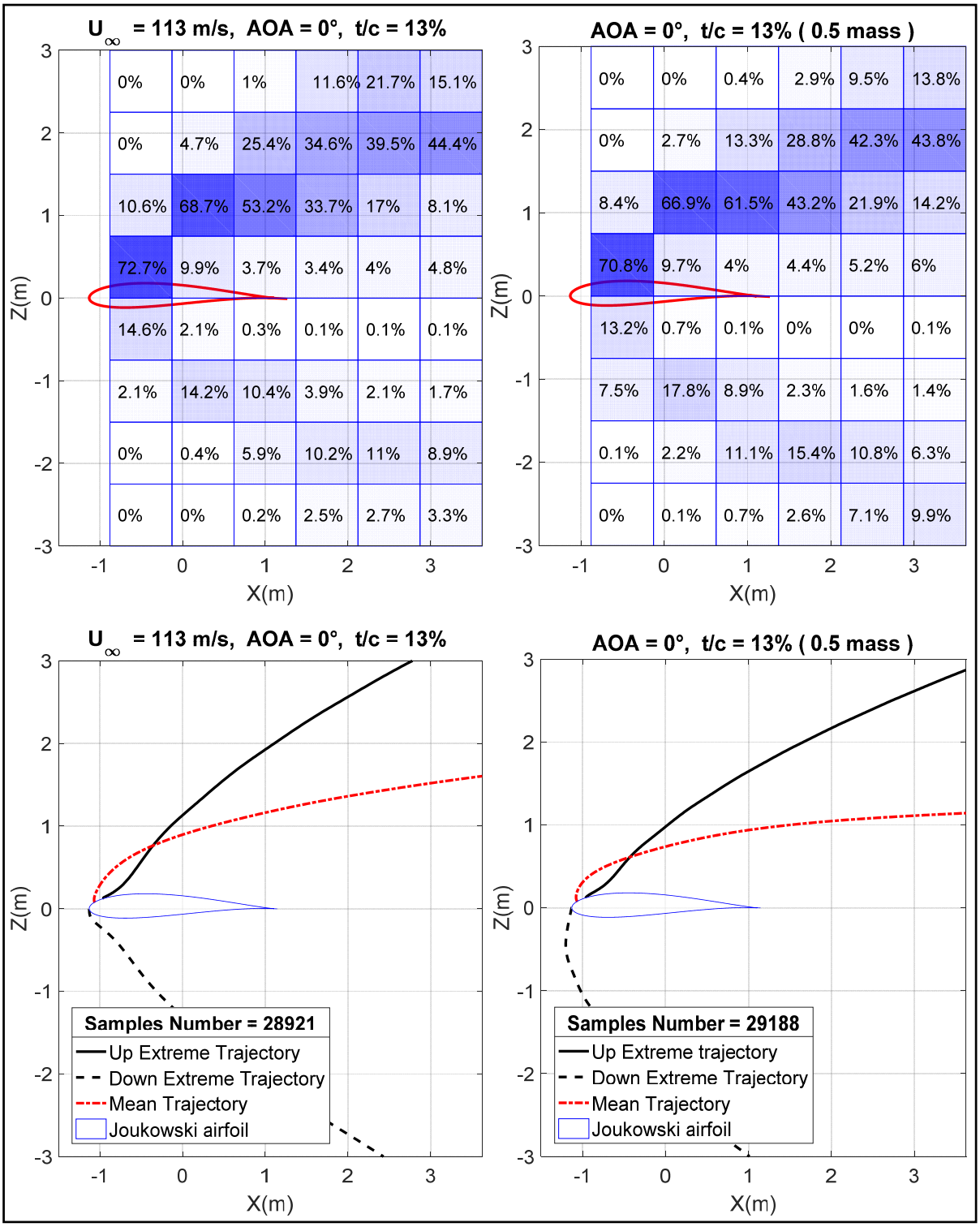

Figure 3.28 Monte-Carlo simulations for different square plate ices around the Joukowski airfoil, left: Ice particle $0.1303 \times 0.1303 \times 0.0365\ m$ and $m_{ice} = 0.5715$, right: Ice particle $6.5 \times 6.5 \times 1.8\ mm$ and $m_{ice} = 0.2857$, $\rho_{air} = 0.770\ kg/m^3$, shedding is from the upside surface of the leading edge, Magnus effect included.

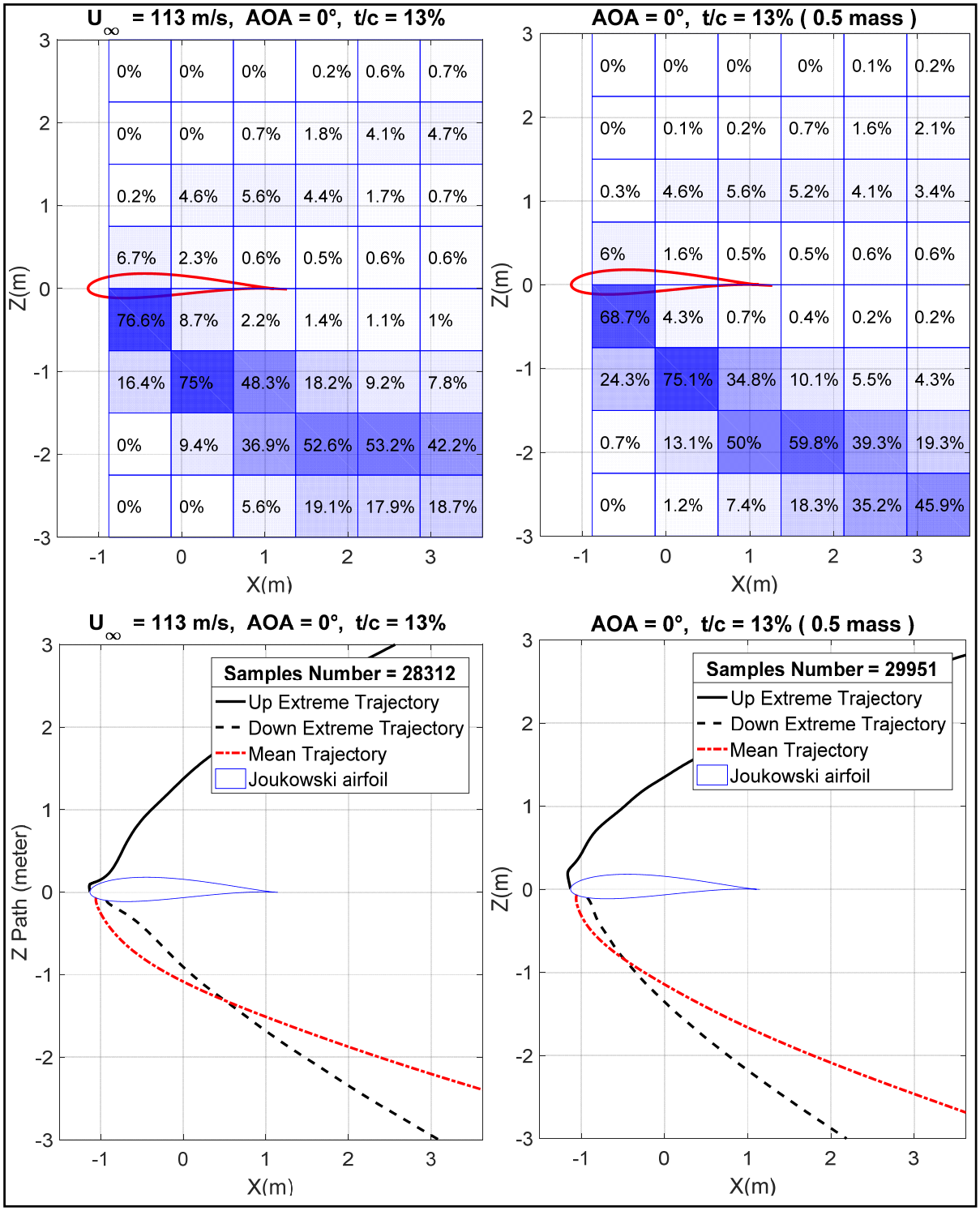

Figure 3.29 Monte-Carlo simulations for different square plate ices around the Joukowski airfoil, left: Ice particle $0.1303 \times 0.1303 \times 0.0365\ m$ and $m_{ice} = 0.5715$, right: Ice particle $0.065 \times 0.065 \times 0.018\ m$ and $m_{ice} = 0.2857$, $\rho_{air} = 0.770\ kg/m^3$, shedding is from the downside surface of the leading edge, Magnus effect included.

3.5.5 Effect of the Magnus coefficients on the probability map

This section is dedicated to compare the ice pass probability maps of the square plate ice piece around the Joukowski airfoil with and without the Magnus effect. As there is not a complete agreement in the literature to include this coefficient on the calculation of the force components on the ice piece, results will show how influential is this effect on the ice trajectory simulation models.

Figure 3.30 compares the results for ice trajectory simulations with and without Magnus effect when the ice pieces are shed from the upside surface of the leading edge. The plot for the trajectories without Magnus effect shows that trajectories tend to be more concentrated. It can be seen that 64.9% of the trajectories exit from the study plane through the same altitude interval between $z = 1.5\ m$ and $z = 2.25\ m$.

Trajectories which are not influenced by Magnus effect are 4.7% less probable to be ingested by an engine behind the airfoil on the horizontal axis. On the other hand, although without Magnus effect, the ice pieces are less seen near the horizontal axis but the mean trajectory has a downward shift in this case.

Figure 3.31 presents the results for this simulation when the shed ices are located on the downside surface of the leading edge. Again in this case, trajectories have more diverse altitudes in their trajectories when Magnus effect is included. When the Magnus effect is not included 86.7% of the trajectories leave the study plane, having an altitude between $z = -1.5\ m$ and $z = -3\ m$, while this percentage for cases with Magnus effect is 60.9 %. Although the mean trajectory has an upward shift toward the horizontal axis, the strike probability of the ice piece with an engine located behind the airfoil has decreased without Magnus effect. While this probability for trajectories with Magnus effect is 1.6 %, any ice piece samples in our simulation has not been ingested by the engine when Magnus effect is not included.

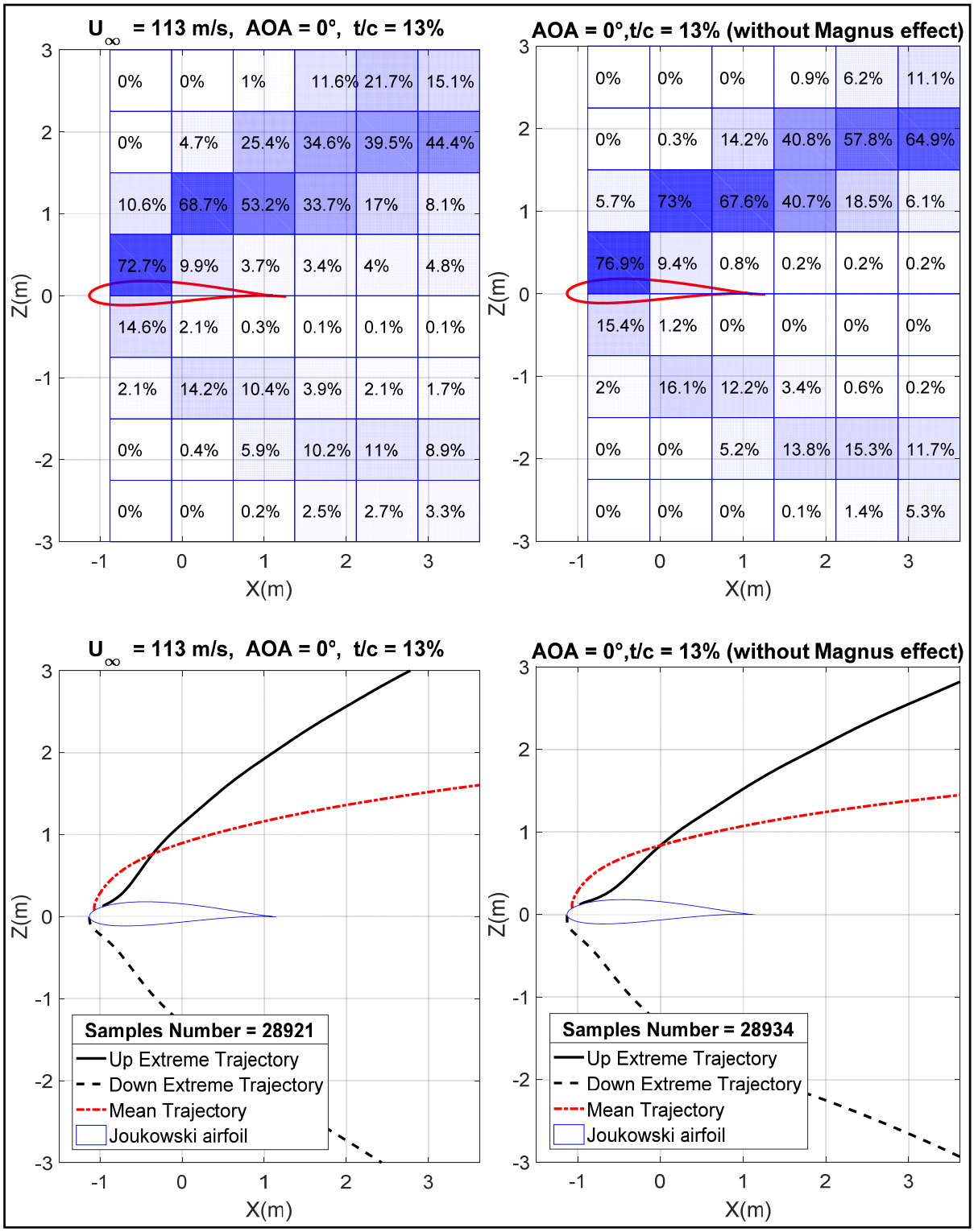

Figure 3.30 Monte-Carlo simulations for square plate ice around the Joukowski airfoil with (left) and without (right) Magnus effect, Ice particle $0.1303 \times 0.1303 \times 0.0365\ m$, $m_{ice} = 0.5715\ kg$, $\rho_{air} = 0.770\ kg/m^3$, shedding is from the upside surface of the leading edge.

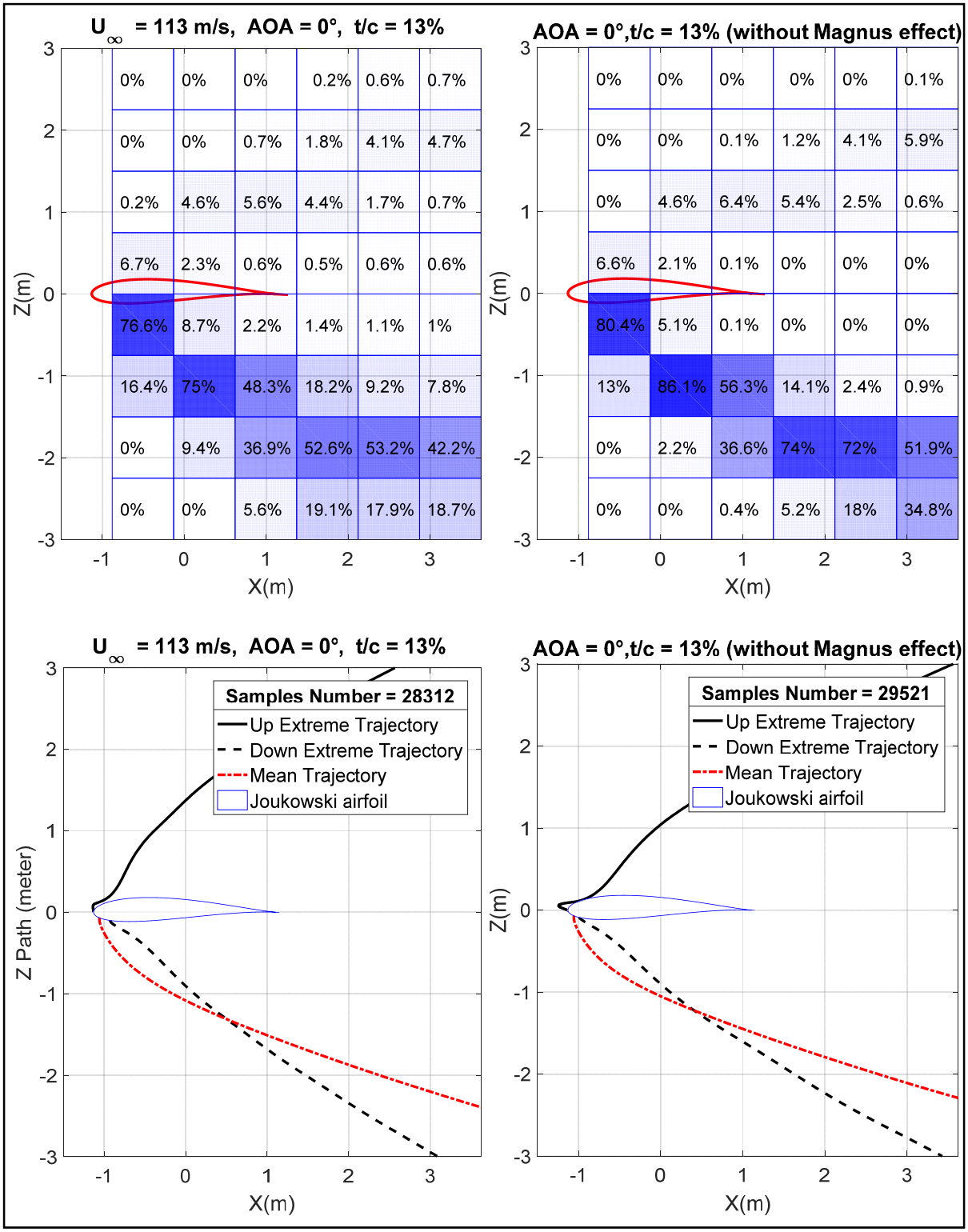

Figure 3.31 Monte-Carlo simulations for square plate ice around the Joukowski airfoil with (left) and without (right) Magnus effect, Ice particle $0.1303 \times 0.1303 \times 0.0365\ m$, $m_{ice} = 0.5715\ kg$, $\rho_{air} = 0.770\ kg/m^3$, Shedding is from the downside surface of the leading edge

3.5.6 Effect of the ice shape on the probability map

The other significant parameter to influence the trajectory of the ice piece is its shape. Each shape of ice has its own aerodynamic coefficients which result in different induced forces and accelerations. Chapter two presented the aerodynamic coefficients for rectangular and sphere ice pieces in chapter three as well as the main ice shape of the research which is a square plate. This section will compare the results of Monte-Carlo simulation for these different ice shapes. The properties of the ice pieces are presented in table 2.2.

Figure 3.32 depicts the result of Monte-Carlo simulation for a sphere ice piece. As in this case higher percentage of the ice samples hit the airfoil itself, the initial number of samples is raised to 80,000. The other different parameter in this case is the initial velocity of the ice piece. The acceleration of the sphere ice piece is significantly less than the other two ice shapes used in the research due to smaller aerodynamic forces. The range of variation for an initial velocity of the sphere ice piece is reduced to being more proportional to its final velocity during its trajectory. In this order 0.01 of the free stream's velocity is used instead of 0.03 of this velocity for the initial velocity of the ice particle.

The probability map on the left side of the figure presents the trajectories initiated from the upper surface of the airfoil. As mentioned in the section 2.5.7 sphere ice piece is moved by drag force and aerodynamic coefficients for lift and moment for this shape of the ice piece are zero. It can be seen that the sphere ice pieces cannot reach high altitude in their trajectory and tend to fall down vertically due to small induced drag forces. The ice ingestion by an engine located behind the airfoil is 48.6%.

The left side of the figure 3.32 illustrates the result for the sphere ice pieces when are shed from the downside surface of the leading edge. A huge number of the trajectories hit the airfoil and only 6675 (out of 80,000) ice samples remain in the Monte-Carlo simulation. 10.9% of the ice samples have trajectories above the airfoil which follow almost the same trajectories as the case when shedding is from the upper surface of the leading edge and impose ingestion risk by an engine behind the airfoil. The ices below the airfoil have more downward vertical movement which are significantly less probable to be ingested by an engine behind the airfoil.

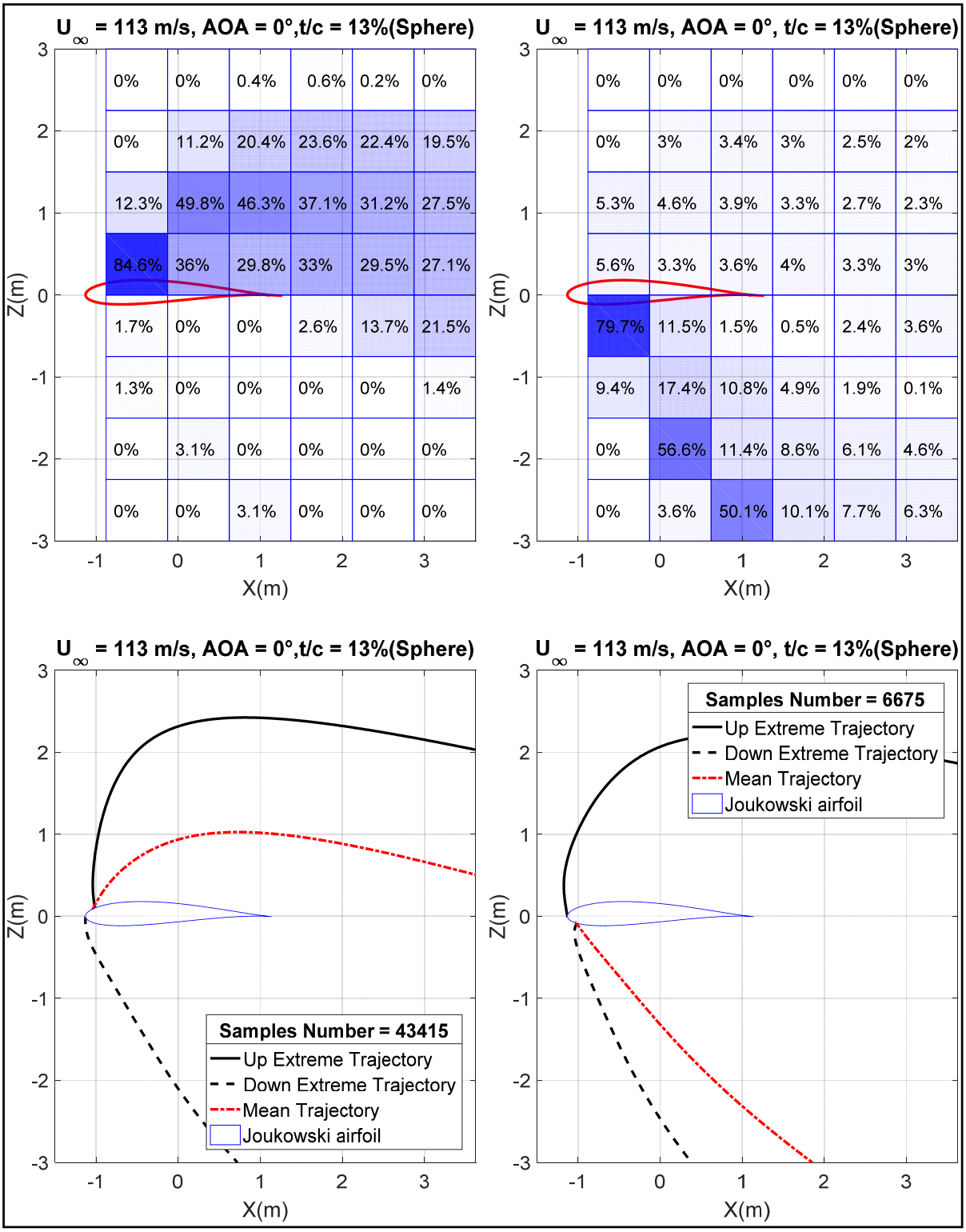

Figure 3.32 Monte-Carlo simulations for sphere ice piece around the Joukowski airfoil, shedding from upside (left) and downside (right) surface of the leading edge, Ice particle $D = 0.106\ m$, $m_{ice} = 0.5715\ kg$, $\rho_{air} = 0.770\ kg/m^3$

In the section 2.2.7 aerodynamic coefficients for the rectangular ice piece were introduced. Using those relations, Monte-Carlo simulation is run for rectangular ice piece.

The square plate ice piece has a dimension of 0.1303 m $\times$ 0.1303 m $\times$ 0.0365 m and a mass of 0.5715 kg. The rectangular plate ice piece has a dimension of $0.1303 \times 0.2606 \times 0.0365$ m with half of the mass density of the square plate ice piece. This means that despite different ice dimensions, both the samples have the same mass. The air free stream velocity is 113 m/s and its density is 0.770 kg/m^3.

Figure 3.33 compares the pass probability map of the square and rectangular ice piece when the trajectories are initiated from the upper side of the leading edge. As shown in the figure, although the mean trajectories in both cases (square and rectangular) are almost the same but rectangular ice particle are more probable to strike an engine behind the airfoil (25.8 %).

Figure 3.34 shows the results for rectangular and square ice pieces when the ices are shed from the downside surface of the leading edge. Although rectangular samples have more downward vertical displacement but higher percentage of these ice pieces are prone to be ingested by an engine behind the airfoil. Comparison between the mean trajectories for both ice shapes does not show substantial differences.

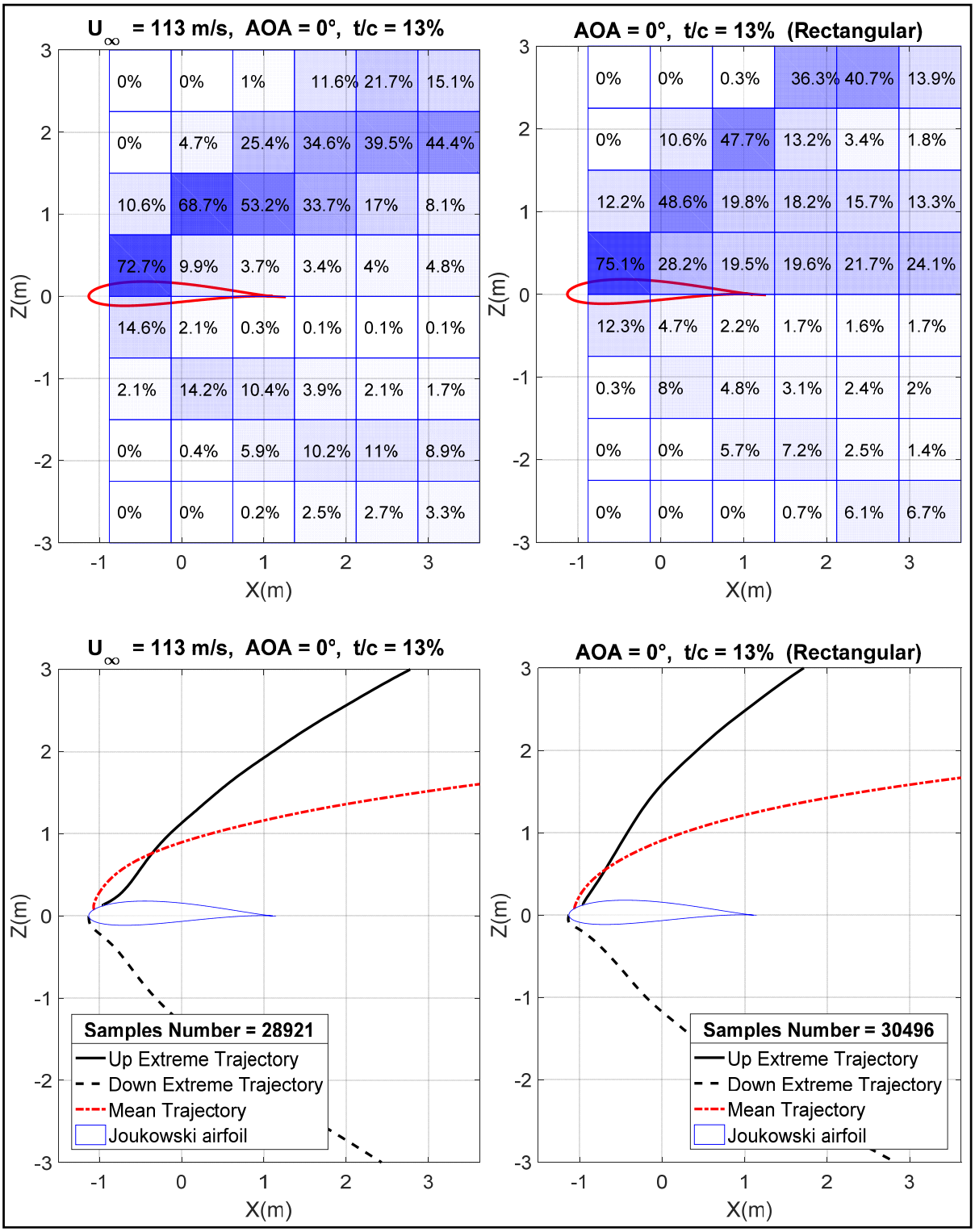

Figure 3.33 Monte-Carlo simulations for square (left) and rectangular ice piece (right) around the Joukowski airfoil, shedding is from upside surface of the leading edge, rectangular ice; $0.130 \times 0.260 \times 0.036\ m$, $m_{ice} = 0.5715\ kg$, $\rho_{air} = 0.770\ kg/m^3$, Magnus effect included

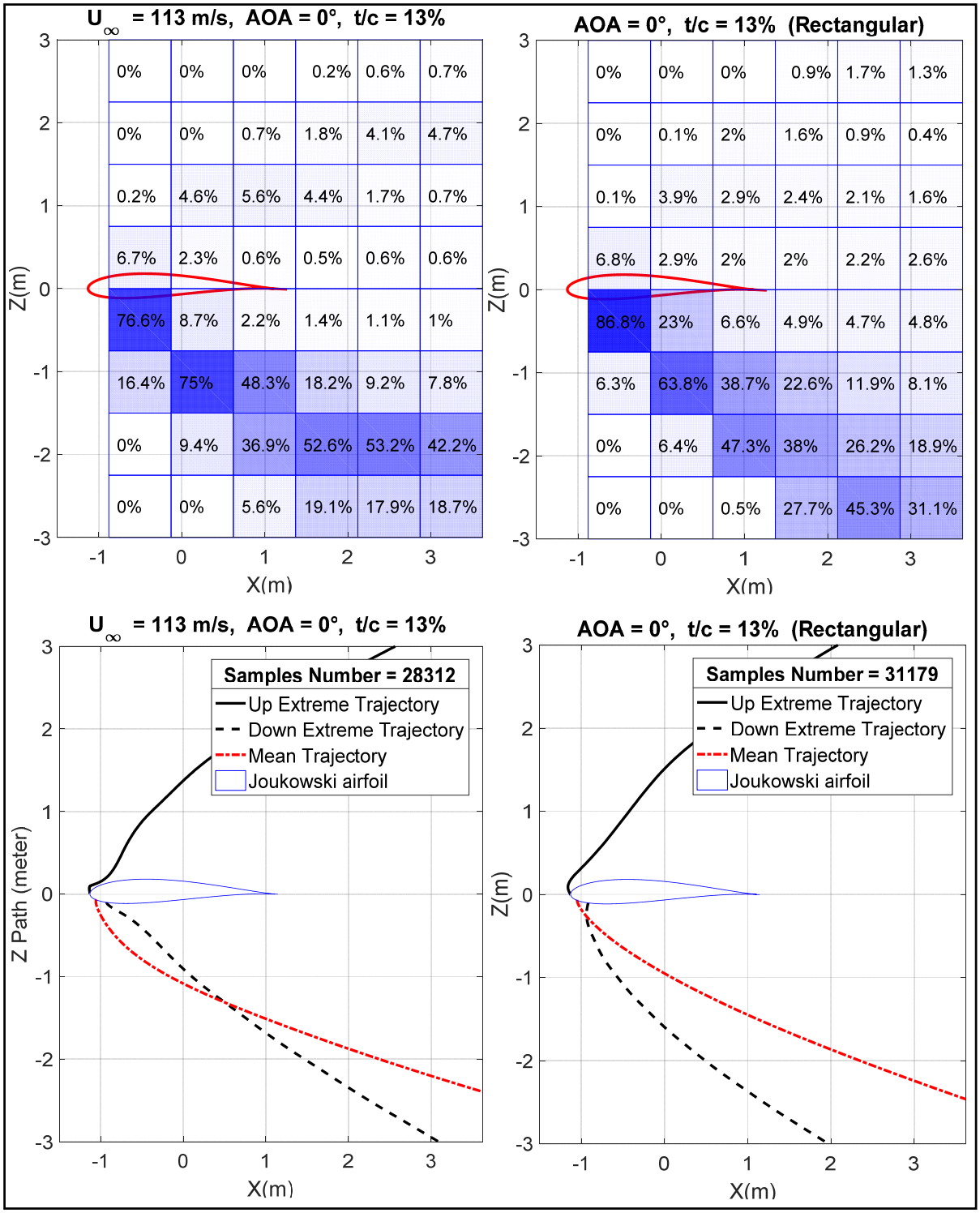

Figure 3.34 Monte-Carlo simulations for square (left) and rectangular ice piece (right) around the Joukowski airfoil, shedding is from downside surface of the leading edge, rectangular ice $0.13 \times 0.26 \times 0.036\, m$, $m_{ice} = 0.5715\, kg$, $\rho_{air} = 0.770\, kg/m^3$, with Magnus effect

Figure 3.35 shows the results of the research and result of the Suares (Suares, 2005) for rectangular ice particles. As mentioned in the section 3.5.1 the initial uncertainties used for Monte-Carlo simulation are different in two researches which yield two different results. Again the result of the Suares (Suares, 2005) shows the concentration of ice pieces in a small area in the plane of the engine which can be because of similar initial parameters.

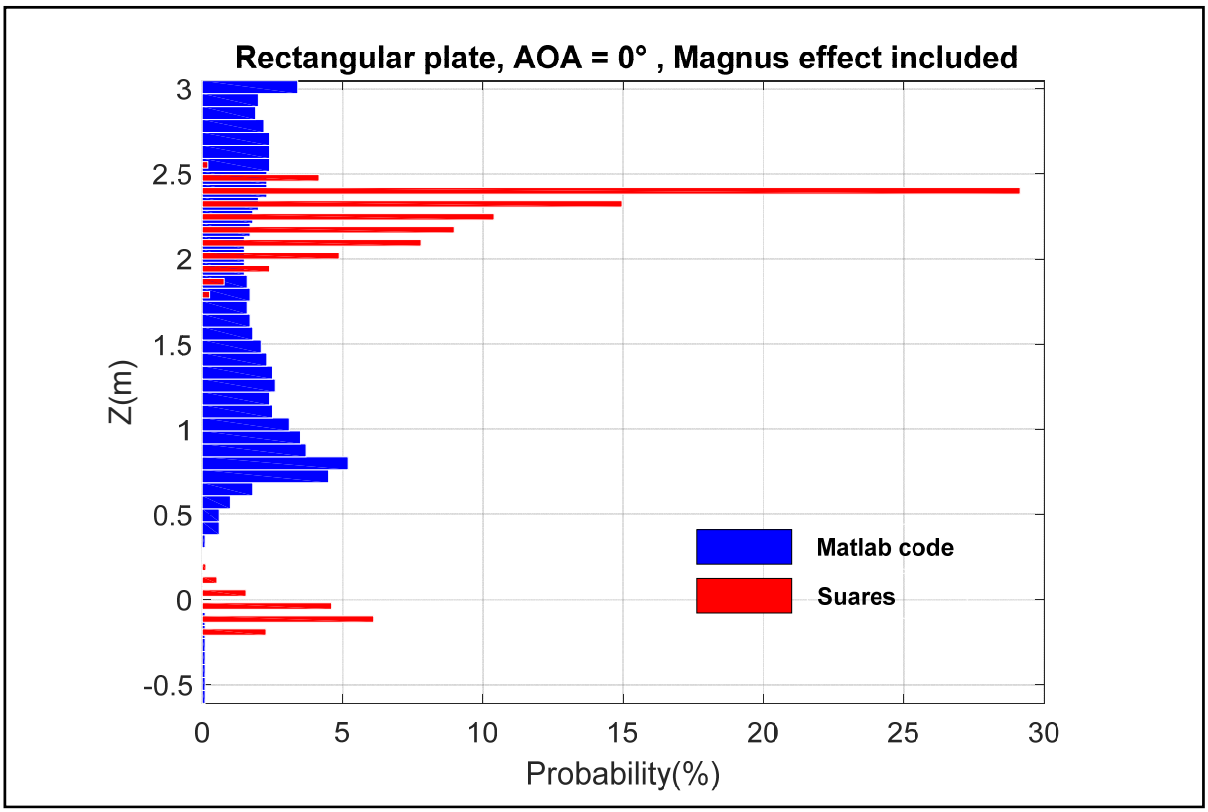

Figure 3.35 Comparison with the results of Suares for trajectories of rectangular ice plate

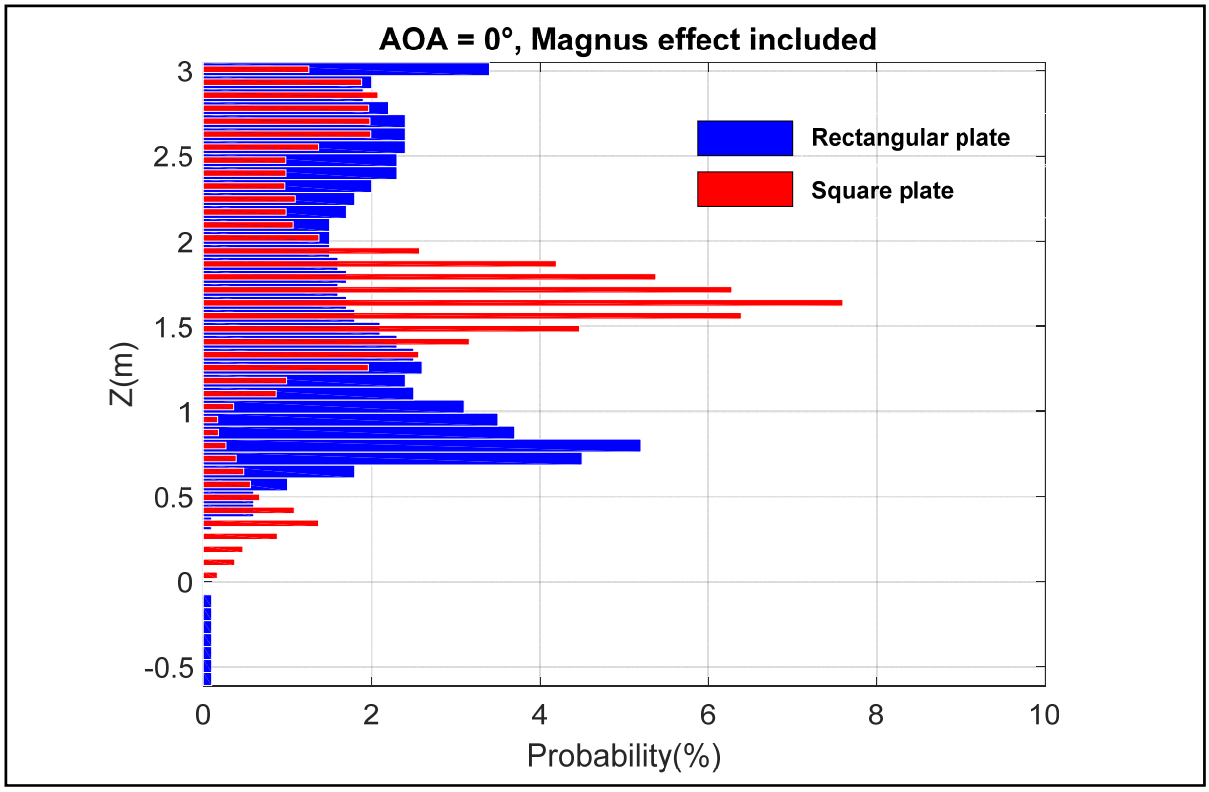

Figure 3.36 Comparison of the Monte-Carlo simulations for square and rectangular ice plates

Figure 3.36 compares the ice pass probability of the square and rectangular ice pieces in the plane of the engine's inlet. Rectangular ice pieces are more probable to be seen near the horizontal axis which increases the risk of ice ingestion by engines. This result can be seen in the probability map in the figure 3.33. Although the ice shedding position in two simulations are different but in both of them ice ingestion risk is higher in the case of rectangular ice shape.

3.5.7 Effect of the normal random initial conditions on the probability map

In previous sections the effect of different parameters on the ice trajectory and ice ingestion probability by the engine behind the airfoil were studied. In all these sections, the random numbers generated for Monte-Carlo simulation were obtained by uniform distribution. Most of the research related to ice trajectory simulations have used uniform random numbers to generate random initial parameters for the ice trajectory (Shimoi, 2010), (Suares, 2005). As

introduced in the chapter of methodology, random numbers can be generated by normal distribution too. Following is the comparison of these two methods and their effect on the probability map of ice trajectory around the airfoil.

Figure 3.37 shows the results for Monte-Carlo simulations with uniform random numbers and Monte-Carlo simulation with normal random numbers. The ice shedding is from the upper surface of the airfoil. As can be seen in Monte-Carlo simulation with normal random numbers, ice pieces are more concentrated in an area. This means that initial conditions in uniform distribution are more different than normal distribution which lead to more divers trajectories. Although there is a significant difference between two probability maps but the ice ingestion risk by the engine is estimated only 0.5% less using normal random numbers.

Figure 3.38 shows the ice trajectory probability maps when the shedding occurs from downside surface of the airfoil. The same difference can be observed in this figure as figure 3.37. The concentration of the ice pieces means more similar initial conditions when the Monte-Carlo simulation uses normal random numbers. The ice ingestion probability by the engine is estimated only 0.3% more using normal random numbers.

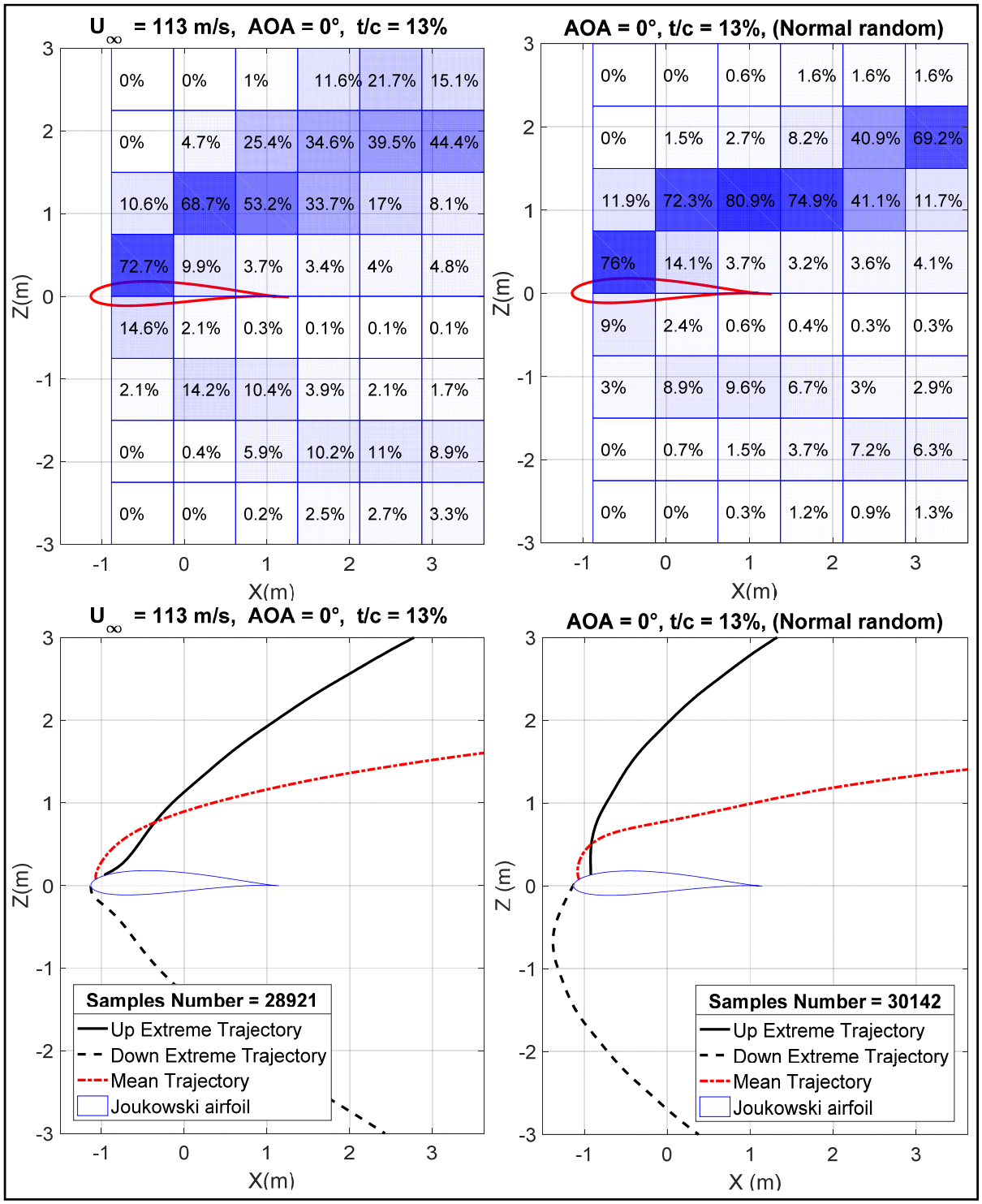

Figure 3.37 Comparison of Monte-Carlo simulations with uniform and normal random numbers , shedding is from upside surface of the leading edge, Ice particle $0.1303 \times 0.1303 \times 0.0365\ m$, $m_{ice} = 0.5715\ kg$, $\rho_{air} = 0.770\ kg/m^3$, Magnus effect included

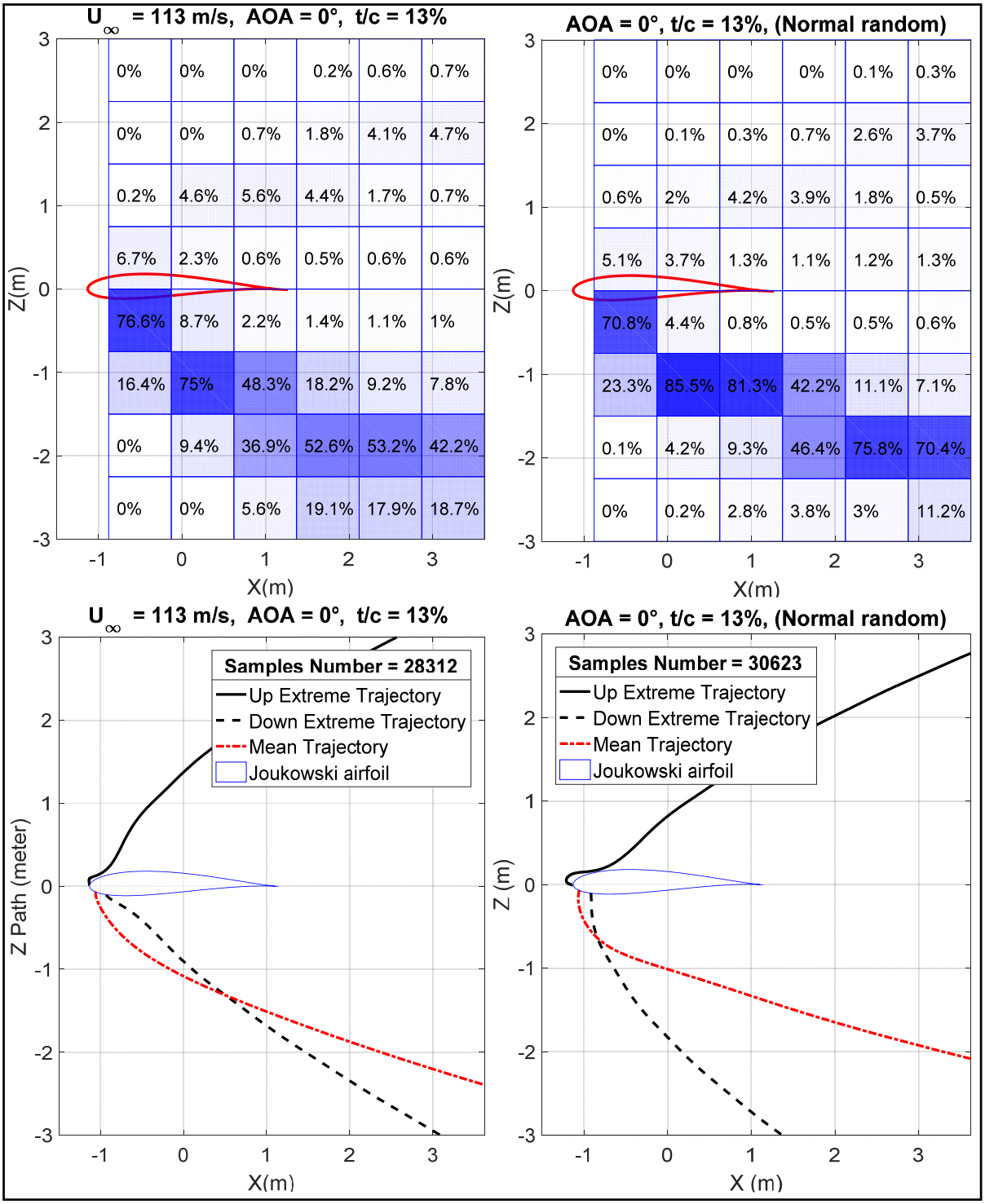

Figure 3.38 Comparison of Monte-Carlo simulations with uniform and normal random numbers , shedding is from downside surface of the leading edge, Ice particle $0.1303 \times 0.1303 \times 0.0365\ m$, $m_{ice} = 0.5715\ kg$, $\rho_{air} = 0.770\ kg/m^3$, Magnus effect included

Using normal random numbers needs to determine the mean number for normal distribution. For initial linear and angular velocities mean number can be zero. The initial angle of the ice piece can be any angle between zero and 180, therefore, using a mean number for this parameter seems to be unrealistic. In figure 3.37 and 3.38 mean number for the angle of the ice piece is zero.

Figure 3.39 and 3.40 show the results for Monte-Carlo simulation when the random number for initial angle of the ice piece is generated using uniform distribution and the initial velocities are generated using normal distribution. These results are compared with the simulations which use only uniform distribution for all initial parameters.

The results show more divers trajectories when the initial angle of the ice piece is obtained by uniform distribution. These results are compared with the simulations which use completely uniform random numbers for initial conditions. It can be seen that the probability maps are similar in two cases and ice ingestion risk does not change significantly. These simulations show again that initial angle of ice piece plays the most important rule in the trajectory of the ice piece and divers initial angle brings about more divers trajectories.

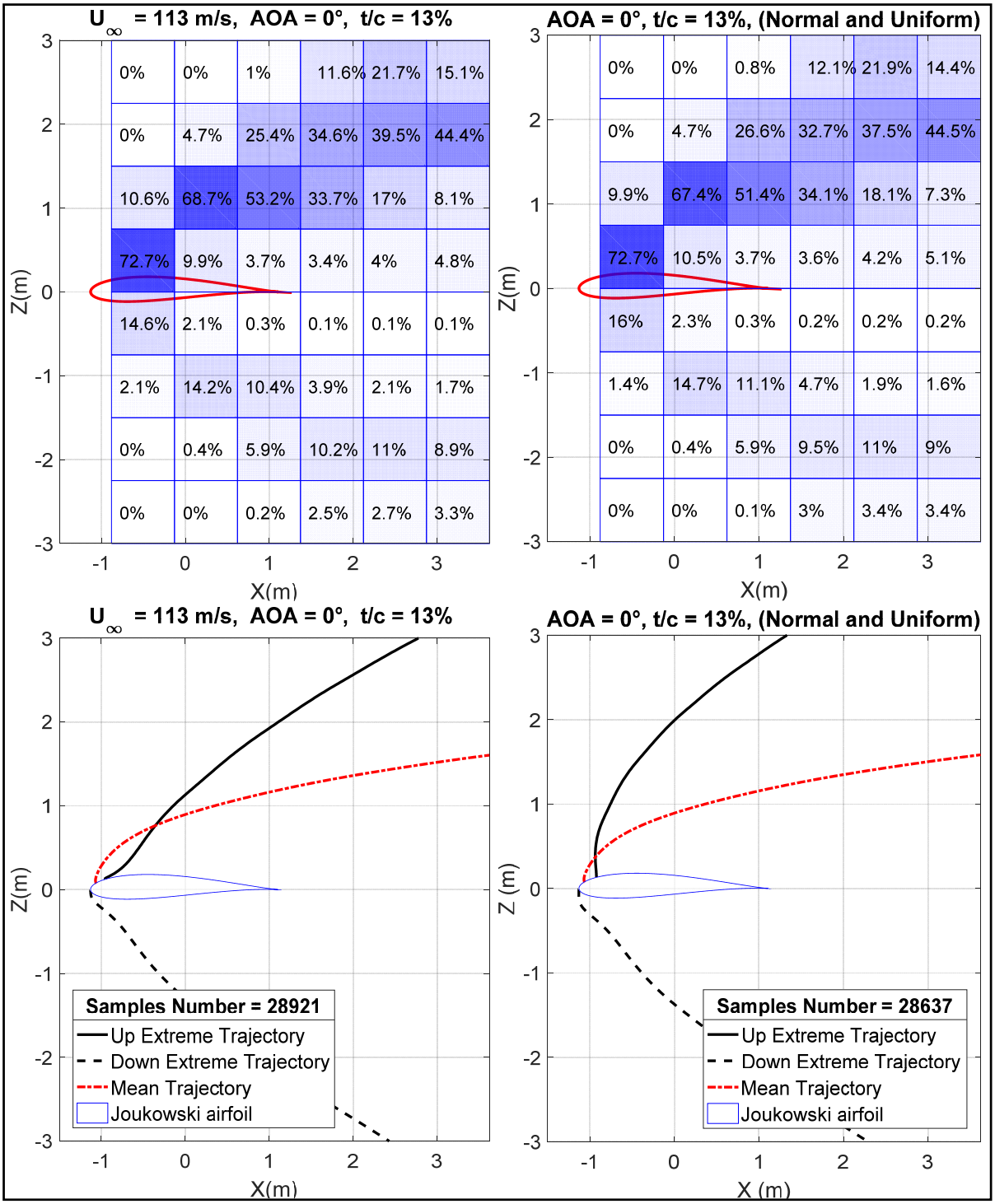

Figure 3.39 Comparison of Monte-Carlo simulations with uniform and normal random numbers, shedding is from upside surface of the leading edge, Ice particle $0.1303 \times 0.1303 \times 0.0365\ m$, $m_{ice} = 0.5715\ kg$, $\rho_{air} = 0.770\ kg/m^3$, Magnus effect included

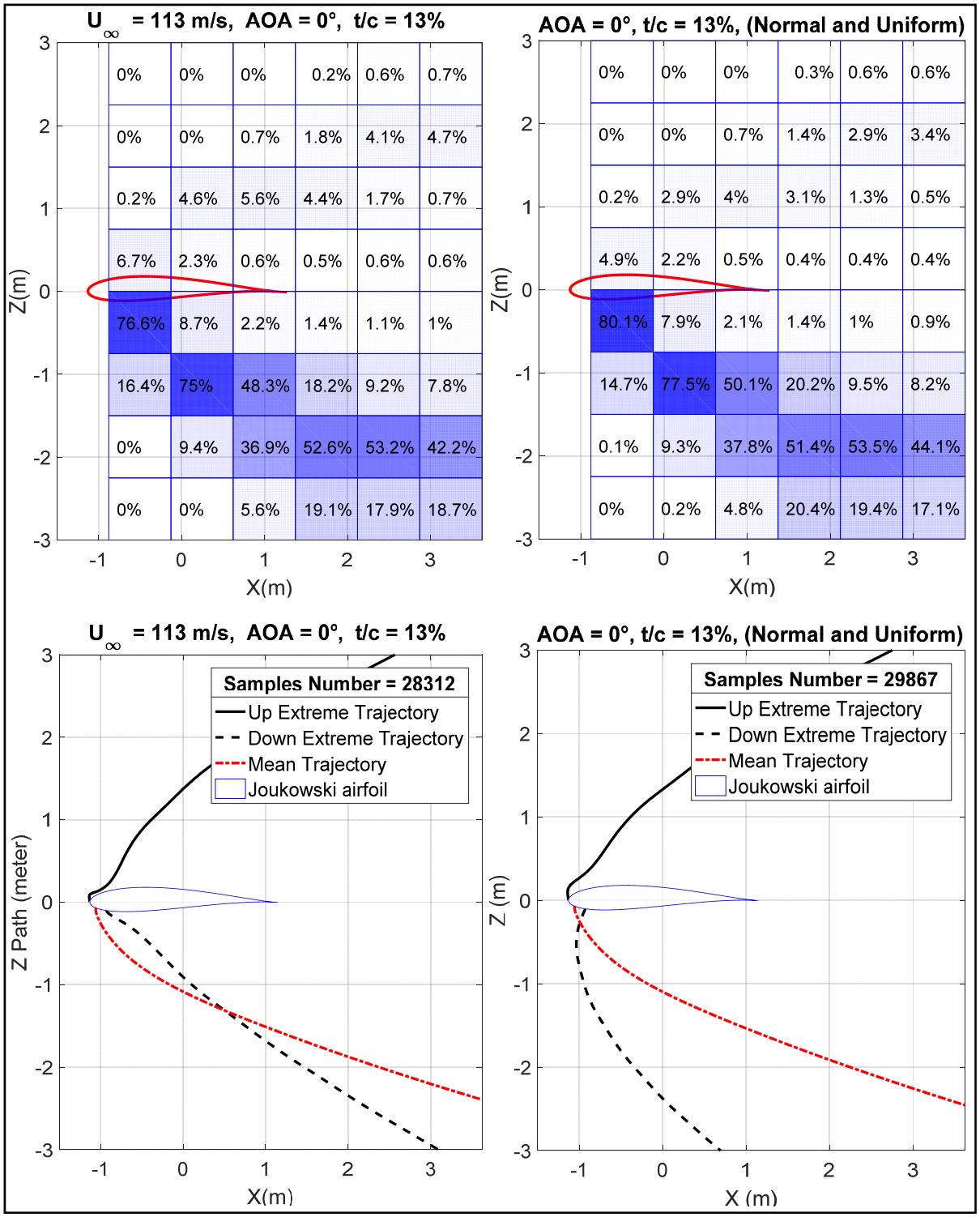

Figure 3.40 Comparison of Monte-Carlo simulation with uniform and normal random numbers , shedding is from downside surface of the leading edge, Ice particle $0.1303 \times 0.1303 \times 0.0365\ m$, $m_{ice} = 0.5715\ kg$, $\rho_{air} = 0.770\ kg/m^3$, Magnus effect included

This chapter was dedicated to the results obtained during the research project. Results for Joukowski airfoil simulation, single two-dimensional ice piece trajectory and finally the results of Monte-Carlo simulations were presented. In the next section the results of the research will be reviewed and conclusions will be presented.

CONCLUSIONS AND RECOMMENDATIONS

Inflight icing and ice shedding threat the flight safety by reducing the performance of the aircraft and by damaging its components. Ice ingestion by aft-mounted engines can damage its internal moving parts or may cause blockage of the airstream inside the compressor of the engine. In this thesis ice piece trajectory was simulated in 2D uniform and un-uniform flow fields. Trajectories in uniform flows were performed to validate the Matlab code of the thesis. Three references were used to compare the simulated trajectories of different square plate ice piece in uniform flows with different velocities and densities. The results of the validations were satisfying and a good agreement were obtained by comparing the results of the thesis with Holmes (Holmes, 2006), Kordi (Kordi, 2009) and Suares (Suares, 2005). These validations were presented and discussed in chapter three.

The main goal of this thesis was simulating the trajectory of the square ice piece in the flow field of the airfoil of the wing of an aircraft. In addition, the influence of the geometry of the airfoil and ice piece on the probability map around the airfoil were studied. In this order and to have the flow field of the airfoil, Joukowski airfoil and its flow field was simulated using potential flow equations. The Matlab code developed for Joukowski airfoil was integrated with the code of 2D trajectory to simulate the trajectory of ice pieces in an un-uniform flow field of the airfoil. In the literature there is no ice piece trajectory simulation in the flow field of the Joukowski airfoil, therefore the code of the ice trajectory in Joukowski airfoil's flow field were verified by conducting several comparative trajectories. Also the results were compared with the results of Suares (Suares, 2005) for NACA 23012. The results of this verification are presented and discussed in chapter three. The results show that developed code generates expected trajectories by different initial conditions and in different flow fields.

Simulation of single ice trajectories with different initial conditions confirms the importance of initial conditions of the shed ice in the trajectory. Initial conditions of the ice piece studied in this thesis are initial orientation of the ice piece, its initial linear and angular velocities and the location of ice shedding. Uncertainties about the initial conditions were studied using Monte-Carlo statistical method. The ice trajectory code was integrated with a developed code

for Monte-Carlo method to simulate ice trajectories with 60000 different initial conditions. The code uses a uniform random number generator to generate different values for the initial conditions of ice shedding.

The results of Monte-Carlo simulations were depicted as ice pass probability maps around the airfoil. These figures are presented in chapter three and show the percentage of pass possibilities through defined areas around the Joukowski airfoil. Also the mean trajectories of each simulation were presented to compare the trajectories with different airfoils and ice pieces. Although the main ice shape for this project was square plate ice piece, trajectories for rectangular and sphere ice pieces were simulated to be compared with the trajectories of square plate ice pieces.

The results of Monte-Carlo simulations were used to study the risk of ice ingestion by an aft-mounted engine. The probability of ice ingestion changes in the simulations with different geometries for the airfoil and ice piece. The results of the Monte-Carlo simulation can be summarized as following:

- **Effect of airfoil's angle of attack:** Ingestion risk by an aft-mounted engine decrease by increasing the angle of attack of the airfoil (AOA) to 4° and 15° degrees when ice shedding occurs from upside surface of the leading edge. Shed ice pieces from downside surface of the leading edge are less ingested by the engine when AOA is 4° but are more likely to be ingested by the engine when AOA is 15°.
- **Effect of airfoil's thickness:** Ice pieces shed from thinner airfoil are more probable to go inside the aft-mounted engine. This higher possibility of ice ingestion was shown for ice shedding from both sides of the leading edge.
- **Effect of airfoil's camber:** Ice pieces shed from upside surface of a symmetric airfoil are more likely to be ingested by the engine. In the case of the downside surface of leading edge, the probability of ice ingestion is slightly less.
- **Effect of ice piece's shape:** Rectangular and sphere ice pieces are more hazardous for aft-mounted engines of an aircraft than square plate ice pieces.

- **Effect of ice piece's size:** While bigger ice pieces shed from upside surface of the leading edge are less probable to be ingested by the engine, bigger ice pieces shed from the downside surface of the leading edge are more likely to go inside the engine.
- **Effect of Magnus effect**: Results confirm that Magnus effect has considerable influence on the ice trajectories. Trajectories with Manus effect in the simulations, have more diverse vertical movement, and trajectories without Magnus effect are more concentrated on the plane of study.

These results are obtained from developed Matlab code for 2D square plate ice piece trajectories in the flow field of Joukowski airfoil. Further works in future are required to develop this Matlab code. following are recommendations to enhance the capability and performance of the code:

- Developing the code to 3D ice trajectory simulation.
- Enhancing the capability of the code to simulate the flow fields of different airfoils.
- Introducing the aerodynamic coefficients of other ice shapes than square, rectangular and sphere to the code.
- Using additional initial conditions for Monte-Carlo simulations such as varying aerodynamic coefficients.

LIST OF REFERENCES

Baruzzi, G. S., Lagacé, P., Aubé, M. S., & Habashi, W. G. (2007). "Development of a Shed-ice Trajectory Simulation in FENSAP-ICE". (No. 2007-01-3360). SAE Technical Paper.

Bin, Y. and Z. Yanpei (2011). "Icing certification of civil aircraft engines". Procedia Engineering 17: 603-615.

Borigo, C. J. (2014). "A novel actuator phasing method for ultrasonic de-icing of aircraft structures". (Doctoral thesis, The Pennsylvania State University, Pennsylvania). Retrieved from https://etda.libraries.psu.edu

Califf, C. and D. C. Knezevici (2014). "Use of a Turbofan Engine to Measure Ice Crystal Cloud Concentration In-Flight". 50th AIAA/ASME/SAE/ASEE Joint Propulsion Conference.

Cao, Y., et al. (2015). "Aircraft flight characteristics in icing conditions". Progress in Aerospace Sciences 74: 62-80.

Chandrasekharan, R., & Hinson, M. (2003). "Trajectory simulation of ice shed from a business jet". (No. 2003-01-3032). SAE Technical Paper.

Cli, R., Grace, J. R., & Weber, M. E. (1978). "Bubbles, drops and particles". Mineola, New York: Dover Publications, INC.

Currie, T. C., Fuleki, D., & Mahallati, A. (2014). "Experimental studies of mixed-phase sticking efficiency for ice crystal accretion in jet engines". Paper presented at 6th AIAA Atmospheric and Space Environments Conference, Reston, VA.

de Castro Santos, L., Papa, R., & Ferrari, M. D. A. (2003, January). "A Simulation Model for Ice Impact Risk Evaluation". Paper presented at 41st Aerospace Sciences Meeting and Exhibit, Reno, Nevada.

Haggerty, J., et al. (2012). "A System for Nowcasting Atmospheric Conditions Associated with Jet Engine Power Loss and Damage Due to Ingestion of Ice Particles". 4th AIAA Atmospheric and Space Environments Conference.

Hargreaves, D. M., Kakimpa, B., & Owen, J. S. (2014). The computational fluid dynamics modelling of the autorotation of square, flat plates. *Journal of Fluids and Structures*, *46*, 111-133.

Hoerner, S. F. (1965). “Fluid-dynamic drag: practical information on aerodynamic drag and hydrodynamic resistance”. Brick Town, New Jersey: Hoerner Fluid Dynamics.

Holmes, J. D., Letchford, C. W., & Lin, N. (2006). “Investigations of plate-type windborne debris—Part II: Computed trajectories”. Journal of Wind Engineering and Industrial Aerodynamics, 94(1), 21-39.

Iversen, J. D. (1979). “Autorotating flat-plate wings: the effect of the moment of inertia, geometry and Reynolds number”. Journal of Fluid Mechanics, 92(2), 327-348.

Johnson, T. (2013). “Conformal Mapping in Wing Aerodynamics” (Technical report).

Kapania, N. R., Terracciano, K., & Taylor, S. (2008). “Modeling the Fluid Flow around Airfoils Using Conformal Mapping”. SIAM Undergraduate Research Online, 1(2).

Kohlman, D., & Winn, R. (2001, January). “Analytical prediction of trajectories of ice pieces after release in an airstream”. Presented at 39th Aerospace Sciences Meeting and Exhibit (p. 680). Reno, Nevada.

Kordi, B., & Kopp, G. A. (2009). “Evaluation of quasi-steady theory applied to windborne flat plates in uniform flow”. Journal of engineering mechanics, 135(7), 657-668.

Mason, J. G., et al. (2006). “The ice particle threat to engines in flight”. Presented at 44th AIAA Aerospace Sciences Meeting, Reno, Nevada.

Newman, S. J. (2011). “Joukowski aerofoil modelling in MATLAB” (Technical report). Southampton: University of Southampton.

Nilamdeen, M. S. (2010). “An uncoupled multiphase approach towards modeling ice crystals in jet engines”. (M.Eng. thesis, McGill University, Montreal, Canada).

Panton, R. L. (2005). “Incompressible Flow”. Hoboken, New Jersey: John Wiley & Sons.

Pellissier, M. P. C. (2010). “Optimization via CFD of aircraft hot-air anti-icing systems”. (M.Eng. thesis, McGill University, Montreal, Canada).

Pope, A. (1951). “Basic wing and airfoil theory”. New York, NY: McGraw-Hill.

Shimoi, K. (2010). “Numerical and experimental investigation of ice shedding”. (Doctoral dissertation, Wichita State University).

Suares, I. G. (2005). “Ice particle trajectory simulation”. (Doctoral dissertation, Wichita State University).

Tachikawa, M. (1983). “Trajectories of flat plates in uniform flow with application to wind-generated missiles”. Journal of Wind Engineering and Industrial Aerodynamics, 14(1-3), 443-453.

Védie, L., Morency, F., & Kubler, N. (2016). “Sensitivity analysis of ice piece trajectory calculation”. Paper presented at 8th AIAA Atmospheric and Space Environments Conference (p. 4351). Washington, D.C.

Veres, J. P., et al. (2012). “A Model to Assess the Risk of Ice Accretion due to Ice Crystal Ingestion in a Turbofan Engine and its Effects on Performance”. Paper presented at 4th AIAA Atmospheric and Space Environments Conference, New Orleans, Louisiana.